

UCSF

UC San Francisco Electronic Theses and Dissertations

Title

Engineering Microvessels through Optimization of the Microenvironment

Permalink

<https://escholarship.org/uc/item/8g43k142>

Author

Cabral, Katelyn Ashley

Publication Date

2021

Peer reviewed|Thesis/dissertation

Engineering Microvessels through Optimization of the Microenvironment

by

Katelyn Ashley Cabral

DISSERTATION

Submitted in partial satisfaction of the requirements for degree of

DOCTOR OF PHILOSOPHY

in

Bioengineering

in the

GRADUATE DIVISION

of the

UNIVERSITY OF CALIFORNIA, SAN FRANCISCO

AND

UNIVERSITY OF CALIFORNIA, BERKELEY

Approved:



Zev Gartner

Chair

DocuSigned by:




Sanjay Kumar

DocuSigned by:



Donald M McDonald

E3CC7DB3648E488...



Todd McDevitt

Committee Members

Acknowledgments

Earning this Ph.D. was one of the most challenging things I've ever done. I could not have accomplished this without the help and support of so many others. I'd like to thank the following people and groups:

Dr. Zev Gartner – Zev has been a source of inspiration and encouragement throughout this Ph.D. His enthusiasm for science is infectious. I admire his creativity, his ability to find connections across different fields of study, and the empathy he shows for his students and postdocs.

The Gartner Lab, both past and present – Dr. Noel Jee, Dr. Michael Todhunter, and Max Coyle welcomed me into the lab, taught me valuable experimental skills, and got me started on my project. Dr. Vasudha Srivastava and Dr. David Patterson gave me advice throughout my Ph.D., and I benefited from their perspectives. Jennifer Hu has been my friend and one of my biggest supporters since we first rotated in the lab. I'm so proud of what she's accomplished during her Ph.D. and I am lucky to have spent the past 6 years working alongside her. Aivy David has been keeping the lab running incredibly smoothly, even during the pandemic, and I appreciate how hard she works to make sure that the supplies I need are there when I need them. In general, the Gartner Lab has had a fantastic work culture, with people who really care about each

other. I found it to be a very supportive environment and I thank all of the past and present members of the Gartner Lab for making it a great place to work.

Collaborators – Although much of my dissertation work was done by myself, I appreciated the opportunities that I had to work with others. I'd like to thank Dr. Rogelio Hernandez-Lopez, Olivia Creasey, Dr. David Patterson, Dr. Olivia Scheideler, Max Coyle, Dr. Vasudha Srivastava, Madu Nzerem, Michael Cronic, Connor Stashko, and Stephen Cutie for their contributions to my graduate work.

I'd like to thank my dissertation committee – Dr. Donald McDonald, Dr. Todd McDevitt, and Dr. Sanjay Kumar, for providing feedback on this dissertation and for giving me insight into how I could improve it.

Carry the One Radio – CTOR has been a fantastic outlet for my creativity. I had so much fun interviewing other scientists and learning about topics different than my dissertation research. CTOR improved my scientific communication skills, and I am truly grateful. The group has accomplished so much since 2016 and I can't wait to see what episodes come out next on my podcast feed.

My family – My family has been a fantastic source of support throughout my Ph.D. I can't wait to move back to Massachusetts and see them more often.

Ian Hawkes – He has been my biggest supporter and best friend during this Ph.D. From the big things (moving across the country) to the small things (tolerating me going into lab to feed cells on the weekend), he has always shown me how much he loves me and wants me to succeed. He gives me strength. I can't wait to marry him this September.

Contributions

A version of Chapter 3 was previously published as:

Cabral, K. A. Patterson, D.M. Scheideler, O.J. Cole, R. Abate, A.R. Schaffer, D.V.

Sohn, L.L. Gartner, Z.J. Simple, Affordable, and Modular Patterning of Cells using DNA. *J. Vis. Exp.* (2021).

Engineering Microvessels through Optimization of the Microenvironment
Katelyn Ashley Cabral
Abstract

Cells need blood vessels to transport nutrients, oxygen, and waste. The lack of vascularization within engineered tissues results in a loss of tissue viability and function, limiting the ultimate success of tissue engineering strategies. Thus, there is a tremendous need to understand how to efficiently grow blood vessels *in vitro* within the context of engineered tissues. As bioprinting and other microfabrication technologies improve in resolution, it has become increasingly possible to define the structure of tissues such as blood vessels by placing the cells in pre-defined positions. Additionally, endothelial cells have an intrinsic ability to self-organize into microvascular networks. My research combines these two ideas: laying down the general structure of the network by cell patterning and then allowing the cells to progress through the later stages of tissue morphogenesis to create a functional capillary network. My dissertation research proposes that we can control and enhance the intrinsic self-organization capabilities of pre-patterned endothelial cells by changing their microenvironment – the chemical, cellular, and physical cues that impinge upon the cells. By adjusting the microenvironment to promote certain cell behaviors involved in vasculogenesis, I was able to guide patterned endothelial cells to self-organize into pre-defined capillary-like vessels.

Table of Contents

1	<i>Introduction</i>	1
2	<i>Recapitulating Vasculogenesis in Vitro</i>	6
2.1	Abstract.....	6
2.2	Introduction	7
2.3	Vasculogenesis <i>In Vivo</i>	9
2.4	The cell behaviors associated with vasculogenesis	9
2.5	Microenvironmental control of vasculogenesis	11
2.5.1	Physical and Mechanical Cues	11
2.5.2	Cellular Cues	13
2.5.3	Soluble Cues.....	16
2.6	Methods for Engineering Microvascular Networks.....	17
2.6.1	Top-down fabrication of vessels	18
2.6.2	Self-organization of endothelial cells seeded within hydrogels into microvascular networks	21
2.6.3	Hybrid approaches to creating vascularized tissues	23
2.6.4	Outlook on engineered microvasculature.....	25
2.7	Summary	26
3	<i>Simple, affordable, and modular patterning of cells using DNA</i>	27
3.1	Abstract.....	27
3.2	Introduction	28
3.3	Methods.....	34
3.4	Results	47

3.5	Discussion	62
4	<i>Microenvironmental control of endothelial cell behaviors that promote microvessel formation in engineered tissues</i>	<i>67</i>
4.1	Abstract.....	67
4.2	Introduction	68
4.3	Methods.....	72
4.4	Results	81
4.5	Discussion	97
4.6	Conclusions	101
5	<i>Effect of Endothelial Cell Density on Endothelial Self-Organization.....</i>	<i>103</i>
5.1	Abstract.....	103
5.2	Introduction	104
5.3	Methods.....	106
5.4	Results	110
5.5	Discussion	120
6	<i>Discussion.....</i>	<i>124</i>
6.1	Accomplishments	124
6.2	Problems Left to Solve.....	126
6.3	Significance within field of microvascular tissue engineering	128
6.4	Unresolved Questions	130
6.5	Future Directions.....	132

6.6 Conclusion..... 133

References134

List of Figures

Figure 1.1 Imposing boundary conditions on endothelial cells and then applying the correct microenvironmental cues to promote self-organization of the endothelial cells into microvessels of pre-defined structure.	3
Figure 2.1 Illustration of endothelial cells undergoing vasculogenesis <i>in vitro</i>	10
Figure 3.1 Example images of the benchtop photolithography setup.....	38
Figure 3.2 Some examples of common failures of this protocol.....	39
Figure 3.3 Overview of CMO-DPAC technique.	47
Figure 3.4 Cells are labeled with CMOs in a stepwise process.	48
Figure 3.5 Photolithography is used to create the DNA-patterned slides that will ultimately dictate the placement of cells.	50
Figure 3.6 Overlapping photopatterns results in presence of both oligos at reduced concentration.	51
Figure 3.7 Adhesion of CMO-labeled cells to DNA patterns increases as a function of CMO concentration during labeling.....	53
Figure 3.8 Quantification of DNA complexes on the cell surface as a function of CMO labeling concentration.	54
Figure 3.9 CMO labeling does not stimulate TLR9 response.....	54
Figure 3.10 CMO-DPAC can be used to create two-dimensional cell patterns that can subsequently be embedded into a three-dimensional hydrogel for culture and/or layered to create multilayered structures.	56
Figure 3.11 Viability of cells after CMO labeling process.....	57
Figure 3.12 Multiple cell types can be patterned without cross-contamination or loss of adhesion.	58
Figure 4.1 Method for measuring cord segment lengths.	78

Figure 4.2 Capillary-sized lines of HUVECs are created using DNA-Programmed Assembly of Cells (DPAC).....	82
Figure 4.3 Extracellular matrix composition influences the initial condensation of patterned lines of HUVECs into cords.....	84
Figure 4.4 Adding collagen I to the ECM resulted in longer cord segments at 24 hours, through a stiffness-independent mechanism.....	85
Figure 4.5 Optimizing the culture media through addition of PMA and removal of FBS results in stable, cohesive HUVEC cords with few sprouts and continuous adherens junctions.	87
Figure 4.6 Adding pro-vasculogenic components to the media did not prevent scattering of HUVECs in patterned cords.....	88
Figure 4.7 The component of FBS that is driving the HUVEC phenotype is a protein greater than 200 kDa.	90
Figure 4.8 Examples of candidate proteins larger than 200 kDa that failed to recapitulate the phenotype of FBS.....	91
Figure 4.9 Observation of cell pairs reveals that FBS increases proliferation and extension of subcellular protrusions but inhibits the formation of stable cell-cell adhesions.	92
Figure 4.10 Extended culture of HUVEC cords in serum-free media led to the formation of stable, lumenized, and mature microvascular networks of controlled dimensions.....	93
Figure 4.11 Multi-layered HUVEC cords also respond to FBS with increased sprouting.....	95
Figure 5.1 The experimental setup for composite DPAC tissues.....	109
Figure 5.2 The spatial context influences the vasculogenesis of HUVECs.....	111
Figure 5.3 Fetal bovine serum (FBS) has no gross morphological effect on the vasculogenesis of GFP-HUVECs uniformly seeded within an MG-COL1 hydrogel.	111
Figure 5.4 Initial cell-cell spacing in the vasculogenesis assay.....	112

Figure 5.5 The addition of a dense population of HUVECs underneath the patterned HUVEC cords results in a more cohesive cord morphology.....114

Figure 5.6 Assessment of proliferation in patterned GFP-HUVEC cords after culture with neighboring, dense endothelial cells.114

Figure 5.7 Comparison of different cell types in adjacent population to cords.115

Figure 5.8 Analysis of secreted proteins found in conditioned media from dense HUVECs.117

Figure 5.9 Reduction of VEGF in the media did not recapitulate the effect of dense, neighboring HUVECs.....118

Figure 5.10 Conditioned media could not recapitulate effect of dense, adjacent HUVEC population on the self-organization of patterned GFP-HUVEC cords.....118

List of Tables

Table 3.1 A troubleshooting guide to identify and resolve potential failures that can arise from this protocol.....	59
Table 4.1 FBS candidate proteins tested.	76

List of Acronyms

ANOVA: analysis of variance

BBB: blood-brain barrier

BSA: bovine serum albumin

CMO: cholesterol modified oligo

DNA: deoxyribonucleic acid

DPAC: DNA programmed assembly of cells

ECM: extracellular matrix

FGF-2: fibroblast growth factor 2

FBS: fetal bovine serum

EGFP: enhanced green fluorescent protein

HBVP: human brain vascular pericyte

HUAEC: human umbilical arterial endothelial cell

HUVEC: human umbilical vein endothelial cell

IL-3: interleukin-3

LMO: lipid-modified oligonucleotide

kDa: kilodalton

MDCK: Madin-Darby canine kidney cells

MESF: molecules of equivalent soluble fluorochrome

MG: Matrigel

MG-COL1: Matrigel-collagen I

MW: molecular weight

PBS: phosphate buffered saline

PDMS: polydimethylsiloxane

PEG: polyethylene glycol

PGMEA: propylene glycol methyl ether acetate

PMA: phorbol 12-myristate 13-acetate

PMSF: phenylmethylsulfonyl fluoride

SCF: stem cell factor

SDF-1 α : stromal cell-derived factor alpha

TGF- β : transforming growth factor beta

TLR9: toll-like receptor 9

VEGF: vascular endothelial growth factor

1 Introduction

As we learn more and more about mammalian biology and physiology, the more we are drawn to the idea of engineering and manufacturing tissues and organs. There are many exciting applications for tissue engineering, including the development of human-specific and even patient-specific disease models¹⁻⁴, the replacement of environmentally unsustainable livestock with lab-grown meat⁵, and eventually the transplantation of engineered organs to meet the demand for healthy, transplantable organs⁶⁻⁸.

Blood vessels serve many essential functions in animal physiology, including delivering oxygen and nutrients to tissues, carrying away carbon dioxide and other wastes, and distributing hormones and other signaling molecules to cells. However, these functions are limited as a function of distance. The oxygen and nutrients delivered by the blood vessels cannot travel more than a few hundred microns through the tissue⁹. Cell-dense, avascular tissues larger than 250 microns in diameter become hypoxic, leading to poor functionality and cell death^{10,11}. This fact is of particular concern in the field of tissue engineering. Upon implantation into a host, engineered tissues do receive some vascularization as host blood vessels invade into the engineered tissue, but this process is too slow, at a rate of approximately 5 microns per hour, to be able to penetrate very far into the hypoxic core of engineered tissues¹². Thus, it is essential that bioengineers include vascular networks within

engineered tissues. The problem of tissue vascularization within engineered tissues has been described as a key limitation for the field^{8,13}.

Even after being cultured outside the body, endothelial cells retain the ability to self-organize into capillary networks. Thus, it is possible to create blood vessels *in vitro* through a “bottom-up” engineering approach by simply placing the endothelial cells into a supportive 3D microenvironment. Under the right culture conditions, cells will migrate towards each other and adhere, resulting in the formation of multicellular elongated structures that will merge into a microvascular network. However, this process is inefficient and takes several days to take place, during which time the center of the engineered tissue may have died. An alternate strategy would be to use bioprinting or other additive manufacturing techniques to seed endothelial cells into defined network structures, and then use microenvironmental manipulation to encourage the pre-patterned endothelial cells to link up with each other and form a perfusable network¹⁴. The hope is that by placing the cells next to each other in the geometry of a blood vessel we could limit the distance that the cells need to move and thus reduce the time required to form complex microvascular networks. However, for this strategy to be successful, we will first have to learn more about the signaling pathways and cellular behaviors that drive the self-assembly of endothelial cells into microvascular networks. Furthermore, we will need to have a keen understanding of what microenvironmental cues, such as extracellular matrix composition, media

additives, cell density, and supporting cell types, can encourage pre-patterned endothelial cells to undergo vasculogenesis and quickly form a microvascular network in the prescribed geometry.

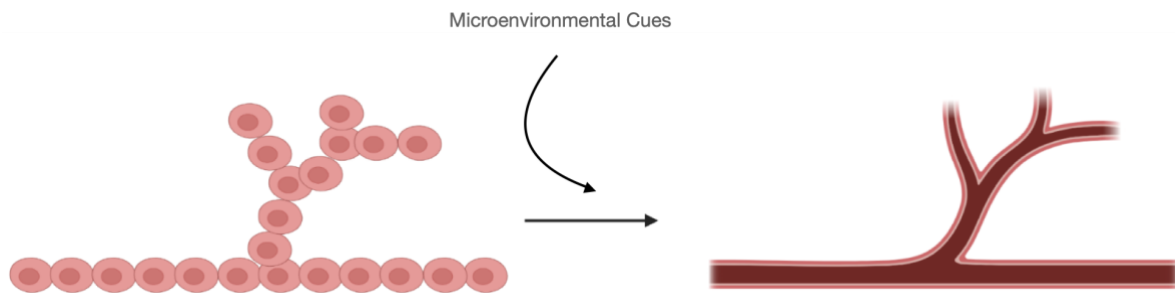


Figure 1.1 Imposing boundary conditions on endothelial cells and then applying the correct microenvironmental cues to promote self-organization of the endothelial cells into microvessels of pre-defined structure.

The goal of my dissertation research was to investigate how the self-organization of pre-patterned endothelial cells into capillaries is influenced by their microenvironment. I aimed to identify some of the minimal cues necessary for pre-patterned endothelial cells to fully reconstitute mature microvasculature, defined as a perfusable endothelial tube with a continuous lumen at least 5 μm wide, an intact basement membrane with laminin and collagen IV, and permeability similar to *in vivo* vasculature of approximately $1 \times 10^{-8} \text{ m/s}^{15}$.

During tissue morphogenesis, cells integrate cues from other cells, the extracellular matrix, mechanical forces, and soluble factors. These

microenvironmental cues drive the cell behaviors underlying the morphogenesis. For engineered tissues, we start with an initial set of components (cells, matrix, soluble factors, et cetera) and aim to drive morphogenesis of the cells to a final tissue state that is functional and mimics the analogous tissue *in vivo*. To control this morphogenesis, tissue engineers can provide the correct microenvironmental cues that will encourage the desired cell behaviors for that stage of morphogenesis (proliferation, migration, formation of cell-cell adhesions, et cetera). However, it is still unclear which microenvironmental cues, and in what spatiotemporal context, will result in a perfusable capillary network.

I developed an assay to systematically and reproducibly test the influence of microenvironmental factors on endothelial self-organization. Using DNA Programmed Assembly of Cells (DPAC), a high precision cell patterning technique¹⁶, I patterned human umbilical vein endothelial cells (HUVECs) into lines 35 microns in width and 2 millimeters in length. I then embedded these HUVEC lines into a 3D hydrogel and cultured them for at least 72 hours before quantitatively assessing the resulting morphology of the HUVEC cords. Using this assay, I tested the effect of a wide variety of microenvironmental cues, including hydrogel composition, growth factors, media additives, endothelial cell density, and mural cells. I found that by optimizing the microenvironment, I could encourage condensation of the HUVECs into multicellular cords and then mature the cords into lumenized microvessels with a

basement membrane. I also found that the context in which the cells receive the microenvironmental cues is important – the spacing, relative positioning, and cell density also influence the self-organization of endothelial cells.

This dissertation summarizes my research investigating the effect of the microenvironment on endothelial self-organization. To provide context for this work, in Chapter 2 I review the relevant scientific literature on the formation of blood vessels both *in vivo* and *in vitro*, what is currently known about the effects of the microenvironment on endothelial self-organization, and how other tissue engineers have approached this problem. In Chapter 3, I describe our refined protocol for a simple, modular, and inexpensive version of the DPAC technique that uses a modular, commercially available cholesterol-modified oligo system to tether the cells and adapts a protocol for photopatterning DNA that can be used outside of a cleanroom. In Chapter 4, I discuss the effects of extracellular matrix properties and media components on the self-organization of patterned endothelial cells into mature microvessels. In Chapter 5, I investigate the effect of cell density on endothelial self-organization. To conclude the dissertation, in Chapter 6 I reflect on the body of work that I have produced during this Ph.D., discuss the lessons learned during the process, address the limitations of my research, and propose some future projects that could build on my findings.

2 Recapitulating Vasculogenesis in Vitro

2.1 Abstract

Vasculogenesis is the process of forming microvascular networks *de novo*. During vasculogenesis, individual endothelial cells must move towards each other, elongate, and form stable connections with each other, ultimately forming a tubular, branched vascular plexus. Although vasculogenesis is often thought of as a developmental phenomenon, this process can also happen *in vitro* when endothelial cells are provided with a supportive 3D microenvironment. Understanding the individual cell behaviors that result in vasculogenesis and the microenvironmental conditions that can encourage those behaviors will enable us to create engineered tissues that are fully vascularized. In this chapter, I will first discuss what is known about developmental vasculogenesis, as there are likely many similarities to vasculogenesis *in vitro*. I will then examine what is known about the individual endothelial cell behaviors that result in self-organization of a collection of cells into a unified branched microvascular network. Next, I will discuss how chemical, mechanical, spatial, and cellular cues from the microenvironment can encourage or discourage vasculogenesis. I will conclude by highlighting some successes made in the creation of pre-vascularized tissues and their applications in basic science and clinical settings.

2.2 Introduction

The circulatory system is essential for vertebrate life, providing oxygen, nutrients, and hormones to all tissues in the body. Due to its essential function, it is the first organ system to achieve functionality during embryonic development¹⁷. The blood vessels that comprise the circulatory system can arise through two distinct morphogenic processes. Vasculogenesis is the *de novo* creation of blood vessels by the self-organization of endothelial progenitors into a vascular plexus. Angiogenesis is the creation of new blood vessels from existing ones, either by branching off (sprouting angiogenesis) or splitting in two (intussusceptive angiogenesis)^{18,19}.

In vivo, only angiogenesis is typically observed after the very early stages of development, and therefore much of the vascular biology literature has focused specifically on angiogenesis, whether that is in the context of cancer²⁰⁻²², wound healing^{23,24}, or normal physiology²⁵. This has led to a much greater understanding of endothelial cell gene expression and behavior, as well as the development of therapies like bevacizumab for cancer and diabetic retinopathy^{21,26}. In comparison, the individual cell behaviors and gene expression that contribute to vasculogenesis *in vivo* are less well studied due to the limited time frame in which it occurs during embryonic development.

However, vasculogenesis is not limited to just early development. Neonatal and adult endothelial cells, as well as endothelial cells derived from pluripotent stem cells, are quite plastic and retain their ability to undergo vasculogenesis even after two-dimensional cell culture²⁷⁻²⁹. In a 3D extracellular matrix (ECM), such as collagen or fibrin, dissociated endothelial cells can migrate, pathfind towards each other, adhere to each other, and undergo shape changes. Over the course of several days, endothelial cells can go from a uniform dispersion of single cells to a complex, branched microvascular network. Given the right fluid flow conditions, this network can ultimately become fully perfused³⁰. This latent ability of endothelial cells to form networks has been used to model tumor vascularization³¹⁻³⁴, support the growth and development of organoids³⁵⁻³⁸, and increase the physiological relevancy of organ-on-a-chip models¹⁶⁻¹⁸.

There is a significant need for the vascularization of large, cell-dense engineered tissues^{8,13}. Angiogenesis from the host vasculature is often insufficient, due to the relatively slow invasion rate of five microns per hour¹². Thus, the concept of pre-vascularizing tissues by incorporating endothelial cell networks into engineered tissues has become of significant interest in recent years^{42,43}. However, for this strategy to be successful, we will first have to learn more about the signaling pathways and cellular behaviors that drive the self-assembly of endothelial cells into microvascular networks. Moreover, we will need to have a keen understanding of what

microenvironmental cues, such as extracellular matrix composition, media additives, and supporting cell types, can encourage pre-patterned endothelial cells to undergo vasculogenesis and quickly form a microvascular network within the constraints of the engineered tissue.

2.3 Vasculogenesis *in vivo*

Blood vessels arise both intra- and extra-embryonically during development⁴⁴. During embryonic vasculogenesis, mesoderm-derived angioblasts begin to proliferate, differentiate towards an endothelial lineage, and migrate towards each other⁴⁵. The angioblasts then aggregate and organize themselves into primitive blood vessels such as the dorsal aorta^{46,47}. These early vessels eventually lumenize and connect to the developing heart to form a perfusable blood vessel network⁴⁸. Endothelial cells in these initial blood vessels undergo further differentiation to specify towards arterial, venous, and lymphatic lineages^{49,50}. After vasculogenesis creates this initial blood vessel network, new vessels are created through the process of angiogenesis⁵¹.

2.4 The cell behaviors associated with vasculogenesis

Endothelial cells participating in the process of vasculogenesis must perform a complex series of behaviors, including migration, pathfinding, proliferation,

elongation, and adhesion to other cells, in order to self-organize into a multicellular vascular structure⁵²⁻⁵⁴ (Figure 2.1). These multicellular structures are further expanded by angiogenesis as new sprouts branch from existing structures and connect different parts of the vascular plexus. The initial vascular plexus must then be further developed through lumenization, maturation, stromal cell recruitment, and pruning of the vascular network. The molecular mechanisms driving these cell behaviors can be difficult to discern, as these behaviors overlap with each other temporally⁵². These cellular behaviors are driven by both intrinsic signals and microenvironmental cues. In this section, I will discuss how the cellular behaviors underlying the morphogenesis of vascular networks are impacted by the cellular, physical, and soluble factors in the microenvironment. Much of what is known about vasculogenesis has been discovered by using *in vitro* and *ex vivo* models and then comparing those results to what has been discovered using animal models such as mouse and zebrafish⁵⁵.

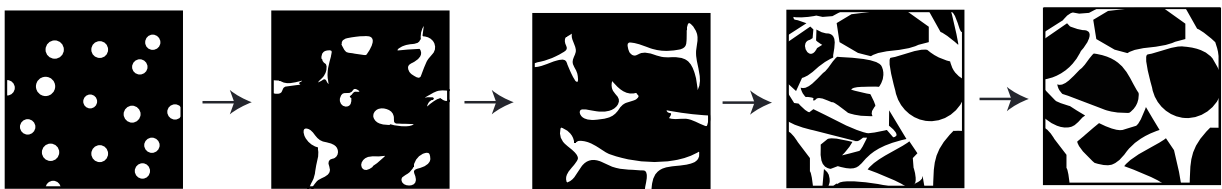


Figure 2.1 Illustration of endothelial cells undergoing vasculogenesis *in vitro*.

The cells are initially rounded after being seeded within the hydrogel. Over time, they begin to extend protrusions and migrate towards each other. Endothelial cells that successfully adhere to each other will elongate as one long, multicellular structure. These multicellular structures will continue to expand the vascular network by connecting with additional endothelial cells. Over time, the network structure is refined into a branched microvascular plexus.

2.5 Microenvironmental control of vasculogenesis

The behavior of cells is dependent on the external cues they receive from their microenvironment. Cells integrate chemical, electrical, and mechanical signals in selecting their behavior. By providing the correct microenvironmental cues, researchers can guide cells and tissues to accomplish target functions. In this section, I will review the physical, cellular, and soluble factors within the endothelial microenvironment that can not only influence whether endothelial cells choose to undergo vasculogenesis, but also the resulting quality and maturity of those microvascular networks. Tissue engineers can direct endothelial cells to undergo vasculogenesis *in vitro* by supplying the endothelial cells with the appropriate microenvironment^{42,56–58}.

2.5.1 Physical and mechanical cues

Endothelial cell behavior is guided by mechanical forces^{58,59}. During vasculogenesis and angiogenesis, endothelial cells exert traction forces on the ECM by pulling on matrix fibers and creating tension^{60,61}. Other endothelial cells will migrate directionally towards each other along these lines of tension, facilitating the formation of microvascular networks^{62,63}. Endothelial cell contractility is required for both vasculogenesis and microvessel stabilization⁶⁴. Cell contractility is influenced by the mechanical properties of the ECM. There have been many tissue engineering studies

attempting to find an optimal ECM to promote vasculogenesis or angiogenesis^{58,59}.

Fibrin and collagen I are the most popular choices of hydrogel to use with engineered microvasculature⁴² and are physiologically relevant due to their pro-angiogenic function in either the early (fibrin) or late (collagen I) stages of granulation tissue²³. The degree of microvascular network formation as well as the resulting structure of the network are affected by hydrogel stiffness⁶⁵⁻⁶⁷. Vasculogenesis has generally been found to increase in softer hydrogels where the cells can exert more traction forces on the ECM⁶¹. Increasing the matrix density of fibrin or collagen gels decreases vasculogenesis due to inhibited transport of nutrients and angiogenic molecules^{27,68}.

One complication with the use of natural hydrogels like collagen and fibrin to study the biomechanics of vasculogenesis is that their properties are hard to disentangle experimentally. Increasing the protein concentration of a collagen gel will also influence its stiffness, porosity, and the number of adhesive ligands available. To separate out the effects of these biomaterial properties on vasculogenesis, Brown et al. cultured endothelial cells within a synthetic, PEG-based hydrogel⁶⁹. They found that increasing the polymer density or increasing the degree of crosslinking led to a decrease in endothelial network formation. Modifying the hydrogel with peptides that were differentially sensitive to cleavage by endothelial-secreted matrix metalloproteinases revealed that the degradability of the ECM should be a key consideration when designing hydrogels for vasculogenesis models.

Interstitial fluid flow, in which fluid moves slowly throughout a tissue, drives vascular morphogenesis *in vitro* in a magnitude-dependent manner, resulting in enhanced microvascular network formation and angiogenic sprouting in the opposite direction of the flow⁷⁰⁻⁷⁴. The interstitial flow acts on the endothelial cells through both through physical means and by the creation of biochemical gradients. The mechanical stresses acting on the endothelial cells are transduced through FAK and Src-mediated signaling, resulting in de-localization of VE-cadherin from cell-cell junctions and differences in actin cytoskeleton organization⁷⁵. Song et al. found that using a dominant-negative form of RhoA blocked the angiogenic sprouting of endothelial cells in response to interstitial fluid flow⁷⁶. However, many labs have observed synergy between the mechanical stresses of interstitial fluid flow and its effects on biochemical gradients^{70,73,77-79}. Gradients of pro-angiogenic molecules such as VEGF are created by the fluid flow, facilitating vascular morphogenesis⁸⁰. The application of interstitial fluid flow to microvascular networks also encourages lumenization, allowing the vessels to become perfused^{30,73}.

2.5.2 Cellular cues

Co-culture of the endothelial cells with mural cells can both stimulate vasculogenesis and promote stabilization and maturation of the microvascular networks. *In vivo*, capillaries are enveloped by pericytes that stabilize the vessel and

regulate endothelial permeability^{81,82}. To recapitulate these cell-cell interactions, many researchers have included mural cells in their vasculogenesis culture models. A variety of cell types have been used, including pericytes⁸³, fibroblasts⁸⁴, mesenchymal stem cells⁶⁷, and adipose-derived stem cells⁸⁵⁻⁸⁷. Although each of these cell types has been demonstrated to improve vasculogenesis *in vitro*, the specific cell type that is used may influence the quality and maturity of the resulting microvascular network⁸⁸. Grainger et al. found that co-culture of endothelial cells with adipose-derived stem cells or bone marrow-derived mesenchymal stem cells resulted in lower permeability and a more mature microvascular structure compared to co-culture with lung fibroblasts or endothelial cells cultured alone⁸⁶. The authors concluded that the choice of stromal cell influences the quality of engineered microvascular networks.

Mural cells can act at multiple stages of vascular morphogenesis and through multiple mechanisms. Fibroblasts and other mural cells can secrete growth factors such as hepatocyte growth factor⁸⁹ to promote endothelial cell survival and encourage endothelial cells to elongate and migrate towards each other⁶⁸. Fibroblasts also remodel the ECM by secreting pro-vasculogenic matrix proteins such as fibronectin⁹⁰ and collagen⁸⁹. Pericytes promote stabilization and maturation of the microvasculature through both the secretion of paracrine factors and direct cell-cell contact^{81,91,92}. Coculture with mesenchymal stem cells⁹³ or pericytes⁹² has been shown to reduce vascular permeability.

Culture with organ-specific cells can influence the maturation and functionality of engineered microvascular networks. There is substantial heterogeneity across capillary networks in different organs. This heterogeneity arises from both intrinsic genetic programs and the influence of the cells in the microenvironment⁹⁴⁻⁹⁶. By culturing endothelial cells with organ-specific stromal cells or parenchymal cells, researchers can engineer microvascular networks with organ-specific characteristics. For example, Campisi et al. developed a model of the blood-brain barrier (BBB) that included stem cell-derived endothelial cells, brain pericytes, and astrocytes⁹². The inclusion of the pericytes and astrocytes altered the structure of the resulting microvascular networks (smaller diameters, more branching) and prevented vascular regression. The presence of the pericytes and astrocytes also matured the microvascular network towards a BBB phenotype, as evidenced by the upregulation of tight junctions and BBB transporter proteins and the significant decrease in microvascular permeability. By including the other cellular components of the BBB niche, Campisi and co-authors were able to recapitulate aspects of the BBB microenvironment and guide the development of BBB-like microvascular networks.

An open question in the field is the extent to which endothelial cells influence each other during vascular morphogenesis. Multiple labs have reported variations in their vasculogenesis culture models as a function of cell density, with most settling on

an initial cell density of 1-2 million cells/mL ECM as “ideal”^{27,97,98}. Each endothelial cell is acting on its own microenvironment – e.g., by secreting cytokines or by exerting tension on the ECM. This idea is supported by the fact that endothelial cells undergo directed migration towards each other during angiogenesis^{62,99}. This would indicate that endothelial cells are sensing and responding to signals produced by other endothelial cells. Collectively, a population of endothelial cells will alter the microenvironment that they are being cultured in, and that could alter their ability to undergo vasculogenesis. In Chapter 5, I will investigate how endothelial cells collectively alter their own microenvironment and how that may drive certain cell behaviors.

2.5.3 Soluble cues

Soluble factors added to the culture media can also stimulate vasculogenesis^{42,100}. Growth factors added to the media or incorporated into the ECM can promote microvascular network formation *in vitro*. VEGF is the most well-studied endothelial growth factor and has been found to be required for both vasculogenesis and angiogenesis. VEGF promotes endothelial cell differentiation, survival, proliferation, and migration¹⁰¹. FGF regulates vascular development through control of endothelial metabolism¹⁰². The combination of VEGF and FGF-2 can prime endothelial cells to enhance vasculogenesis *in vitro* driven by the addition of SDF-1 α ,

IL-3, and SCF^{103,104}. TGF- β promotes endothelial proliferation and the synthesis of ECM proteins¹⁰⁰. The addition of a phorbol ester (PMA) has been demonstrated to enhance endothelial proliferation and vascular network formation through activation of protein kinase C¹⁰⁵⁻¹⁰⁷.

2.6 Methods for Engineering Microvascular Networks

The quest to engineer blood vessels *in vitro* has been a major focus of the tissue engineering community for over two decades^{8,13,42,43}. The specific goals vary from research group to research group, however. Some researchers want to build vascular networks so that they can create perfused, viable tissues that can be successfully implanted, while others are more interested in building blood vessels so that they can understand more about the biology of blood vessel development, maturation, and maintenance. Another common application of engineered microvasculature is to create more physiologically relevant models of human disease *in vitro*. To meet these varied goals, a variety of techniques have been used to engineer blood vessels, including the use of biofabrication techniques to create the structure of vessel networks, directed self-organization of endothelial and stromal cells into vascular networks, and hybrid approaches that combine both the initial structure of prefabricated vascular networks with the intrinsic self-organization capabilities of endothelial cells.

2.6.1 *Top-down fabrication of vessels*

Vessels can be engineered by using bioprinting or other fabrication technologies to create empty channels within a tissue that can subsequently be lined with endothelial cells. Spreading and proliferation of the endothelial cells results in a complete endothelial monolayer around the channel. A simple method for accomplishing this is to mold collagen hydrogels around a small-diameter needle. After gelation, the needle is removed, leaving behind a cylindrical void that can be used for seeding cells^{108–111}. A drawback to this approach is that the resulting vessel structure is typically a straight channel without branching. Zheng et al. expanded on this concept by micromolding collagen around PDMS stamps, resulting in more complex microvessel networks¹¹². Although these models are simple, they can be effective for studying vascular inflammation¹⁰⁸, thrombosis¹¹², and permeability¹¹³.

Another strategy involves 3D-printing sacrificial channels within cell-laden hydrogels^{114–116}. After gelation of the hydrogel, the fugitive ink can be washed away, leaving behind an empty channel that can optionally be lined with endothelial cells. Recently, Jennifer Lewis' group printed a sacrificial gelatin network into a shear-thinning bath composed primarily of organoids, resulting in a large (2.5 mL) vascularized tissue with physiologically high cell density¹¹⁷. In a creative application of the fugitive ink strategy, Maharjan et al. bioprinted photosynthetic algae within a cellulose bioink¹¹⁸. This provided oxygen to support the initial survival of the

surrounding hepatic tissue. After the initial oxygenation period, the algae and cellulose were enzymatically removed, leaving behind microchannels that were then seeded with endothelial cells.

To fully recapitulate the structure of native vasculature *in vitro*, researchers have developed methods that can create vascular networks that mimic the complex and intertwining structures found *in vivo*. Kinstlinger et al. used selective laser sintering of isomalt to create complex, interpenetrating vessel networks within a wide array of hydrogels and other materials¹¹⁹. These vessel networks exhibited biologically realistic branching characteristics and could be procedurally generated to fill a given hydrogel volume. Grigoryan et al. developed a technique to improve the resolution of stereolithography within hydrogels by using food dyes to block excess light¹²⁰. Using this method, the authors were able to generate entangled vascular networks within PEGDA hydrogels. They applied this technique to the development of a sophisticated alveolar model of blood oxygenation and a multi-material engineered liver tissue. Laser-based degradation of hydrogels to create voids has also been used effectively to engineer intertwining microvascular networks within hydrogels^{121–124}. A major challenge in the field of vascularized tissue engineering is scalability – creating an organ-scale multiscale vascular network. Lee, Hudson, and colleagues applied freeform reversible embedding of suspended hydrogels (FRESH) to bioprint a model of a large section of a human heart, including the vasculature down to 100 μm -

diameter microvessels¹²⁵. Technological progress is advancing rapidly in this field towards the goal of creating hierarchical, multiscale architecture that recapitulates structures found *in vivo*.

The last few years have brought about significant advances in the top-down creation of vascular networks *in vitro*. Though initial biofabrication techniques such as collagen micromolding around needles were limited in terms of vessel geometry, advancements in several different types of bioprinting have allowed for the creation of sophisticated vascular networks that recapitulate the complex structures of native vasculature^{117-121,125}. One limitation, however, is that these vascular networks are typically limited to vessels around 100 μm in diameter or larger, in contrast to capillaries, which range about 5-15 μm in diameter. This is due to both the limited resolution of bioprinting techniques¹²⁶ as well as the inability to line very small channels with endothelial cells without clogging¹²⁷. Rayner et al. recently found a solution to this problem by seeding larger, adjacent channels with endothelial cells and allowing the cells to migrate into the narrow channels over several days¹²⁴. Using this approach, the authors were able to create an endothelialized glomerulus model with organ-specific microvascular architecture.

2.6.2 *Self-organization of endothelial cells seeded within hydrogels into microvascular networks*

Capillary-sized microvessels can be engineered “from the bottom-up” by seeding a monodispersion of endothelial cells within a hydrogel and allowing the cells to self-organize into networks over the course of 3-14 days⁵⁴. Within this approach, there is substantial variance in the methodologies used between different research groups^{43,55,128,129}. Although the most widely used endothelial cell type are human umbilical vein endothelial cells (HUVECs), primary human adult endothelial cells¹³⁰, endothelial colony forming cells¹³¹, or induced pluripotent stem cell-derived endothelial cells^{29,132} can also be used. These endothelial cells may be cultured alone or with one of several types of supportive mural cells (pericytes⁸³, fibroblasts⁸⁴, mesenchymal stem cells⁶⁷, adipose-derived stem cells⁸⁵⁻⁸⁷, etc.) Biomaterials used for culturing the endothelial networks include fibrin¹³³, collagen I^{27,134}, synthetic hydrogels made of poly(ethylene glycol)⁴², and combinations of these materials^{67,83,136}. Slight variations in culture conditions, such as starting cell density and the mechanical properties of the hydrogel, can influence both whether the endothelial cells will self-organize into networks and the properties of those resulting networks^{27,133,137}.

In the last decade, vasculogenesis models have been successfully integrated with microfluidic chips, resulting in perfusion of the microvascular networks. In these microfluidic models, a central tissue chamber containing endothelial cells and stromal cells is flanked by media channels on either side^{84,131,138}. The application of interstitial

fluid flow across the tissue chamber enhances vasculogenesis and promotes the lumenization of the developing microvascular networks^{30,73,139}. The microvascular network may eventually anastomose with the media channels, resulting in full perfusion of the microvascular network and permitting the influx of molecules, tracer beads, and other cells^{140,141}. This approach has led to the creation of more complex organ-on-a-chips to model normal physiology and disease^{40,142,143}.

There are several advantages to engineering microvascular networks by promoting the self-organization of endothelial cells within a hydrogel. First, it allows researchers to study the individual cell behaviors underlying vasculogenesis and how these behaviors are impacted by both intrinsic and extrinsic factors. This may improve our understanding of how vasculogenesis happens in the early embryo, which is difficult to observe in many organisms, especially humans. The microvascular networks created using this process are generally on the order of capillaries, with a width of 1-2 cells wide, and are therefore useful for modeling capillary-specific biological processes such as tumor cell extravasation¹⁴³.

The main drawback to this “bottom-up” approach is that it takes several days to a few weeks for the cells to self-organize and mature into functional vessels⁴³, during which time the cells in the center of an engineered tissue may have become hypoxic and died. Another disadvantage to building vessels through self-organization

of randomly seeded cells is that the resulting network structure may not match the hierarchical structure found *in vivo*, leading to poor blood flow. White et al. found that pre-vascularized tissues made using self-organization of endothelial cells and fibroblasts had a tendency to clot upon implantation into the host¹⁴⁴. Upon further investigation, they found that the microvascular network did not follow physiological vessel branching rules. Murray's law states that when a vessel branches, the sums of the cubed radii of the daughter vessels should equal the cubed radius of the parent vessel¹⁴⁵. If vessels split but remain the same diameter after splitting, the shear rate drops, which can result in thrombus formation.

2.6.3 Hybrid approaches to creating vascularized tissues

An alternate strategy is to impose some initial tissue geometry or other physical boundary conditions to establish the general structure of the tissue, and then allow the cells to finish the morphogenesis process through their inherent self-organization capabilities^{146–149}. Bioprinting or other biofabrication techniques can be used to seed endothelial cells in defined network structures. Tissue engineers can then further guide the pre-patterned endothelial cells to connect with each other and form a perfusable network through manipulation of the microenvironment to drive specific cell behaviors. By placing the cells next to each other in a rough network shape, one could limit the distance that the cells need to move and thus reduce the time required

to form complex microvascular networks. Additionally, this could allow for the creation of physiologically relevant hierarchical structures.

Recent advancements in bioprinting have demonstrated the feasibility of this approach. Brassard and colleagues applied their bioprinting-assisted tissue emergence (BATE) technology to place high-density (up to 100 million cells/mL) solutions of endothelial cells within an ECM with tightly controlled tissue geometry¹⁴. Over time, the endothelial cells self-organized into a tube with a perfused lumen. Angiogenesis could be triggered by stimulation with VEGF. Yang et al. extruded an iPSC-EC-containing hydrogel into a bath of cell-dense collagen microbeads¹⁵⁰. Over 72 hours, the endothelial cells sprouted from the initial cord into the surrounding construct. Microvessels with controlled geometry can also be created by using DNA-mediated adhesion to pattern endothelial and stromal cells within a single plane and then embedding the patterned cells within an ECM¹⁶. This approach was used to measure the impact of stromal cells such as fibroblasts, mesenchymal stem cells, and pericytes on the branching of HUVEC microvessels.

An alternate approach for pre-vascularizing tissues is to pre-form endothelial cells into cords by allowing them to condense around collagen I within PDMS micromolds¹⁵¹. By combining these endothelial cords with cell aggregates made of hepatocytes and fibroblasts, Stevens et al. were able to create liver microtissues that

could then be transplanted into a host and expanded *in situ*¹⁵². Imposing this initial structure on the tissue was found to improve the function of the liver microtissue. Compared to uniformly seeded endothelial cells, the pre-patterned endothelial cords also had higher expression of genes known to be expressed by endothelial cells during liver regeneration. This suggests that imposing some structure on the endothelial cells within engineered tissues may influence their functionality.

2.6.4 Outlook on engineered microvasculature

The best method for engineering microvascular networks is dependent on the intended application. Studies that aim to better understand the cellular dynamics during vasculogenesis should use systems where the endothelial cells are initially uniformly dispersed within a hydrogel and must progress through each step of vascular morphogenesis. These studies can shed light on the “rules” that govern vasculogenesis and endothelial cell behavior. If the aim is to instead engineer large, complex tissues that can ultimately be used for transplantation, one should use scalable biofabrication methods such as the bioprinting of sacrificial materials to create microvessel networks. Although the bioprinted vessels are not quite capillary-sized, they are capable of efficiently perfusing the tissue, which is the most important function for that application. Hybrid techniques, in which the cells are initially placed into vascular network structures but allowed to undergo morphogenesis into microvessels *in vitro*, are a relatively new but versatile method of engineering blood

vessels. I foresee two potential applications for which hybrid techniques are best suited. The first application is to be used in conjunction with larger, bioprinted vessels as part of a multi-material printing strategy for large, implantable tissues. By printing large (millimeters to hundreds of microns) networks of sacrificial inks with smaller branches of endothelial cell-laden bioinks (10-100 μm), one could create complex multiscale vasculature that mimics physiological structures, is efficient for fluid flow and nutrient diffusion, and can be easily anastomosed with host vasculature. Another application for hybrid microvessel formation is the perfusion of organoids and other 3D cell culture models of physiology and disease.

2.7 Summary

Endothelial cells must perform a series of cell behaviors as they go through the different stages of vasculogenesis and self-organize into microvascular networks. Bioengineers can direct these behaviors and encourage vascular morphogenesis by imposing initial boundary conditions and providing the endothelial cells with a supportive microenvironment. Understanding how endothelial cells integrate various mechanical, cellular, and soluble cues during vasculogenesis will shed light on how blood vessels form *in vivo* and help bioengineers to engineer complex microvascular networks for *in vitro* studies.

3 Simple, affordable, and modular patterning of cells using DNA

This work was published in The Journal of Visualized Experiments in 2021. It has been adapted for inclusion in this dissertation.

Katelyn A. Cabral, David M. Patterson, Olivia J. Scheideler, Russell Cole, Adam R. Abate, David V. Schaffer, Lydia L. Sohn, Zev J. Gartner

Author Contributions: K.A.C, D.M.P., and Z.J.G conceived the project. K.A.C, D.M.P., and O.J.S. developed the protocol and performed experiments. K.A.C. and D.M.P. analyzed data. R.C. and A.R.A. provided technical advice. D.V.S., L.L.S., and Z.J.G. supervised the experiments. K.A.C. wrote the manuscript with feedback provided by all authors.

3.1 Abstract

The relative positioning of cells is a key feature of the microenvironment that organizes cell-cell interactions. To study the interactions between cells of the same or different type, micropatterning techniques have proved useful. DNA Programmed Assembly of Cells (DPAC) is a micropatterning technique that targets the adhesion of cells to a substrate or other cells using DNA hybridization. The most basic operations in DPAC begin with decorating cell membranes with lipid-modified oligonucleotides,

then flowing them over a substrate that has been patterned with complementary DNA sequences. Cells adhere selectively to the substrate only where they find a complementary DNA sequence. Non-adherent cells are washed away, revealing a pattern of adherent cells. Additional operations include further rounds of cell-substrate or cell-cell adhesion, as well as transferring the patterns formed by DPAC to an embedding hydrogel for long-term culture. Previously, methods for patterning oligonucleotides on surfaces and decorating cells with DNA sequences required specialized equipment and custom DNA synthesis, respectively. We report an updated version of the protocol, utilizing an inexpensive benchtop photolithography setup and commercially available cholesterol modified oligonucleotides (CMOs) deployed using a modular format. CMO-labeled cells adhere with high efficiency to DNA-patterned substrates. This approach can be used to pattern multiple cell types at once with high precision and to create arrays of microtissues embedded within an extracellular matrix. Advantages of this method include its high resolution, ability to embed cells into a three-dimensional microenvironment without disrupting the micropattern, and flexibility in patterning any cell type.

3.2 Introduction

The positioning of cells with respect to one another in a tissue is an important feature of the microenvironment^{153–156}. Techniques used to pattern live cells into

spatially controlled arrangements are valuable experimental tools for studying differentiation^{4,5,159,160}, cell motility¹⁶¹, morphogenesis^{162,163,146}, metabolism¹⁶⁴, and cell-cell interactions^{159,165}. A variety of methods exist for patterning cells, each with their own advantages and drawbacks^{3,4}. Methods that create adhesive islands of extracellular matrix (ECM) proteins, such as microcontact printing and laser-cut stencils, are simple and scalable. However, it is difficult to pattern more than one or two cell types at a time because the adhesive properties of different cell types to different ECM molecules are often similar^{166–168}. More complex micropatterns can be created with light-induced molecular adsorption (LIMAP), a technique that uses UV light to ablate PEG-coated regions and allow for subsequent protein adsorption^{169,170}. This process can be repeated to create high-resolution micropatterns with multiple cell types. However, cross-binding of cells to the different protein patches can occur, resulting in poor pattern specificity¹⁷⁰. Physical methods such as seeding cells onto micromechanical reconfigurable culture devices can create structured co-cultures with dynamic control, but without the flexibility in pattern design of microcontact printing or LIMAP^{165,160}. Unlike the other techniques, bioprinting can create three-dimensional arrangements of cells within hydrogels^{171,172}. However, bioprinted constructs have much lower resolution than other micropatterning techniques, with an average feature size on the order of hundreds of microns¹²⁶. An ideal cell patterning method would have high resolution, pattern multiple cell types, use equipment and reagents that are easily accessible, and have the ability to embed successful patterns into a hydrogel for

three-dimensional (3D) cell culture. In this article, we present CMO-DPAC, a cell micropatterning technique that uses the flexibility and speed of DNA hybridization to target cell adhesion to a substrate. This method has been adapted from our previous protocols^{16,173} to make it more affordable, modular, and accessible. Using the current protocol, any lab should be able to set up a fully functional system without any specialized equipment or expertise.

DNA Programmed Assembly of Cells (DPAC) is a powerful tissue engineering technique that patterns cells at single-cell resolution with precise control over cell-cell spacing and tissue geometry. In DPAC, cell membranes are decorated with DNA oligonucleotides (oligos) using two lipid-modified oligos designed to hybridize on the cell membrane. Because the oligos are conjugated to hydrophobic lipids, they rapidly partition to the cell membrane¹⁷⁴ where they hybridize, increasing the net hydrophobicity of the non-covalently bound molecules, and thereby enhancing their lifetime at the cell surface¹⁷⁵. The oligos are presented on the cell surface in a manner where they can hybridize with complementary oligos on other cells or DNA-functionalized glass slides to create defined 2D or 3D cell patterns with prescribed composition, cell-cell spacing, and geometry^{16,173}. The patterned microtissues can be cleaved off the surface enzymatically and embedded into a hydrogel for prolonged 3D culture. When used in combination with primary cells or stem cells, the resulting collections of cells can undergo morphogenesis and form into organoids^{16,176,177}.

DPAC has been applied to investigate the dynamics of adult neural stem cell fate in response to competing signals^{158,178}, to study self-organization of mammary epithelial cells^{16,177}, and to generate “tissue origami” through mesenchymal condensation¹⁷⁶.

DPAC allows for the precise placement of multiple cell populations and has substantially better resolution than extrusion-based bioprinters (on the order of microns)^{16,126}. In addition, unlike ECM-based patterning methods such as microcontact printing, DPAC does not require differential adhesion of the different cell types to an ECM-coated surface^{16,166}. It is ideal for answering questions about how the composition of a tissue affects its behavior, how cells integrate multiple cellular and microenvironmental cues when making decisions^{158,178}, and how pairs of cells interact with each other. An advantage of this method over other micropatterning methods is that it can be used for 3D cell culture in a single imaging plane, facilitating time-lapse studies of tissue self-organization and organoid morphogenesis^{16,176,179}.

Despite these advantages, successful implementation of DPAC has required the synthesis of custom oligonucleotide reagents and access to specialized equipment for DNA patterning^{16,173}, limiting widespread adoption. For example, the optimal lipid-modified oligos (LMOs) used in the original protocol must be custom synthesized, modified to have a lignoceric acid or palmitic acid, and purified¹⁷⁵. This process requires the use of a DNA synthesizer and a high-performance liquid chromatography

instrument, as well as the purchasing of the associated reagents such as methylamine, a controlled substance that is subject to both institutional and federal regulations. As an alternative, LMOs can be custom purchased in bulk, but this requires a significant up-front investment in the technology.

To overcome these limitations, we have developed a revised version of DPAC that uses commercially available cholesterol-modified oligos (CMOs) in place of the custom-synthesized LMOs. To further reduce costs and to increase the flexibility of the platform, we have changed to a modular, three-oligo system. Instead of ordering a new cholesterol-modified oligo for each unique cell population, a user of this protocol can instead use the same cholesterol-modified oligos (“Universal Anchor” and “Universal Co-Anchor”) for every cell population and then employ an inexpensive, unmodified oligo (“Adapter Strand”) that hybridizes with both the Universal Anchor and either the amine-functionalized DNA on the surface or the Adapter Strand of another cell type.

Another limitation of the original DPAC protocol was that it created the DNA-patterned slides by using a high-resolution liquid printer (Nano eNabler, BioForce Nanosciences)^{16,173}. While this instrument boasts extraordinary resolution and low reagent requirements, it is not available to most institutions and has a relatively low printing rate (approximately 1 feature patterned per second). Recently, two

photolithographic methods have been developed to pattern DNA features onto surfaces. Viola and colleagues used a polyacrylamide and benzophenone coating that covalently bound single-stranded DNA oligos upon exposure to UV light¹⁷⁹. Using this method, they were able to create tissue scaffolds that underwent large-scale, programmed shape changes as a result of cell contractility and self-organization. Scheideler et al. developed a method that uses UV exposure of a positive photoresist to selectively expose amine-modified DNA oligos to an aldehyde-functionalized slide¹⁷⁸. After baking and reductive amination, the amine-modified DNA is covalently bound to the surface. This method was used to investigate the response of adult neural stem cells to spatially presented self-renewal and differentiation cues. This article adapts Scheideler et al.'s protocol to create the DNA patterns that will capture CMO-labeled cells. This photopatterning protocol can be performed without using a clean room. It uses inexpensive and commercially available equipment that is easily deployed on a benchtop or fume hood. The use of inexpensive or DIY (do-it-yourself) photolithography equipment increases accessibility to researchers without access to clean room facilities and allows researchers to try the technique without a large investment of time or resources^{180,181}. However, better resolution and the alignment of multiple DNA features can be achieved by using the commercial spin coater and mask aligner commonly found in cleanroom facilities.

Here, we describe a method to pattern cells at single-cell resolution using

DNA-based adhesion. First, photopatterning with a positive photoresist is used to create high-resolution patterns of amine-modified DNA onto an aldehyde-modified glass substrate. Next, the slide is treated to reduce non-specific cell attachment and PDMS flow cells are created to confine cells over patterned regions. Cells are then labeled with short DNA oligonucleotides that are functionalized with cholesterol and as a result insert into the cell membrane. The cells are then flowed over the DNA micropatterns. Hybridization between the cell-surface DNA and the DNA on the glass surface results in specific adhesion of the cells to the DNA pattern. Non-adherent cells are washed away, revealing the adherent cell pattern. This process can be repeated to pattern multiple cell types or to create multi-layered structures. If desired, the cells can be fully embedded into an ECM for 3D cell culture.

3.3 Methods

Experimental design:

CMO-DPAC is a versatile technique that can be applied to a wide variety of experimental schemes. Experimental considerations should include the feature size, feature spacing, number of unique cell populations involved, and the arrangement of cells with respect to one another.

Photomasks for photopatterning the DNA were created using AutoCAD (Autodesk). These photomasks were used to delineate four to five separate regions within the dimensions of a microscope slide. Within each region, enclosed features were drawn in the desired size, shape, and spacing. These features would be used to pattern the DNA, which would then form a template for the cell adhesion. Aligned photomasks were created by creating a master drawing with all sets of features and then saving versions that correspond to each cell type. From the AutoCAD drawings, high-resolution (at least 20,000 dots per inch) photomasks were ordered from CAD/Art Services with the features transparent and the larger regions black.

Photopatterning DNA onto aldehyde-functionalized slides (adapted from Scheideler et al.¹⁷⁸):

For experiments requiring the patterning of multiple cell types, fiducial markers were fabricated on the aldehyde-functionalized slide (Nexterion AL, Schott) before any DNA patterning to facilitate alignment of features. Metal fiducial markers were created on the slide by first applying positive photoresist and photopatterning as described below. Thin films of titanium were then deposited onto the slide using electron-gun evaporation¹⁷⁸. Excess metal and photoresist were removed using acetone before proceeding to the DNA photopatterning.

Photolithography was used to pattern the DNA onto the aldehyde-

functionalized slide. Slides were first labeled by using a diamond scribe to write on the surface. Double-sided tape or a vacuum was used to attach an aldehyde-functionalized slide to the rotor of a spin coater (SCK-100, Instras Scientific). Drops of positive photoresist (Shipley 1813, Kayaku Advanced Materials) were added on top of the slide by disposable pipette (Figure 3.1). The slide was then spun at 3000 rpm for 30 seconds, followed by a soft-bake on a 100 °C hotplate for 1.5 minutes to crosslink the photoresist. The slide was then covered with the photomask and exposed to UV light 365 nm wavelength, 360 mW, 5 inches from slide, total radiant energy density 100 mJ/cm²) for 2 minutes (Figure 3.1). UV light breaks the polymer bonds in the photoresist underneath transparent regions of the photomask, creating regions where DNA will later be able to adhere. The slide was developed by immersion in MF-321 developer solution (Kayaku Advanced Materials) for 3-5 minutes (Figure 3.1) before being rinsed with water and dried under an air stream. After drying, the slide was inspected for quality under a microscope. A successfully patterned slide should have sharply defined edges for each feature, no cracking, and no feature distortion at the edges. Examples of correct and incorrect photolithography are provided in Figure 3.2. See Table 3.1 for troubleshooting suggestions if photolithography does not provide the desired feature quality.

Droplets of a 20 μM solution of 5' amine-modified oligo in DNA patterning buffer (50 mM of sodium phosphate in water, pH = 8.5) were added onto each

photopatterned region of the slide. A pipette tip was used to gently spread the droplet across the entire region, being careful not to scratch the slide (Figure 3.1). Baking the slide in a 65°C oven until the DNA solution was fully dried onto the slide surface (about 1 hour) resulted in a reversible covalent bond between the DNA and the surface, as the amine on the oligo formed a Schiff base with the aldehydes on the slide surface. Reductive amination of the baked slide with 0.25% sodium borohydride (Sigma-Aldrich) in PBS for 15 minutes converted the Schiff base to a secondary amine, resulting in an irreversible bond. At this point, the DNA was irreversibly and covalently attached to the slide and all unreacted aldehyde functional groups were converted to alcohols. The photoresist was no longer needed and was removed by rinsing with acetone. Photopatterned slides were stored in a vacuum desiccator under dry conditions for up to 3 months before use.

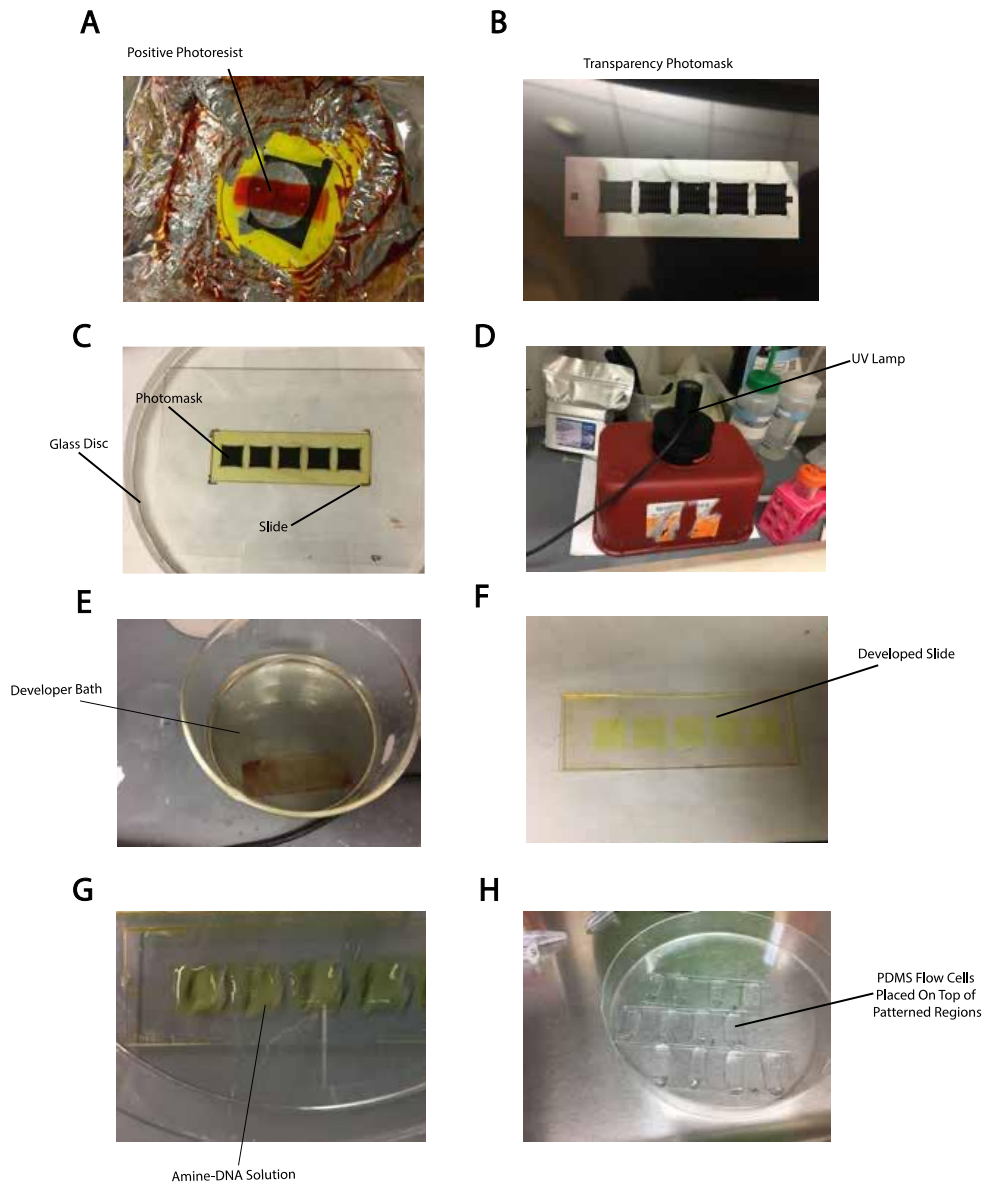


Figure 3.1 Example images of the benchtop photolithography setup.

A) Slide on spin coater, covered with positive photoresist, before spin coating. B) Picture of transparency photomask. C) During exposure, the photomask is sandwiched between the photoresist-coated slide and a glass disc. D) Housing for UV lamp was made from a re-purposed sharps container. E) Slide immersed in developer solution. F) Developed slide. G) Amine-modified DNA solution spread on patterned regions of the slide. H) PDMS flow cells placed on top of patterned regions of the slide.

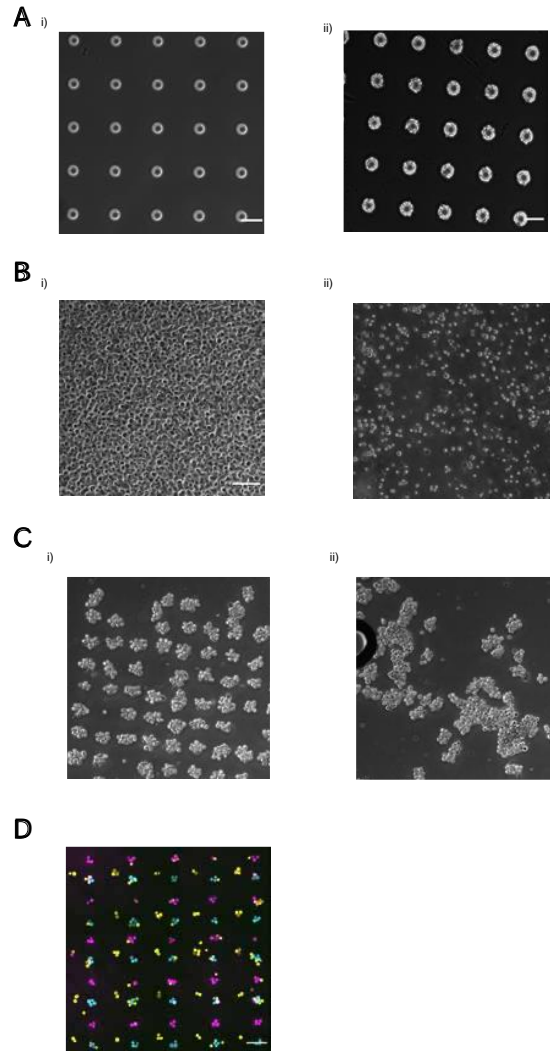


Figure 3.2 Some examples of common failures of this protocol.

A) i) Under-baking before UV exposure or over-developing features post-exposure can result in features that have jagged edges and may be irregular in size. ii) An example of a correctly photopatterned slide that has clean edges around features, uniform feature size, and no obvious cracks in the pattern. Scale bar = 50 μm . B) Cell density is critical to patterning efficiency. When observing the cells on top of the pattern under a microscope, few gaps should exist between cells, as evidenced by the example image on the left. Scale bar = 50 μm . C) Patterned cells can be sensitive to fluid forces arising from overly vigorous pipetting, which can damage and dislodge the patterned cells. Multilayered cell aggregates are particularly vulnerable, as one cell at the bottom is supporting a structure of multiple cells. i) An array of cell aggregates successfully embedded into Matrigel. ii) A grid of cell aggregates that dislodged because of pipetting viscous Matrigel too vigorously. D) Clumping of cells can occur, particularly with epithelial cells. These clumps are usually homotypic but can be heterotypic (cells adhering to already patterned cells of a different type) if the cells are particularly sticky. Image shows three different populations of MCF10As were patterned onto an array composed of three different single-cell sized DNA spots (15 μm). Most DNA spots have 2-4 cells attached. Clumping can be resolved by EDTA treatment or by filtering out the clumps before patterning. Scale bar = 100 μm .

Surface treatment of slide (adapted from Todhunter et al.¹⁷³):

It is advantageous, though not required, to modify the slide's surface chemistry to render it more inert and hydrophobic. Non-specific cell attachment is reduced on these surfaces¹⁸², thereby alleviating non-specific binding of cells to un-patterned areas of the slide. Additionally, if the patterned cells will ultimately be embedded within a hydrogel and transferred off the slide, the surface treatment is essential for reliable movement of the cell-laden hydrogel across the slide without distortion or tearing. Silanizing with (tridecafluoro-1,1,2,2-tetrahydrooctyl) dimethylchlorosilane (Gelest) results in the presence of hydrophobic fluoroalkyl groups on the slide surface. Slides were first rinsed with 10% acetic acid and then dried under an air stream. In a glass Coplin jar, the silanization solution was prepared by mixing 60 mL methylene chloride (dichloromethane), 0.6 mL of triethylamine (Sigma-Aldrich), and 0.6 mL of (tridecafluoro-1,1,2,2-tetrahydrooctyl) dimethylchlorosilane. The slide was added to the Coplin jar containing the silane solution and the reaction progressed for 15 minutes under gentle shaking. The slide was then rinsed sequentially with methylene chloride, ethanol, and water, before being dried under an air stream.

Preparation of PDMS flow cells:

Rectangular PDMS flow cells (dimensions 10 mm x 15 mm x 200 microns) are used to concentrate the cells over the patterned regions of the slide. For experiments

cultured in 3D, the flow cells form a mold for the hydrogel. An SU-8 master wafer for the flow cells was created by spin coating SU-8 2075 (Microchem) onto a silicon wafer (500 rpms for 10s, followed by 1000 rpm for 30s) to create features approximately 200 μm in height¹⁸³. The wafer was baked at 95°C for 45 minutes to remove excess solvent. The wafer was then exposed to UV light (365nm) traveling through a photomask for a radiant energy density of 350 mJ/cm². The wafer was then baked at 95°C for 12-15 minutes. The wafer was developed by immersion in SU-8 Developer Solution (PGMEA) for 15 minutes. After development was complete, the wafer was dried and baked for 5 additional minutes.

Polydimethylsiloxane (PDMS) was prepared by mixing polydimethylsiloxane elastomer and crosslinker in a 10:1 ratio (by mass). The PDMS solution was de-gassed in a vacuum desiccator for 15-30 minutes to remove bubbles before it was poured onto the SU-8 master wafer. The PDMS was cured by baking in a 60°C oven for 3 hours.

Shortly before starting a CMO-DPAC experiment, the required number of PDMS flow cells were cut out from the master wafer. Plasma oxidization with 10 cc/min room air for 90 seconds rendered the surfaces of the flow cells hydrophilic. The flow cells were then cut to have 1-2 mm of PDMS remaining on each side and then the top and bottom of the flow cell were cut open to create an inlet and outlet.

Using the photomask as a reference, PDMS flow cells were placed on top of the slide in the location of each patterned region. 50 μL of phosphate buffered saline (PBS) + 1% bovine serum albumin (BSA) was added to the inlet of each flow cell, as shown in Figure 4.1. Blocking with BSA minimizes non-specific cell adhesion to the slide surface.

Labeling cells with cholesterol-modified DNA oligos (CMOs):

For each set of cells in the experiment, we mixed 3 μL of a 100 μM stock solution of the cholesterol-modified Universal Anchor Strand with 3 μL of a 100 μM stock solution of an Adapter Strand. Incubation for 1 minute pre-hybridized the oligos. 69 μL of PBS was then added to create a 4 μM Universal Anchor + Adapter solution. For each set of cells in the experiment, we added 3 μL of a 100 μM Universal cholesterol-modified Co-Anchor Strand stock solution to 12 μL of PBS, creating a 20 μM solution.

Adherent cells were treated with trypsin to remove the cells from the culture flask. After neutralization with media, the cell suspension was centrifuged to pellet the cells. The cell pellet was resuspended in 1 mL of ice-cold PBS or serum-free media. 1-3 million cells were transferred to a 1.5 mL microcentrifuge tube and centrifuged at 160 x g for 4 minutes.

To label the cells with CMOs, the cell pellet was resuspended in 75 μ L of ice-cold PBS or serum-free media. We made sure to keep the cells in an ice bucket throughout the labeling and washing process to maximize cell viability and minimize loss of the cholesterol-modified oligos from the cell surface. 75 μ L of the 4 μ M Universal Anchor + Adapter solution was added to the microcentrifuge tube containing the cell suspension. After being mixed thoroughly by pipetting, the microcentrifuge tube was incubated for 5 minutes on ice. 15 μ L of the Universal Co-Anchor Solution was then added to the microcentrifuge tube. The microcentrifuge tube was again mixed by pipetting and incubated for 5 minutes on ice.

Excess oligos were removed from the cell suspension by adding 1 mL of ice-cold PBS or serum-free media to the microcentrifuge tube, mixing, and centrifuging at 160 x g for 4 minutes at 4°C. Discard the supernatant. This was repeated for a total of three times. Cells that were particularly prone to clumping (e.g., MDCKs) were passed through a 40 μ m filter before the final wash.

Cell patterning:

The cells were resuspended in ice-cold PBS or serum-free media to create a cell-dense solution of at least 25 million cells/mL. For one slide using four of the 10 x 15 mm x 200 μ m PDMS flow cells described in Step 4, about 100 μ L of this dense cell suspension is required. Although most of these cells will not adhere to the

pattern and will ultimately be discarded, having an extremely concentrated solution of cells over the pattern dramatically improves the efficiency of cell patterning. 25 μ L of cell suspension was added to the inlet of each flow cell on the patterned slide. By removing the PBS + 1% BSA solution from the outlet, the cell suspension could fill the PDMS flow cell. The slide was incubated on ice for 30 seconds. At this point, looking at the flow cell under a microscope showed densely packed cells with little to no gaps visible between cells (Figure 3.2). Cells were cycled through the flow cell by repeatedly removing 5 μ L of cell suspension from the outlet of the slide and adding it back into the inlet. Flowing the cells over the pattern multiple times increased the probability that a cell will flow over a given DNA spot and be captured. Excess cells were washed out by gently adding ice-cold PBS or serum-free media until a visual inspection of the slide under the microscope confirmed that there were no excess cells remaining. This process was repeated for each set of cells in the pattern. For patterns in which multiple cell types are directly patterned by the surface template, we started with the least abundant cell type of the pattern and finished with the most abundant cell type. We note that it is advisable to do each round of cellular assembly sequentially instead of pooling the cells, even in conditions where the cells are all labeled with orthogonal DNA sequences. Pooling the cells effectively dilutes each cell population and reduces patterning efficiency. After the final round of cell assembly was complete, the next steps varied on the specific experiment. If the cells were

intended to remain on the glass, media was added to a Petri dish containing the slide and forceps were used to nudge the PDMS flow cells off the slide.

Transfer of patterned cells into hydrogel for 3D culture:

For experiments where the cells were embedded in an ECM and cultured in 3D, 50 μL of a hydrogel solution (e.g., Matrigel, collagen I) containing 2% DNase was added to the inlet of each flow cell. Aspiration of excess fluid from the outlet drove the hydrogel solution into the flow cell. For viscous hydrogel precursors, tilting the slide slightly was required to help the hydrogel flow into the flow cell. The slide was then incubated at 37°C for 30-45 minutes (depending on hydrogel gelation kinetics) to allow the hydrogel to set and to cleave the DNA-based adhesion between the cells and the surface. To fully embed the patterned cells, the flow cells had to be removed from the slide and placed onto a drop of unpolymerized hydrogel solution. 50 μL of hydrogel precursor was added to a well of a 2-well chamber slide or a 6-well plate. 10 μL of PBS was pipetted on either side of each flow cell and a razor blade was used to distribute the PBS along the full length of the flow cell and gently lift the sides of the flow cell so that the PBS rushes underneath the hydrogel. This allowed for the “floating” of the hydrogel across the slide, allowing for transfer without distortion or tearing. The razor blade was then used to gently move the flow cell to the edge of the glass slide. The slide was then inverted, and the flow cells remained on the slide due to surface tension. The razor blade was used to nudge the flow cell off the slide so that it

landed on top of the razor blade. Curved forceps were used to transfer the flow cell, cell side down, from the razor blade onto the droplet of hydrogel precursor solution. The hydrogels containing the patterned cells were then incubated at 37°C for an additional 30-45 minutes so that the hydrogel containing the patterned cells can bind to the hydrogel underlay, resulting in the full embedding of the patterned cells. The PDMS flow cells were removed by immersing them in media, loosening the adhesion between the hydrogel and the flow cell. The PDMS flow cells were then gently nudged off the hydrogel using curved forceps.

Confirming labeling efficiency:

To confirm that the cells were being labeled successfully with CMOs, we used a fluorescently modified oligonucleotide that was complementary to the surface adhesion sequence of the Adapter Strand being used in the experiment. CMO labeled cells were mixed with a 2 μ M solution of the fluorescently labeled complementary oligonucleotide and incubated for 5 minutes on ice. After 3 wash steps to remove excess oligos, the cells were analyzed by flow cytometry and compared to an MESF standard. This data allowed us to calculate the number of CMO complexes per cell as a function of CMO labeling concentration.

3.4 Results

This technique makes it possible to pattern cells in 2D and 3D with high precision and without the use of custom reagents or expensive cleanroom equipment. Figure 3.3 shows an overview of the process. First, DNA-functionalized slides are created through photolithography. Next, cells are labeled with CMOs. The cells are then flowed over the slide, where they attach only to the DNA-functionalized regions of the slide. After excess cells are washed away, the desired pattern of cells is revealed. These cells can be cultured on the slide or embedded in a hydrogel containing DNase and transferred off the slide for 3D cell culture.

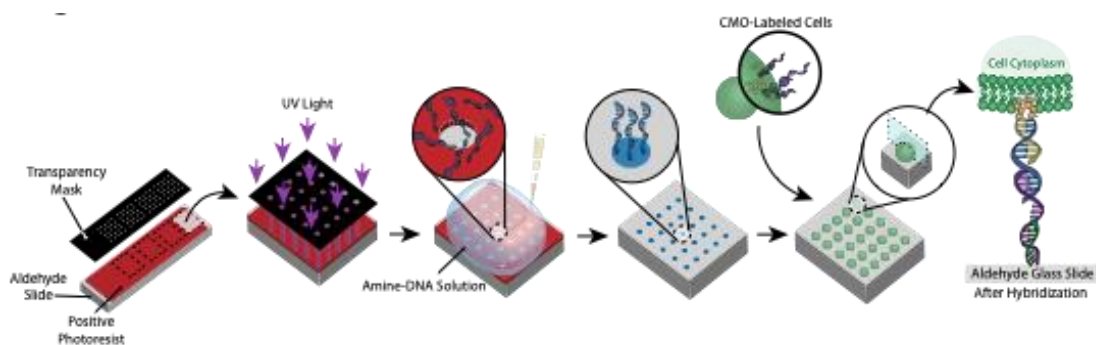


Figure 3.3 Overview of CMO-DPAC technique.

A DNA-patterned slide is created by coating an aldehyde-functionalized glass slide with a positive photoresist, covering it with a transparency mask in the desired pattern, and exposing it to UV light. The UV-exposed photoresist is washed away with developer, leaving exposed regions of the aldehyde slide and allowing the binding of amine-functionalized DNA to the surface. Cells are then labeled with CMOs and flowed over the surface. The DNA on the cell membrane hybridizes to the DNA on the surface, resulting in adhesion.

Labeling of cells with CMOs allows for their attachment to the DNA patterned slide (Figure 3.4). First, the cholesterol-modified Universal Anchor Strand is pre-hybridized with the Adapter Strand. Next, the Universal Anchor + Adapter solution is

mixed 1:1 with the cell suspension. The cholesterol on the Universal Anchor + Adapter complex inserts into the cell membrane. Addition of the cholesterol-modified Universal Co-Anchor Strand, which hybridizes with the Universal Anchor Strand, improves the stability of the CMO complex in the cell membrane by increasing the net hydrophobicity of the duplex¹⁷⁵. After washing out the excess DNA from the cell suspension, the cells are flowed over the slide. Hybridization between the Adapter Strand and the Surface DNA Strand results in attachment of cells to the DNA-patterned regions of the slide.

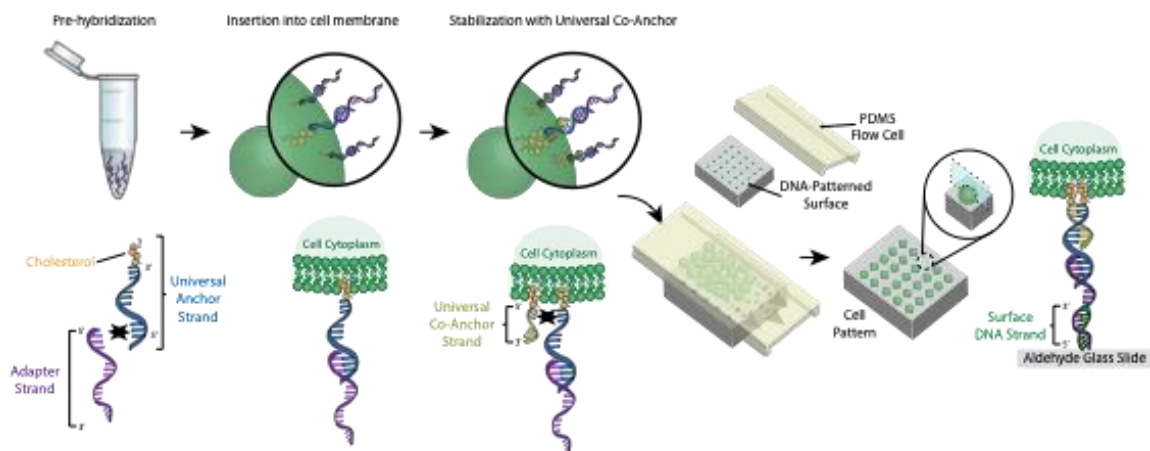


Figure 3.4 Cells are labeled with CMOs in a stepwise process.

First, the cholesterol-modified Universal Anchor Strand is pre-hybridized with the Adapter Strand. Next, the Universal Anchor + Adapter solution is mixed with the cell suspension. The cholesterol on the Universal Anchor + Adapter complex inserts into the cell membrane. After incubation, the cholesterol-modified Universal Co-Anchor Strand is added to the cell suspension, where it hybridizes with the Universal Anchor Strand and inserts into the cell membrane. The addition of the second cholesterol molecule increases the net hydrophobicity of the DNA complex and stabilizes it within the membrane¹⁷⁵. After washing out the excess DNA, the cells are concentrated and added to a PDMS flow cell on top of the patterned surface. The 3' end of the Adapter Strand hybridizes with the Surface DNA Strand on the glass slide, resulting in adhesion to the slide specifically in regions functionalized with complementary DNA.

The pattern of the cells is created by using photolithography to restrict the attachment of amine-modified DNA oligos to specific regions of an aldehyde-modified glass slide¹⁷⁸ (Figure 3.5). Positive photoresist is spin-coated onto an aldehyde-functionalized slide. A transparency photomask is then placed on top of the slide and the slide is exposed to UV light. After developing, the regions of the slide that were exposed to UV light are no longer coated in photoresist and thus have exposed aldehyde groups. A 20 μ M solution of amine-modified DNA oligos is then dropped onto the slide and spread to cover the patterned regions. Baking followed by reductive amination results in a covalent bond between the amine-modified DNA and the slide. Remarkably, this process can be repeated to pattern multiple oligos without any loss of functionality of the previously patterned oligos (Figure 3.5). However, care should be taken to avoid overlapping patterns, which results in the presence of both oligos at a reduced concentration (Figure 3.6). Multiple cell populations can be patterned sequentially by using Adapter Strands that differ in their modular domain (the 20 bases closest to the 3' end).

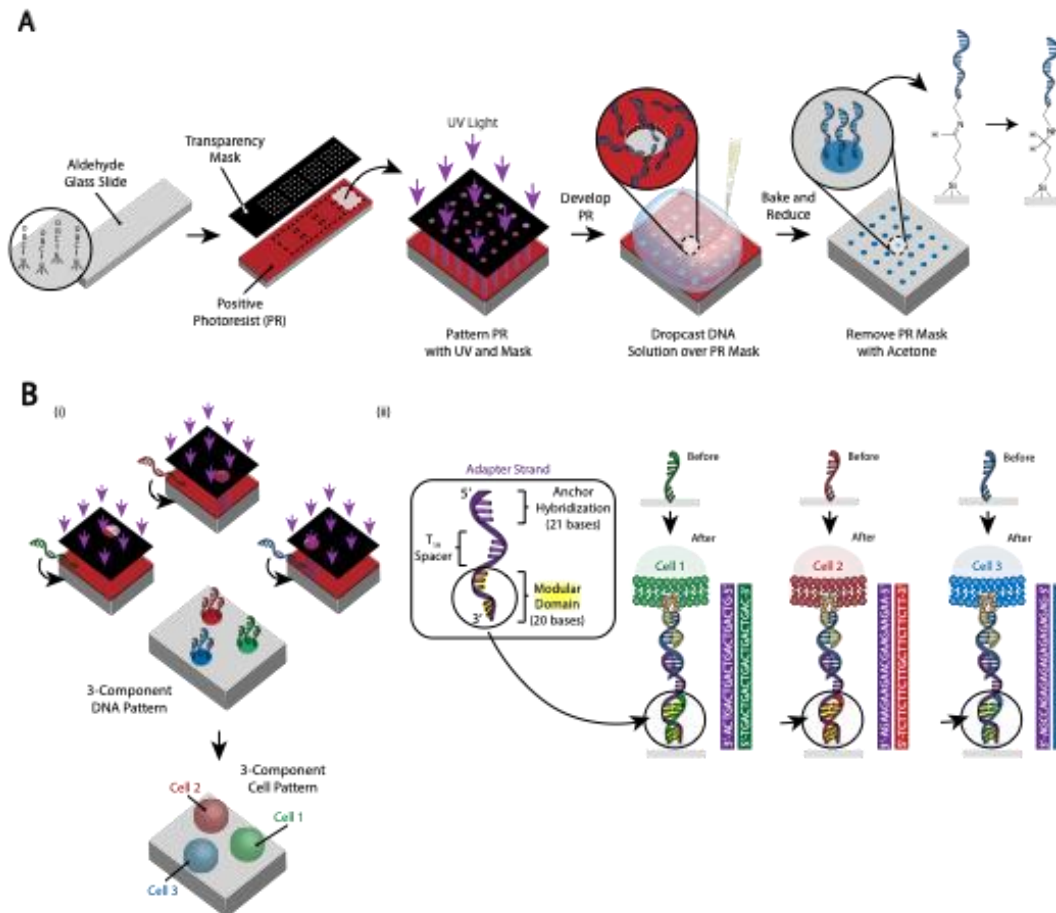


Figure 3.5 Photolithography is used to create the DNA-patterned slides that will ultimately dictate the placement of cells.

A) Overview of photolithography process. An aldehyde-functionalized slide is spin-coated with a positive photoresist. UV light shines onto the slide through a transparency photomask that is transparent where cell adhesion is desired. After the slide is developed, the regions that were previously exposed to UV light now have exposed aldehyde groups. A 20 μM solution of an amine-functionalized DNA oligo is then dropped onto the slide and spread over the patterned regions. The slide is then baked to induce the formation of Schiff bonds (C=N) between the amine and aldehyde groups, a reversible covalent bond¹⁷⁸. Subsequent reductive amination with 0.25% sodium borohydride in PBS converts the Schiff base to a secondary amine by reductive amination, resulting in an irreversible bond between the DNA and the slide. The remaining photoresist can then be removed by rinsing with acetone. B) This process can be repeated to create multi-component DNA patterns and therefore perform experiments with multiple cell populations. i) After the first oligo is patterned, the slide is again coated in photoresist and the protocol proceeds as before. Alignment of the photomasks using fiducial markers is necessary for patterning multiple DNA strands. ii) Each cell type being patterned differs in the 20-base modular domain of the Adapter Strand. By using orthogonal sets of complementary oligos, multiple cell types can be patterned without cross-adhesion.

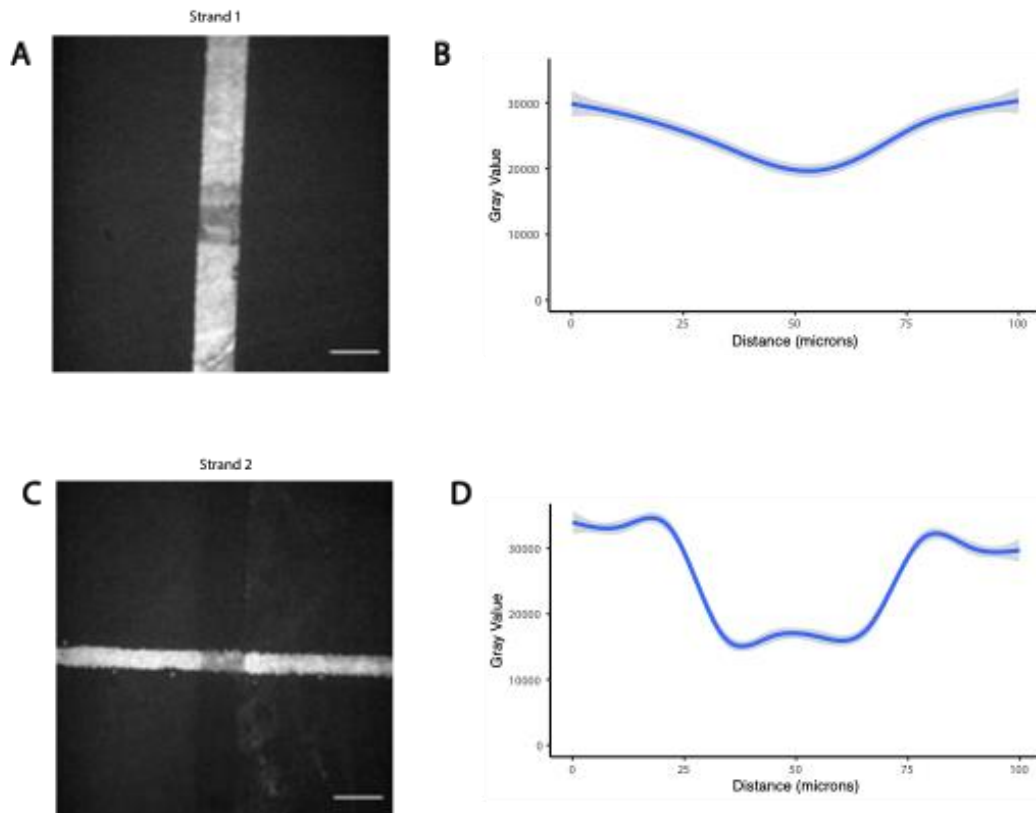


Figure 3.6 Overlapping photopatterns results in presence of both oligos at reduced concentration.

Two orthogonal amine-modified oligos were photopatterned sequentially, first a vertical line (Strand 1), followed by a horizontal line that overlapped it (Strand 2). The oligos were then visualized by hybridization with fluorescent complementary oligos. A) Fluorescence image of Strand 1. B) Quantification of the fluorescence profile of Strand 1 over a 100 μm vertical line spanning the overlap. C) Fluorescence image of Strand 2. D) Quantification of the fluorescence profile of Strand 2 over a 100 μm horizontal line spanning the overlap. Scale bar = 50 μm .

Although this photopatterning protocol was developed by Scheideler et al. in the context of a clean room, we have demonstrated that it is possible to achieve similar results with an inexpensive, “home-brew” photolithography setup that fits easily within a chemical fume hood. The setup includes a \$400 spin coater made of a DC motor, digital controller, and CD cake box, as well as a UV lamp that was assembled from individual components and housed in a repurposed sharps container. The main

advantage of the home-brew photolithography setup is that it is very affordable (<\$1000 for all equipment) while still being able to create single-cell-sized features. However, the use of inexpensive equipment does have its limitations – for example, it is more challenging to precisely align fiducial markers to pattern multiple DNA oligos without use of a mask aligner. We recommend this inexpensive photolithography setup for labs that do not have convenient access to a clean room or that want to try this method without a large investment.

To identify optimal conditions for DNA-programmed cell adhesion, we systematically varied the concentrations of DNA strands on cell surfaces and measured the efficiency of cell adhesion to DNA-modified glass surfaces. The concentration of Universal Anchor + Adapter Strand and Universal Co-Anchor in labeling solutions were varied across several orders of magnitude (Figure 3.7), resulting in 10^4 - 10^6 DNA complexes per cell (Figure 3.8). Cell adhesion was dose-dependent, with minimal cell adhesion to the DNA pattern when cells were labeled with CMOs at a concentration of 0.05 μM or less, and high occupancy at a concentration of 2.5 μM and higher. We therefore used a 2 μM solution of Universal Anchor + Adapter Strand and 2 μM solution of Universal Co-Anchor in most experiments. Cell adhesion would also be expected to decrease if the amount of DNA used on the glass surface decreased¹⁷⁸ or if mismatches between the Adapter Strand

and surface strand increased. CMO labeling using Adapter Strands without CpG repeats did not stimulate TLR9 in HEK cells expressing mouse TLR9 (Figure 3.9).

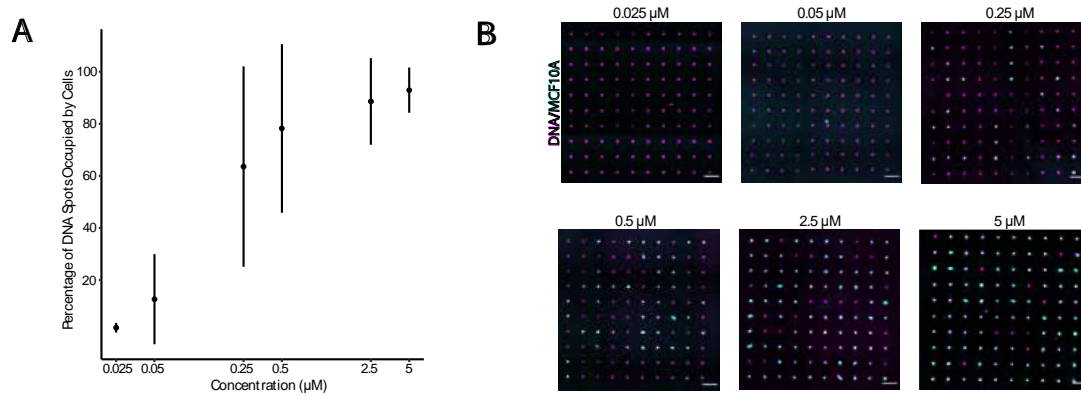


Figure 3.7 Adhesion of CMO-labeled cells to DNA patterns increases as a function of CMO concentration during labeling.

In this experiment, the Universal Anchor + Adapter Strand (pre-hybridized) and the Universal Co-Ancor were used at equal concentrations. Concentration refers to the concentration of CMO in the cell suspension during CMO labeling of cells. A) Quantification of the percentage of 15 μm diameter DNA spots that were occupied by CMO-labeled MCF10A cells as a function of CMO concentration during cell labeling. Data represented as the mean \pm standard deviation from three experiments. B) Representative images of the DNA patterns (magenta) and adhered MCF10As (cyan) at different concentrations of CMO. Scale bar = 100 μm .

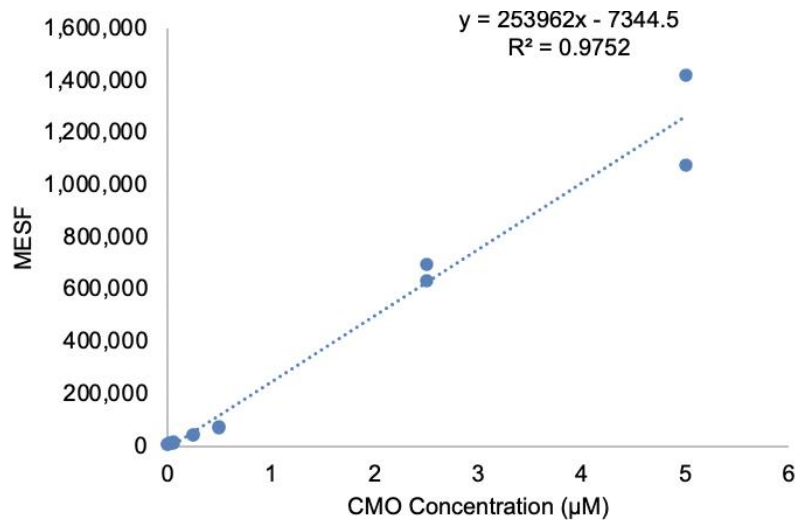


Figure 3.8 Quantification of DNA complexes on the cell surface as a function of CMO labeling concentration.

HUVECs were labeled with different concentrations of CMO solution, washed, and then incubated with a fluorescent complementary strand. An MESF (Molecules of Equivalent Soluble Fluorochrome) microsphere kit was used to do quantitative flow cytometry and estimate the number of DNA complexes on the cell surface as a function of CMO concentration during labeling.

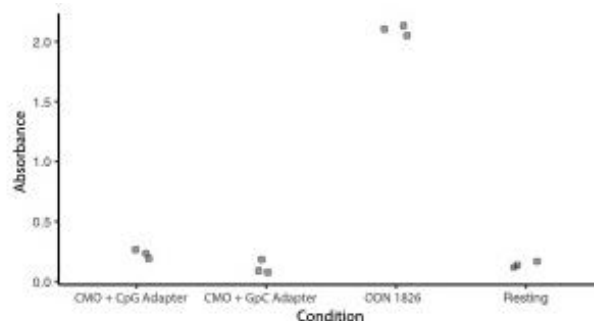


Figure 3.9 CMO labeling does not stimulate TLR9 response.

An experiment was carried out to see whether CMO labeling would trigger the DNA-detection mechanism of TLR9 and whether this would be affected by CpGs in the Adapter Strand sequence. HEK cells expressing mouse TLR9 were incubated overnight with 0.2 µM of either ODN 1826 (a CpG-containing TLR9 agonist), CMO Universal Anchor + Universal Co-Anchor + Adapter Strand containing the same sequence as ODN 1826 (CMO-CpG), or CMO Universal Anchor + Universal Co-Anchor + Adapter Strand containing a similar sequence but with replacement of the CpGs with GpCs (CMO-GpC). TLR9 stimulation would result in the production of SEAP (secreted embryonic alkaline phosphatase). SEAP secretion was quantified by a colorimetric assay (absorbance). Treatment conditions were compared to resting cells that were only treated with PBS. Incubation with CMO-GPC did not stimulate TLR9 expression. Incubation with CMO-CpG was slightly higher than resting cells but much lower than ODN-1826.

We provide several demonstrations that this method provides reproducible and efficient DNA-programmed cell adhesion. For example, human umbilical vein endothelial cells (HUVECs) labeled with CMOs adhered to DNA patterns with high efficiency. CMO-labeled HUVECs adhered as well as LMO-labeled HUVECs (Figure 3.10). Cells patterned using CMO-DPAC retained their viability and functionality. Cells labeled with CMOs were stained by calcein AM and ethidium homodimer to assess viability (Figure 3.11). Differences in viability compared to unlabeled control cells were small (94% vs 97%). Single MDCKs patterned via CMO-DPAC and transferred into Matrigel were able to proliferate and polarize correctly after 5 days of culture (Figure 3.10). DPAC also provides a means of elaborating patterns of cells into the third dimension (Figure 3.10). For example, multilayered, multicellular aggregates can be created by alternating layers of cells labeled with complementary CMOs (Figure 3.10). These experiments demonstrate that the protocol is reproducible, does not negatively affect cell viability or functionality, and yields cellular patterns that can be successfully cultured within a single imaging plane in a 3D ECM.

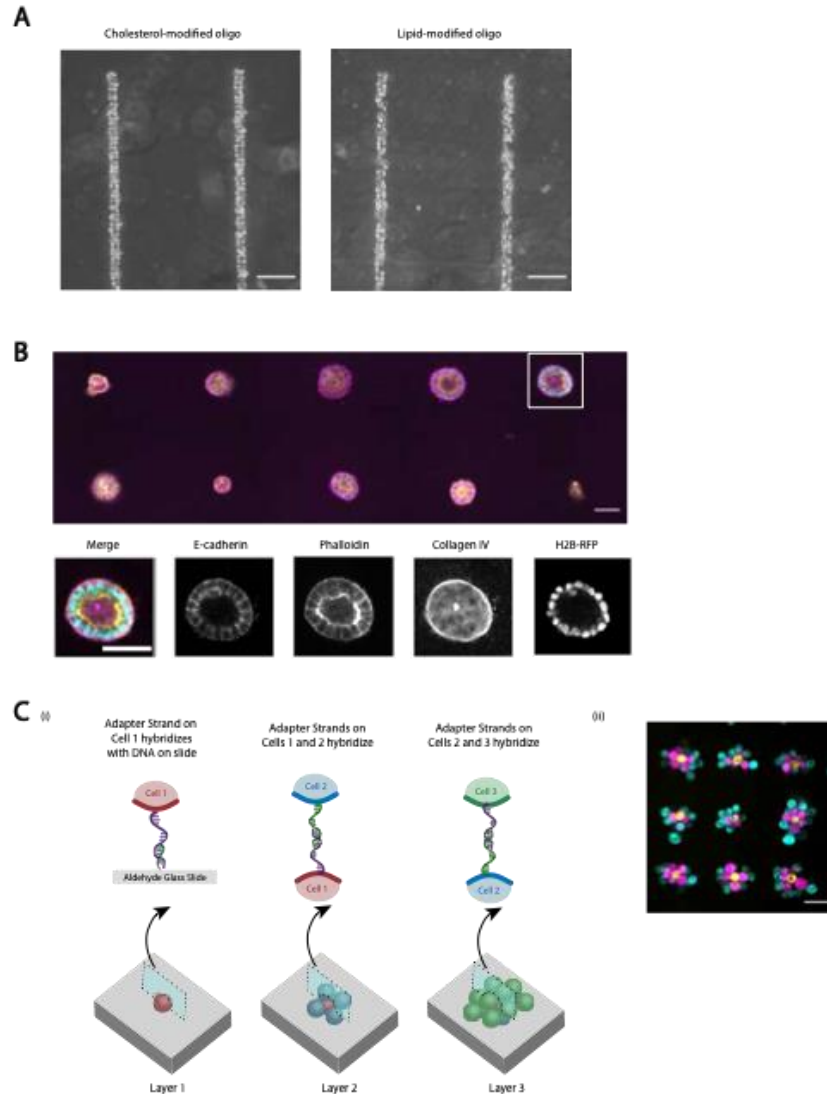


Figure 3.10 CMO-DPAC can be used to create two-dimensional cell patterns that can subsequently be embedded into a three-dimensional hydrogel for culture and/or layered to create multilayered structures.

A) Direct comparison between CMO-labeled human umbilical vein endothelial cells (HUVECs) and LMO-labeled HUVECs adhered to a linear DNA pattern. Both methods of cell labeling result in nearly 100% occupancy of the DNA pattern. B) Single Madin-Darby Canine Kidney cells (MDCKs) expressing H2B-RFP were patterned onto 15 µm diameter spots spaced 200 µm apart and subsequently embedded in Matrigel. After 120 hours of culture, the resulting epithelial cysts were fixed and stained for E-cadherin, actin, and collagen IV. Spheroid in white box is shown in detail. Scale bar = 50 µm. C) Multilayered cellular structures can be created by labeling separate cell populations with complementary Adapter Strands and patterning sequentially so that each new addition of cells adheres to the cell layer before it. (i) A schematic of the sequential patterning of cell populations to create multilayered structures. (ii) Three-layered cell aggregates of MCF10As (visualized using dyes) were created using this process. Scale bar = 50 µm.

By providing orthogonal DNA sequences to direct cell adhesion, DPAC provides a means of patterning multiple cell types on a single surface. To implement this feature of DPAC, DNA patterns generated by photolithography must be aligned with respect to one another. Metal fiduciary markers deposited onto the slide allowed for the alignment of multiple photomasks and therefore the patterning of multiple cell types at once. MCF10As stained with different unique dyes were labeled with orthogonal CMOs and patterned to create a visualization of the UC Berkeley and UCSF logos (Figure 3.12). This experiment demonstrates that multiple unique cell populations can be patterned together with high precision and without cross-contamination.

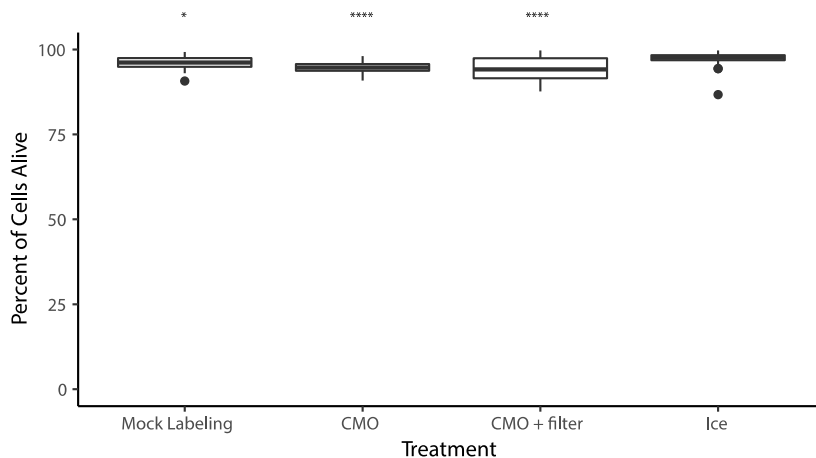


Figure 3.11 Viability of cells after CMO labeling process.

To assess how the protocol impacts viability, HUVECs were split into four populations: one remained on ice for 1 hour, one was mock labeled with PBS but otherwise taken through all centrifuge and wash steps, one was labeled with CMOs, and one was labeled with CMOs and filtered through a 40 μm filter to remove clumps. The cells were then stained with calcein AM and ethidium homodimer to assess the number of alive and dead cells. All treatments resulted in significantly decreased viability than the ice control (one-way ANOVA with Tukey post-hoc analysis), but median viability for CMO-labeling (with or without filtering) was about 94%. Data collected from three independent experiments. * = $p < 0.05$. **** = $p < 0.0001$.



Figure 3.12 Multiple cell types can be patterned without cross-contamination or loss of adhesion.

Multiple amine-modified DNA oligos were patterned sequentially onto an aldehyde slide and aligned through use of metal fiducial markers. Three populations of MCF10As (cyan, magenta, yellow) were stained with unique dyes labeled with complementary CMOs, and patterned onto the slide, resulting in an image of the UC Berkeley and UCSF logos. Scale bar = 1 mm.

Successful patterning of cells using CMO-DPAC requires high-quality photolithography, sufficient concentration of oligo on the cell surface, a high density of cells over the pattern, and sufficient washing. Failure of any one of these steps affects the final product. Figure 3.2 includes example images of correct and incorrect photolithography, the desired cell density over the pattern to create fully occupied patterns, the loss of patterned cells due to overly vigorous pipetting during subsequent steps of DPAC, and undesired clumping of cells. Table 3.1 includes a list of common failure points and the suggested troubleshooting. The use of fluorescent

complementary oligos is recommended as a tool for troubleshooting to confirm the presence of patterned DNA on the slide and the presence of CMOs on the cell surface by flow cytometry.

Table 3.1 A troubleshooting guide to identify and resolve potential failures that can arise from this protocol.

Result	Possible Cause(s)	Suggested Fixes
Photolithography – features are cracked	Inconsistent or inadequate soft-bake	Increase time of soft-bake up to 3 minutes; verify actual temperature of hotplate and increase temperature as necessary
Photolithography – features are not sharp or have photoresist remaining within them	Under-development	Increase time that slide spends in developer solution; incorporate gentle agitation
Photolithography – features inconsistent across slide	UV light may not be centered or not focused properly	Adjust UV light setup to ensure collimated light of uniform intensity
Cells don't adhere to patterned spots with high efficiency	Not enough DNA on surface	Confirm that DNA is present on surface by hybridizing the slide with fluorescent complementary oligos and then imaging under microscope
	Cells are inadequately labeled with CMO	Add fluorescent complementary oligos to cell suspension and confirm fluorescence via flow cytometry
	Not enough cells over pattern	Collect cells by washing out from PDMS flow cell, centrifuge, and re-suspend in lower volume to concentrate the cells

Result	Possible Cause(s)	Suggested Fixes
	Too much remaining CMO in cell suspension, hybridizing with DNA on slide	Add another wash step. Be sure to remove as much supernatant as possible with each wash.
	Too much internalization of CMO due to time and temperature	Work quickly after labeling the cells with CMO; keep cells and slide on ice and use ice-cold reagents
Cells clump	Cells were not adequately separated during trypsinization	Use PBS + 0.04% EDTA during cell washes; pass cell suspension through 40 μ m filter before the final wash
Cells adhere non-specifically	If in one specific area – could be due to scratches on slide, misalignment of PDMS flow cells, or spillage of DNA outside the pattern region	Avoid scratches, be careful to align the PDMS flow cells to the pattern region
	If cells are adhering everywhere – inadequate blocking or washing	Add in more washes after patterning the cells; pipet more vigorously during washes; block with 1% BSA for longer before starting cell patterning; silanize slide, or confirm silanization was successful by measuring contact angle of water droplet
Bubbles form within flow cell	Pipetting errors, uneven hydrophilic surface created during plasma oxidation	If bubbles are small, add PBS to the inlet of the flow cell and they may be washed out. If bubbles are larger, apply gentle pressure to the PDMS flow cell, nudging the bubbles towards the inlet or outlet.

Result	Possible Cause(s)	Suggested Fixes
Cells initially adhere to pattern but are removed during washes, patterning of other cell types, or adding the hydrogel precursor	The shear forces from pipetting too vigorously can cause the cells to detach from the surface	Pipet more gently during subsequent washes, rounds of cell patterning, or adding hydrogel precursors. Because the hydrogel precursors are viscous, they are more likely to cause the pattern to dislodge, so take extra caution. Multilayered structures tend to be top-heavy and are more susceptible to being dislodged.
Tissue deforms during 3D transfer	Hydrogel sticks to slide	Confirm hydrophobicity of slide using contact angle measurements
		Use razor blade to lift PDMS fully on both edges, allowing PBS to float under the tissue
		This can happen with pure collagen hydrogels – consider adjusting the protein concentration or composition of hydrogel
	Cells don't transfer with the hydrogel and remain on the slide	Increase Turbo DNase concentration or increase incubation time
	Hydrogel is not solid enough	Increase incubation time and/or optimize the gelation mechanism for the hydrogel in question (e.g., for collagen, make sure pH is correct)
Hydrogel tears upon removing PDMS	Make PDMS flow cells hydrophilic using plasma oxidation before beginning experiment so that they detach easily upon adding media. Use forceps very gently to detach the PDMS.	

3.5 Discussion

Here we present a detailed protocol for high-resolution patterning of cells in 2D and 3D for *in vitro* cell culture experiments. Unlike previously published versions of this method, the protocol presented here focuses on usability: it does not require highly specialized equipment and all reagents can be purchased from vendors instead of requiring custom synthesis. Unlike other cell micropatterning methods, this method is rapid and cell-type agnostic: it does not require specific adhesion to extracellular matrix proteins¹⁶⁶. Cells patterned by CMO-DPAC can be embedded within an ECM such as Matrigel or collagen, resulting in 3D cultures with much higher spatial resolution than is currently possible with extrusion printing-based methods¹²⁶. CMO-DPAC can be used to create hundreds to thousands of microscopic features per slide, allowing for many replicates to be performed at the same time.

One of the most important parameters in the success of this protocol is the density of cells added to the flow cells on top of the patterned slide. Ideally, the density should be at least 25 million cells/mL. When loaded into the flow cells, this density of cells results in a nearly close-packed monolayer of cells above the pattern (Figure 3.2). These high cell densities maximize the probability that a cell will settle directly on top of a DNA spot and adhere. Reducing the cell density will decrease the

overall patterning efficiency. Another critical step in this protocol is thoroughly re-suspending the cells in PBS or serum-free media before adding the CMO solution. The CMOs partition very rapidly into cell membranes and adding the CMO solution directly to a cell pellet will result in heterogeneous labeling of cells. After adding the CMO solution to the cell suspension, it is important to mix thoroughly by pipetting so that the cells are uniformly labeled with the CMOs. After the incubations, it is necessary to thoroughly wash out the excess CMOs through multiple centrifugation and wash steps. Excess free CMO present in the cell suspension will bind to the patterned amine-modified DNA on the glass slide, blocking hybridization and adhesion of the CMO-modified cells in suspension. Time is also a key consideration for this protocol. It is important to work as quickly as possible when using CMOs and to keep the cells on ice to minimize internalization of the CMOs and maximize cell viability. Flow cytometry experiments have shown that CMOs do not persist as long on the cell surface as LMOs, with 25% loss of CMO complexes over two hours of incubation on ice¹⁸⁴. Furthermore, the viability of cells will decrease as the cell handling time increases. Viability can be maximized by working quickly, keeping cells on ice, using ice-cold reagents, and using serum-free media to provide some nutrients.

Although CMO-DPAC can be a powerful way of studying cell biology by patterning cells with high precision, it does have its limitations. CMO-DPAC experiments can be challenging, particularly as the experimental complexity is added

with multiple cell types, layers, or 3D cell culture. Experimental failures can be common when starting this protocol, as described in Table 3.1. Therefore, we recommend that new users institute quality control checks (confirming that DNA is present on the slide, confirming that cells are sufficiently labeled with DNA, confirming that excess cells have been thoroughly washed away, etc.) to make sure that the experiment succeeds and to identify steps that may require further optimization.

Cholesterol is a bioactive molecule whose internalization may influence cell metabolism, gene expression, and membrane fluidity^{185,186}. A previous study compared the effects on gene expression of CMO- and LMO-labeled cells using single cell RNA sequencing. CMO-labeled HEK cells had altered gene expression compared to unlabeled and LMO-labeled cells¹⁸⁴. Labeling cells with CMOs resulted in the differential expression (> 1.5-fold) of eight genes relative to unlabeled controls, including AP2B1, which has been linked to cholesterol and sphingolipid transport (GeneCards), and MALAT1, a long non-coding RNA that regulates cholesterol accumulation¹⁸⁷. While minor, these transcriptional responses may nevertheless be of concern if the experiment in question is studying metabolism, membrane dynamics, or other cholesterol-associated pathways in cells.

This protocol is flexible and can be adjusted to meet the needs of each

experiment. Because the CMO inserts itself into the lipid membrane instead of using any specific receptor, the method is cell type agnostic (HUVECs, MCF10As, HEKs, and MDCKs have been demonstrated here). Although cholesterol is a different hydrophobic anchor than our previously published LMOs, we have thus far found them to behave similarly. Thus, we would expect the CMOs to work with any of the wide variety of cell types that we have previously published with LMOs, including but not limited to neural stem cells, fibroblasts, peripheral blood mononuclear cells, tumor cells, and primary mammary epithelial cells^{16,158,176,178,184}. CMO labeling does not stimulate TLR9, suggesting that the protocol is compatible with immune cells.

Membrane incorporation of the CMO is a function of total cell size and the degree of negative charge in the cell glycocalyx¹⁸⁸. Thus, we have included a protocol for testing the extent of membrane incorporation that is amenable to rapid optimization. The specific features of each cell pattern will inevitably vary based on the experimental design. Although the photopatterning protocol described above for patterning the DNA is recommended, any method of spatially confining droplets of amine-DNA solution should work, such as the use of high-resolution droplet printers. The pattern resolution and minimum feature spacing will vary based on the method used. It is also theoretically possible to combine the DNA-photopatterning sections of this protocol with other methods that have been used to label cells with DNA, such as with DNA hybridized to membrane-expressed zinc fingers¹⁸⁹, using NHS-conjugated DNA¹⁹⁰, and reacting azido sialic acid residues on the cell surface with phosphine-conjugated

DNA¹⁹¹. CMO-DPAC can be applied to a variety of experiments that require tight control over cell-cell spacing, including studies of the interactions between pairs of cells, co-culture experiments looking at the transfer of signals from “sender” cells to “receiver” cells, and investigations of the effect of nearby extracellular cues on stem cell differentiation^{158,178}. The method can also be used to create microtissues that can be used to study cell migration in three dimensions, the self-organization of cells into tissues^{16,176}, and the dynamic interplay between cells and the ECM¹⁷⁶. We hope that this technique will provide researchers with an accessible platform to explore new applications of high-resolution DNA-based cell patterning in their own labs.

4 Microenvironmental control of endothelial cell behaviors that promote microvessel formation in engineered tissues

Authors: Katelyn A. Cabral, Vasudha Srivastava, Maxwell C. Coyle, Connor Stashko, Valerie Weaver, Zev J. Gartner

Author Contributions: K.A.C, M.C.C., and Z.J.G conceived the project. K.A.C., V.S., M.C.C., and C.S. performed experiments. K.A.C. analyzed data. V.W. and Z.J.G. supervised experiments. K.A.C. wrote the manuscript with feedback provided by V.S. and Z.J.G.

4.1 Abstract

The formation of orderly microvascular networks for tissue engineering remains a major challenge. Bioprinting provides a strategy for pre-organizing endothelial cells into the geometry of microvascular networks but the microenvironmental cues necessary to promote their self-organization into cohesive microvessels remains unclear. To identify the critical microenvironmental cues, we reconstituted microvessel formation *in vitro* by patterning thin lines of endothelial cells within a 3D ECM and observed how microenvironmental parameters influenced their self-organization into microvessels. At the level of ECM, we found that the inclusion of fibrillar matrices such as collagen I into the ECM positively influenced the

condensation of patterned cells into extended geometries such as cords. At the level of media components, we discovered that a high molecular weight protein-based component of fetal bovine serum (FBS) negatively influences the condensation of endothelial cells to a stable and extended geometry. FBS destabilized cord structure by promoting cell protrusions and more transient cell-cell adhesions. Endothelial cords cultured in the absence of FBS were able to lumenize, incorporate mural cells, deposit a basement membrane, and support fluid flow. These optimized conditions allow the constructions of branched and perfusable microvascular networks directly from patterned cells and may prove useful in future tissue engineering efforts.

4.2 Introduction

Tissue engineers provide cells with critical microenvironmental and boundary conditions, but the cells must ultimately build themselves into tissues through the process of self-organization^{14,146,147}. Self-organization occurs across multiple, sequential steps and involves a variety of individual and collective cell behaviors^{146,192}. This is true for epithelial tissues as well as vasculature—an essential component of many tissue-engineered constructs. Many efforts have optimized for microenvironmental conditions that promote the formation of vascular networks from uniformly dispersed cells^{27,43,56}. However, the formation of microvessels from uniformly dispersed cells is a multi-step process that involves coordination of a variety

of distinct cell behaviors required for vessel formation including proliferation, mechanical polarization, motility, adhesion stabilization, and lumenization⁵³. Emerging bioengineering approaches are allowing greater control over this process, leveraging elements of top-down and bottom-up control to promote more orderly vessel formation along paths that rely on smaller subsets of these cell behaviors. However, optimal deployment of these methods in tissue engineering will require a more detailed understanding of the influence of each component of the microenvironment on specific stages of endothelial cell self-organization.

Top-down and bottom-up methods represent two broad strategies for tissue engineering¹⁹³. In the top-down approach, a variety of bioprinting and microfabrication techniques have been used to fabricate hollow channels within hydrogels that are subsequently seeded with endothelial cells. The cells adhere to the channel walls and ultimately form an endothelial monolayer^{109,112,115,120,121,124}. This approach excels at creating vascular structures that are hundreds of microns to millimeters in diameter and that follow specifically designed paths, often straight lines. However, the creation of capillary-sized vessels is challenging with the top-down approach, both due to the resolution limits of bioprinting and because narrow channels will clog with cell suspension^{193,108}.

In the bottom-up approach, endothelial cells are seeded within an extracellular matrix (ECM) such as collagen or fibrin^{27,43,63,67}. When the necessary microenvironmental cues and boundary conditions are incorporated, the endothelial cells will self-organize through the processes of vasculogenesis and angiogenesis, resulting in the formation of microvascular networks. If interstitial fluid flow is applied to the engineered tissue, these capillaries can lumenize and ultimately become perfused^{30,84,194}. A major advantage of this strategy is that it builds on the process believed to govern microvessel formation *in vivo*. A challenge, however, is that since it takes between 3-7 days to complete due to the slow speed of angiogenesis (approximately 5 $\mu\text{m}/\text{hour}$)¹², the center of thick, cell-dense tissues will begin to suffer from hypoxia without media perfusion^{10,195}. An additional challenge is that the structure of the vessels cannot be readily controlled using this strategy, which precludes the formation of *de novo* vascular networks with the hierarchical structure found *in vivo* that optimize fluid transport^{145,196}.

Bioprinting and other biofabrication techniques that allow for the rapid placement of cells within ECMs and at a high density represent a potential hybrid top-down and bottom-up approach^{14,171}. Placing cells into the structure of a vascular network could result in more efficient vasculogenesis, recapitulating native-like vessel architecture and creating vascular networks that are structurally optimized for fluid flow^{148,149}. For example, laser printing was used to deposit droplets of endothelial cells

and smooth muscle cells at high density on top of Matrigel¹⁹⁷. This resulted in the creation of microvascular networks in a stereotyped branch-and-stem shape on top of an ECM. Recently, Brassard et al. demonstrated the bioprinting of high-density cell solutions within Matrigel or collagen hydrogels¹⁴. Over time, the cells self-organized and condensed into a single cohesive structure in the geometry dictated by the initial print. The authors used this technique to print intestinal organoid tubes and lumenized blood vessels. This strategy allowed for control over the final structure while allowing and encouraging cells to undergo their natural morphogenetic processes. However, due to the limitations in cell density and nozzle geometry, the authors were not able to explore the role of microenvironmental conditions in controlling the self-organization and function of continuous microvessels narrower than 250 microns.

To investigate the formation of microvessels in this size range, we used DNA Programmed Assembly of Cells (DPAC), a high-resolution cell patterning technique that allows the formation of close-packed and cell dense tissues, fully embedded in biologically relevant ECM, and with near single-cellular resolution in X and Y. We created capillary-sized lines of endothelial cells within a 3D ECM and observed their self-organization into microvessels under the influence of different microenvironmental cues. We found that by adjusting the microenvironment, specific cell behaviors involved in vasculogenesis can be encouraged or discouraged, ultimately

leading to the orderly self-organization of the cells into perfusable networks and across length scales that have not been previously achieved.

4.3 Methods

The methods used for creating PDMS flow cells, creating DNA-patterned slides, and labeling cells with cholesterol/lipid-modified oligos are described in Chapter 3.

Cell culture:

Human umbilical vein endothelial cells (HUVECs) were obtained through Lonza and cultured in EGM-2 (Lonza). HUVECs were used between passages 4 and 6. Human brain vascular pericytes (HBVPs) were cultured in DMEM + 10% FBS + penicillin/streptomycin and used between passages 11 and 13. EGFP-HUVECs and EGFP-HBVPs were created by transducing with a pSicoR-EF1a-EGFP lentiviral vector. mCherry-HUVECs were created by transducing with a pSicoR-EF1a-mCherry lentiviral vector. HUVECs with cytosolic EGFP and nuclear mScarlet were created by transducing with a pSicoR-EF1a-EGFP-H2B-mScarlet lentiviral vector. All lentiviruses were made by the UCSF Viracore. Polybrene (1 $\mu\text{g}/\text{mL}$) was used to enhance viral transduction. Cells were sorted for their fluorescence on a BD Aria II flow cytometer.

ECM hydrogel formulation:

Ice-cold growth factor reduced Matrigel (Corning, three different lots) was mixed with 2% Turbo DNase and neutralized rat tail collagen I (Corning, three different lots) for a total protein concentration of 8 mg/mL. The ratio of Matrigel to collagen varied by experiment. Non-specific staining of the ECM was achieved by mixing the hydrogel precursor solution with 1% Alexa Fluor 647 NHS Ester (Invitrogen).

Rheology:

Shear rheology data was collected using an AR 2000ex rheometer (TA Instruments). 300 μ L gels were deposited onto the base of the rheometer, which was heated to 37°C. Then, a 25 mm flat plate probe was lowered, and the sample was compressed into a barrel. Approximately 250 μ L of mineral oil (Sunmark™) was applied around the perimeter of the sample to prevent evaporation. Time sweep data was collected with 1% strain at a frequency of 1 rad/s until the loss and storage moduli reached steady-state values, approximately 30 minutes to an hour. The elastic modulus, E , was calculated by the formula $E = 2(1 + \nu)G^*$, where Poisson's ratio ν was assumed to be 0.5 and where G^* is the complex modulus found using the measured storage and loss moduli: $G^* = (G'^2 + G''^2)^{1/2}$.¹⁹⁸

Atomic force microscopy:

For AFM measurements, 300 μL gels were deposited directly onto glass slides. 15 mm round coverslips coated in a thin layer of hydrophobic Rain-X solution were immediately placed on top to flatten the gels. Coverslips were removed after polymerization at 37°C for one hour. Then, the surrounding areas were marked with a hydrophobic barrier and gels were submerged in approximately 500 μL of PBS. Measurements were obtained with a MFP3D-BIO inverted optical AFM mounted on a Nikon TE2000-U inverted fluorescent microscope (Asylum Research). Gels were indented with silicon nitride cantilevers with borosilicate glass spherical tips 5 μm in diameter (Novascan Tech). Cantilevers had a nominal spring constant of 0.06 N/m and were calibrated using the thermal oscillation of the tip. Gels were indented at 2 $\mu\text{m/s}$ loading rate with a 1.8 nN force trigger. Gel stiffness was computed using the Hertz model with a sample Poisson Ratio of 0.5.

Media optimization experiments:

Unless otherwise stated, endothelial cords were cultured in EGM-2 (EBM-2 with the addition of EGM-2 BulletKit) (Lonza). For most experiments, 50 ng/mL phorbol-12-myristate-13-acetate (PMA) (Sigma-Aldrich) was added to the media. For serum-free media, the FBS was omitted from the EGM-2 (normally comprising 2% of the volume). Recombinant human VEGF-A (VEGF-165), recombinant human FGF-

basic (146 aa), recombinant human TGF- β 1, recombinant human stem cell factor (SCF), recombinant human stromal cell-derived factor-1 α (SDF-1 α), and recombinant human interleukin-3 (IL-3) were all purchased from R&D Systems.

FBS:

Multiple lots and formulations of FBS were used to validate our results, including the FBS included in EGM-2 Bulletkits (Lonza), FBS from the UCSF Cell Culture Facility, and charcoal/dextran stripped FBS (Gemini Bio). For experiments using heat inactivated FBS, the FBS was heated to 56°C for 30 minutes. The FBS was fractionated by centrifuging through molecular weight cutoff filters (200 kDa, Sterlitech). The resulting concentrate and filtrate were then diluted with PBS to the same volume as the FBS before filtration. To degrade the proteins in FBS, 100 μ g/mL of proteinase K (Fisher Scientific) was added to the FBS and then incubated at 55°C for 1 hour before being neutralized with 100 μ g/mL PMSF (phenylmethylsulfonyl fluoride, Millipore Sigma). Exosomes were purified from FBS by adding 0.2 volumes of Total Exosome Isolation Reagent (Invitrogen), incubating at 4°C for 30 minutes, and then centrifuging for 10 minutes at 10,000 x g to pellet the exosomes before removing the exosome-depleted supernatant.

FBS candidate protein experiments:

Candidates for the active component of FBS were proteins larger than 200 kilodaltons in mass, known to be present in serum, and known in the literature to be associated with endothelial cells or angiogenesis. Recombinant versions of these proteins were added into serum-free EGM-2 at the concentrations listed below.

Table 4.1 FBS candidate proteins tested.

Candidate Protein	Molecular Weight	Concentration in Media	Supplier
Alpha-2-macroglobulin	800	44 µg/mL	Sigma-Aldrich
Apolipoprotein B	240	20 µg/mL	Sigma-Aldrich
Butyrylcholinesterase	260	100 ng/mL	R&D Systems
Factor V (bovine)	330	200 ng/mL	Enzyme Research Laboratories
Fibrinogen	340	40 µg/mL	Sigma-Aldrich
Fibronectin	220	5 µg/mL	Sigma-Aldrich
Inter Alpha Inhibitor Protein	225	10 µg/mL	Athens Research and Technology
PAPP-A2	220	0.5 ng/mL	R&D Systems
PTPRF	213	200 ng/mL	R&D Systems
PTPRS	217	200 ng/mL	Sigma-Aldrich
VWF	500	10 µg/mL	EMD Millipore

Immunofluorescent staining:

Tissues were fixed after 72 hours of culture with 2% PFA for 45 minutes at room temperature. The tissues were then permeabilized for 15 minutes with 1% Triton X-100 (Sigma-Aldrich) and blocked overnight with 10% goat serum. To avoid

cross-reactivity with the Matrigel, tissues that would later be treated with anti-mouse antibodies were first blocked with AffiniPure Fab Fragment Goat Anti-Mouse IgG (H+L) (Jackson Laboratories) before applying the primary antibodies. Primary antibodies used: VE-cadherin (ab33168, Abcam), podocalyxin (PODXL Monoclonal Antibody (3D3), Invitrogen), ZO-1 (ZO-1 Monoclonal Antibody, Invitrogen), collagen IV (ab6586, Abcam), claudin-5 (Claudin 5 Monoclonal Antibody (4C3C2), Invitrogen), laminin α 5 (ab14509, Abcam). Primary antibodies were incubated with the tissues overnight before being removed by three 1-hour washes. Fluorescent secondary antibodies and fluorescently conjugated phalloidin were incubated with the tissues overnight before being removed by three 1-hour washes.

Microscopy:

Most experiments were imaged using a 10x air objective on a spinning disc confocal microscope (Zeiss). For the cell pair experiments, the cells were first incubated for 12 hours before being placed onto a laser scanning microscope (Zeiss) and imaged with a 25x oil immersion objective once per hour for 48 hours. Cells undergoing time-lapse microscopy were fed with media supplemented with 50 mM HEPES and ProLong Live Antifade Reagent (Thermo Fisher).

Image quantification:

Cord morphology was quantified using FIJI¹⁹⁹. Segmented lines were used to trace and measure the continuous length of each segment of cord (as visualized by cytoplasmic EGFP) along the original patterned axis (Figure 4.1). Sprouts were identified based on their orientation (perpendicular to the patterned cord) and the presence of long, thin subcellular protrusions. Disconnected cells that had migrated at least one cell length from the cord were also included in the count of sprouts, as we had observed that the sprouts that were initially branching from the main cord tended to detach and migrate over time.

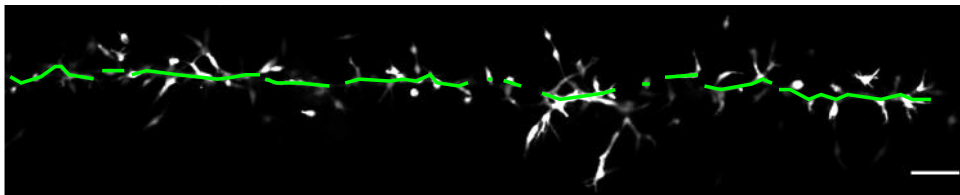


Figure 4.1 Method for measuring cord segment lengths.

Using FIJI software, segmented lines were used to trace the cord along its axis (horizontally) and measure the lengths of individual segments of cord, which could be as small as a single cell or up to two millimeters long. The cells were visualized using cytoplasmic EGFP.

The behavior of cell pairs was quantified by several metrics. The number of cell protrusions per cell at 60 hours of culture was manually counted. Cell protrusions were defined as extensions of the cytoplasm (labeled with EGFP) that were narrower than the nucleus and at least two microns in length. The number of frames that the

cells of each pair were in contact was manually counted. If a cell had divided, either daughter cell could be considered as the partner of the other original cell.

Statistics:

All statistical analyses were performed using Graphpad Prism 9 software. For analyses comparing two experimental conditions, an unpaired t-test was performed. For analyses comparing three or more experimental conditions, a one-way analysis of variance (ANOVA) was used to compare the means, followed by Dunnett's multiple comparisons test.

Methods for perfusion:

Aluminosilicate glass micropipettes with a long tether were prepared using a P-97 micropipette puller (Sutter Instruments). The pulled pipettes were cut 3-5 mm from the tip using a razor blade to get 10-25 μm diameter pipettes with jagged ends. The pipettes were filled with PBS or PBS containing 2 μm -diameter, blue, fluorescent beads (FluospheresTM Carboxylate-Modified Microspheres, Thermo Fisher Scientific) or 1 $\mu\text{g}/\text{mL}$ rhodamine 123 (Thermo Fisher Scientific). The pipette was mounted on a Narishige MM-89 micromanipulator connected to a syringe. The endothelial cords were cut on one end to create an opening, and the micropipette was used to puncture the opposite end of the cord. Once the tip of the micropipette was within the lumen of the cord, the syringe was used to create a positive pressure and induce flow of

Surface Oligo: 5' (Amine C6) ACTGACTGACTGACTGACTG 3'

Universal Anchor: 5'-

TGAATCTCTGGGTGCCAAGGGTAAGCATCCAGCTGTCACT -{Chol}-3'

Universal Co-Anchor: 5'-{Chol} AGTGACAGCTGGATGCTTAC -3'

Adapter Strand A prime:

CCTTGGCACCCAGAGATTCAATTTTTTTTTTTTTTTTTTTTTTTTCAGTCAGTCAG
TCAGTCAGT

4.4 Results

To investigate the microenvironmental cues that promote vessel formation from prepatterned endothelial cells, we began by creating a reproducible assay where the effect of different microenvironmental cues could be investigated beginning from a common set of spatial starting conditions. We created cell-dense, 35 μm -wide, two millimeter-long lines of human umbilical vein endothelial cells (HUVECs) using DPAC (Figure 4.2)^{16,200}. This technique allows for the placement of layers of cells with single-cell precision in a 2D plane, which can then be fully embedded within a 3D hydrogel. Using this technique, we were able to reproducibly pattern cell-dense,

capillary-sized lines of endothelial cells. To our knowledge, this is the finest spatial control that has been demonstrated in the context of engineered microvessels.

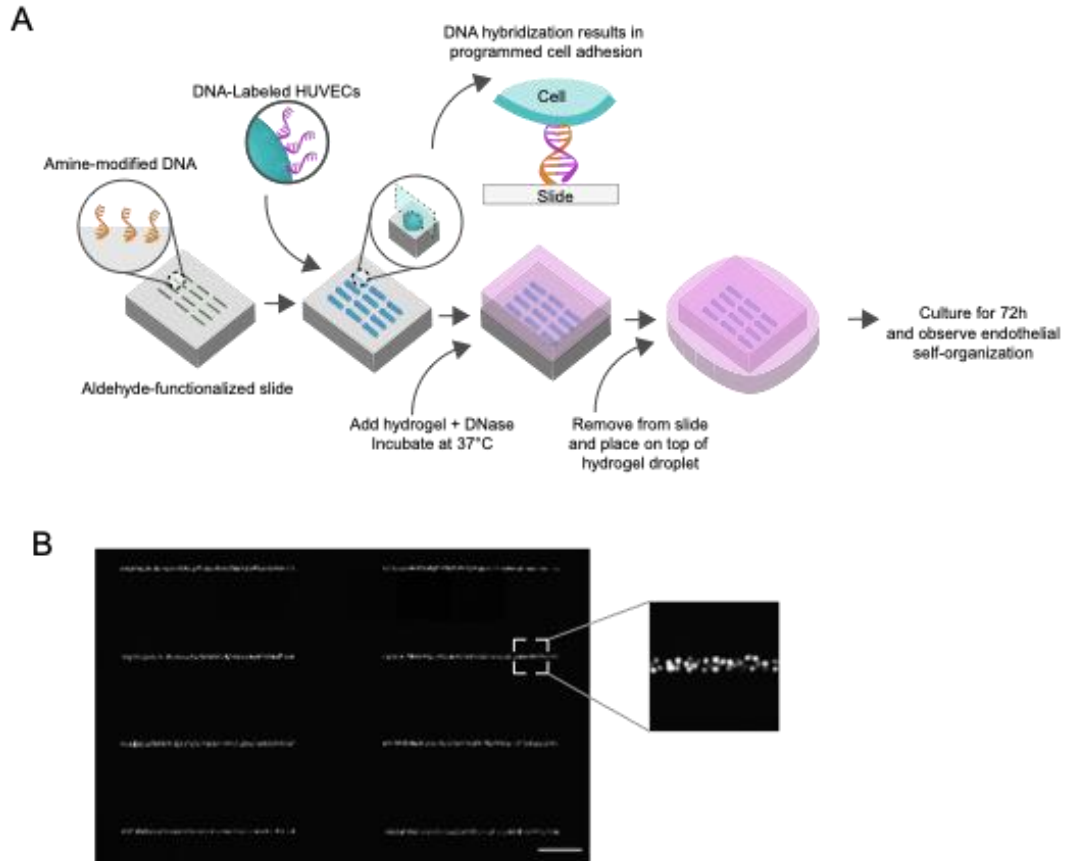


Figure 4.2 Capillary-sized lines of HUVECs are created using DNA-Programmed Assembly of Cells (DPAC).

A) Diagram of the cell patterning process. First, photolithography is used to selectively expose regions of an aldehyde-functionalized slide¹⁷⁸. An amine-modified DNA oligonucleotide solution is then dropped onto the surface. After baking and reductive amination, the amine-modified DNA is covalently bonded to the slide in the pre-defined pattern. HUVECs are then labeled with a set of cholesterol-modified complementary oligos that insert into the cell membrane. Upon passing the cells over the surface, the DNA hybridizes, adhering the HUVECs to the surface only in the regions defined by the DNA pattern. Typically, twelve lines ($35\ \mu\text{m} \times 2\ \text{mm}$) are patterned per tissue. The HUVECs are then embedded in a hydrogel containing 2% DNase. After gelation, the hydrogel containing the patterned HUVECs is removed from the slide and placed on top of another droplet of hydrogel. The result is HUVECs that have been patterned with high precision in a single 2D plane but embedded within a 3D ECM. The HUVECs are then cultured for at least 72 hours to observe endothelial self-organization in response to microenvironmental cues. B) Images of patterned HUVEC cords immediately after being fully embedded within the hydrogel. Scale bar: $500\ \mu\text{m}$.

We first investigated components of the ECM microenvironment that could promote the coalescence of micropatterned HUVECs into long multicellular cords (Figure 4.3). We narrowed our focus to combinations of basement membrane proteins (e.g. Matrigel) and stromal ECM (e.g. collagen I), as these conditions have been used to support the culture of organoids from a variety of tissues^{201–203}. Focusing first on growth factor reduced Matrigel (MG), we found that HUVEC lines cultured for 24h initially broke up and condensed into several cell “droplets” (Figure 4.3). In contrast, identical HUVEC lines cultured in a composite ECM of 6 mg/mL growth factor reduced Matrigel and 2 mg/mL collagen I (MG-COL1) were better able to adopt an extended morphology over the same 24h period. Controlling for constant protein concentration (8 mg/mL), we found that increasing the collagen I concentration in the hydrogel increased the length of the cord segments (Figure 4.4). It has been previously established that increasing matrix stiffness can increase endothelial spreading and lead to increased angiogenic outgrowth^{66,204}. However, there was no significant difference in the elastic modulus (E) between 8 mg/mL MG and MG-COL1 hydrogels, as measured by bulk hydrogel rheology (Figure 4.4) Cells are capable of modifying their ECM microenvironment, for example by synthesizing ECM, concentrating ECM components, and aligning them anisotropically^{176,205,206}. Fluorescently labeling the Matrigel or MG-COL1 precursor solutions with AlexaFluor 647-NHS Ester revealed that HUVEC lines cultured in pure Matrigel were unable to remodel the ECM (Figure 4.3). In contrast, HUVEC lines cultured in MG-COL1 gels

were able to concentrate the ECM into sheaths around themselves. During vasculogenesis, endothelial cells are known to compact and align collagen I between themselves, creating lines of tension that facilitate cell migration and elongation towards each other^{60,62,63}. Moreover, the creation of collagen layers around neovessels and other branched structures has been previously reported^{12,206}. The results suggest that patterned endothelial cells require collagen I to remodel their ECM, exert tension upon it, migrate, and elongate towards each other, ultimately leading to the creation of long, multicellular structures.

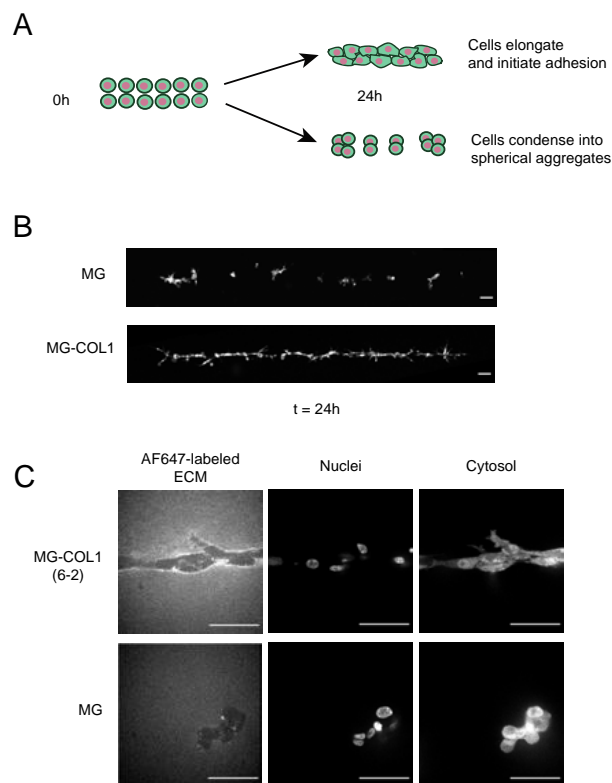


Figure 4.3 Extracellular matrix composition influences the initial condensation of patterned lines of HUVECs into cords.

A) Diagram showing the condensation of patterned HUVECs into either a single continuous structure or several smaller structures. B) After 24 hours of culture, patterned lines of HUVECs in MG broke up into several smaller, rounded sections (top). Patterned lines of HUVECs in MG-COL1 hydrogels were able to condense into a single cord structure (bottom) Scale bar = 100 μm .

C) HUVEC cords with fluorescent nuclei (H2B-mScarlet) and cytoplasm (EGFP) were cultured in either MG or MG-COL1 that had been stained with an Alexa Fluor 647 NHS Ester dye to visualize the ECM.

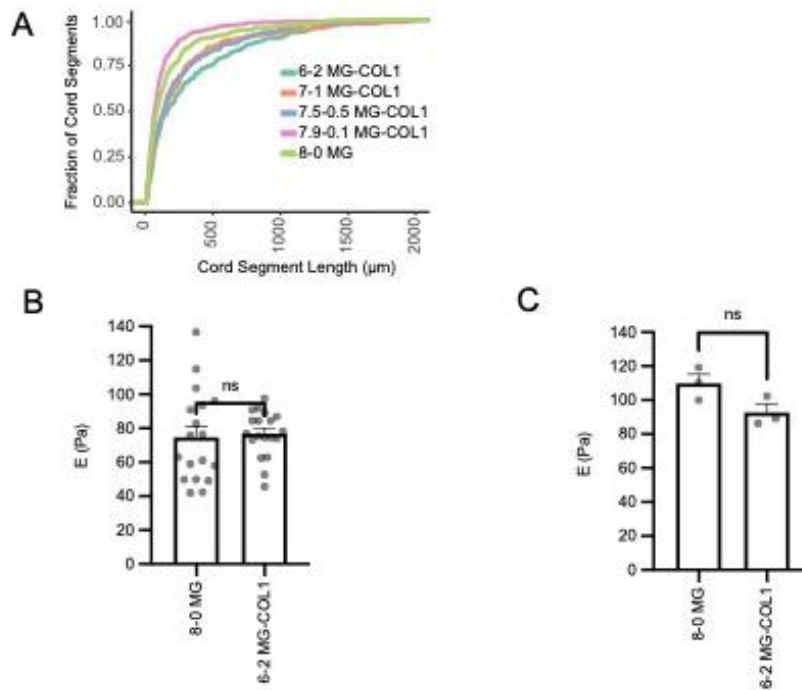


Figure 4.4 Adding collagen I to the ECM resulted in longer cord segments at 24 hours, through a stiffness-independent mechanism.

A) An empirical cumulative distribution function plot of the length of cord segments at 24h as a function of hydrogel composition. Hydrogels varied in the ratio of Matrigel to collagen I but maintained a total protein concentration of 8 mg/mL. B) Measurement of hydrogel stiffness (E) by rheology. T-test, not significant. C) Measurement of hydrogel stiffness (E) by atomic force microscopy. T-test, not significant.

While collagen I-containing gels support initial HUVEC elongation into cord-like structure over 24 hours (Figure 4.4), they failed to maintain this architecture and mature. Instead, we found these same cells scattered over the course of the following 48 hours (Figure 4.5). During this process, many cells exhibited tip-cell like morphology with many subcellular protrusions^{207,208}. We hypothesized that the

presence or absence of specific factors in the standard EGM-2 culture media were contributing to this phenomenon through inappropriate activation of cellular pathways necessary to maintain and stabilize cellular junctions. Phorbol 12-myristate 13-acetate (PMA) is an activator of protein kinase C and has been previously shown to promote angiogenesis^{105,209,210}. When added at 50 ng/ml, we found that PMA reduced the scattering of the HUVECs, allowing for some longer segments of cord (Figure 4.6). Stem cell cytokines such as SDF-1 α , IL-3, and SCF can promote vascular tube morphogenesis¹⁰³, but they had no effect in our assay (Figure 4.6). Similarly, the addition of pro-angiogenic, pro-vasculogenic growth factors FGF-2 (50 ng/mL), VEGF-A (50 ng/mL), and TGF- β (50 ng/mL) had no effect on cord morphology (Figure 4.5). In stark contrast, omitting fetal bovine serum (FBS), normally 2% of the volume of EGM-2, had a dramatic effect on cord morphology. Instead of scattering, the HUVECs remained tightly adhered to one another and maintained the original patterned shape (Figure 4.5). There was also a reduction in the number of sprouts arising from the main cord (Figure 4.5). Staining for VE-cadherin revealed that adherens junctions are impacted by FBS (Figure 4.5), having a more ragged appearance at cell-cell junctions and exhibiting punctate staining within the cell, consistent with endocytosis and an angiogenic morphology^{211,212}. These results suggest that FBS encourages a pro-angiogenic phenotype, leading to the loosening of adherens junctions and breakdown of endothelial cord structure. Combining these

findings with those of microenvironmental ECM, we conclude that matrices containing fibrillar collagen I promote more extended morphologies than pure Matrigel, and that factors within FBS further promote cell scattering from patterned morphologies over longer time periods (Figure 4.5).

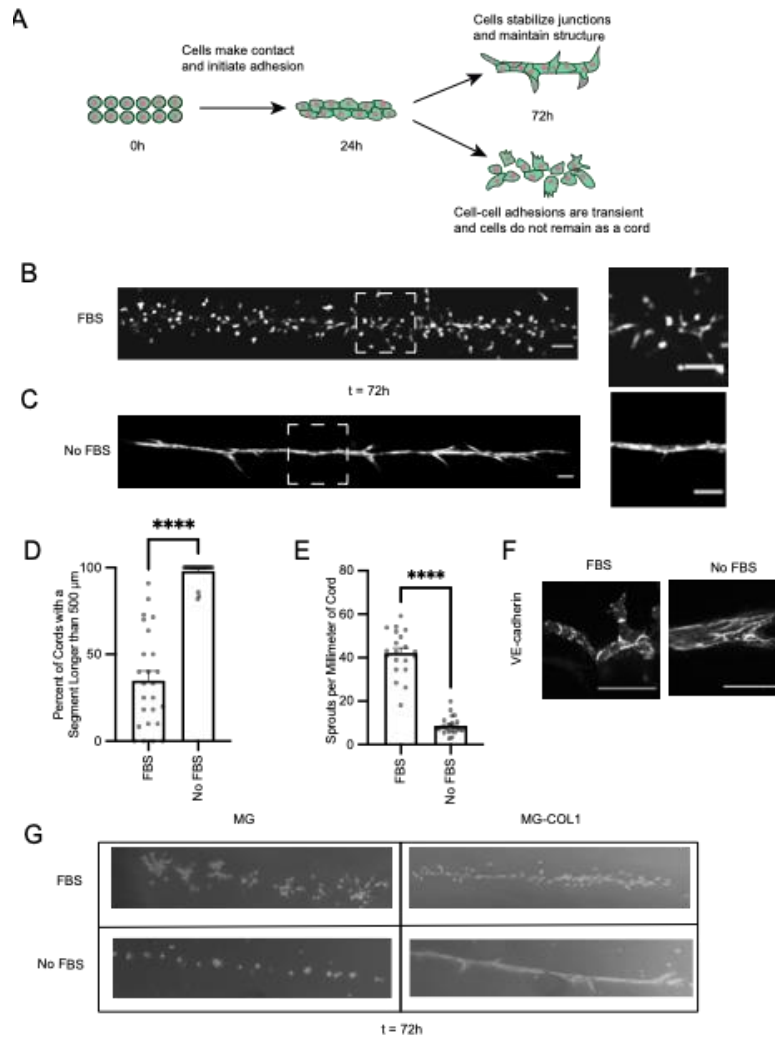


Figure 4.5 Optimizing the culture media through addition of PMA and removal of FBS results in stable, cohesive HUVEC cords with few sprouts and continuous adherens junctions.

A) Diagram showing that after the initial condensation of the patterned HUVECs into a single continuous structure, we need to find microenvironmental conditions to maintain that structure and stabilize the cord. B) After 72 hours of culture in EGM-2 media, HUVEC cords embedded in MG-COL1 scattered into small segments and individual cells. C) After 72 hours of culture in EGM-2 media without FBS, the HUVEC cords maintained one cohesive structure in the approximate shape of the original patterned vessel. D) The percent of cords that had at least one

segment longer than 500 μm in length at 72 hours of culture in EGM-2 + PMA that either contained or omitted FBS. Bars represent mean \pm SEM and with each data point representing one independent tissue. T-test, $p < 0.0001$. E) The number of angiogenic sprouts per millimeter of HUVEC cords cultured for 72 hours in either FBS-free EGM-2 + PMA or FBS-containing EGM-2 + PMA. Data represented as mean \pm SEM and with each data point representing one independent tissue. T-test, $p < 0.0001$. F) VE-cadherin staining in HUVEC cords cultured in either FBS-free EGM-2 + PMA or FBS-containing EGM-2 + PMA. Scale bar = 50 μm . G) Comparison of HUVEC cords grown in either MG or MG-COL1, and in media containing or omitting FBS, after 72h of culture.

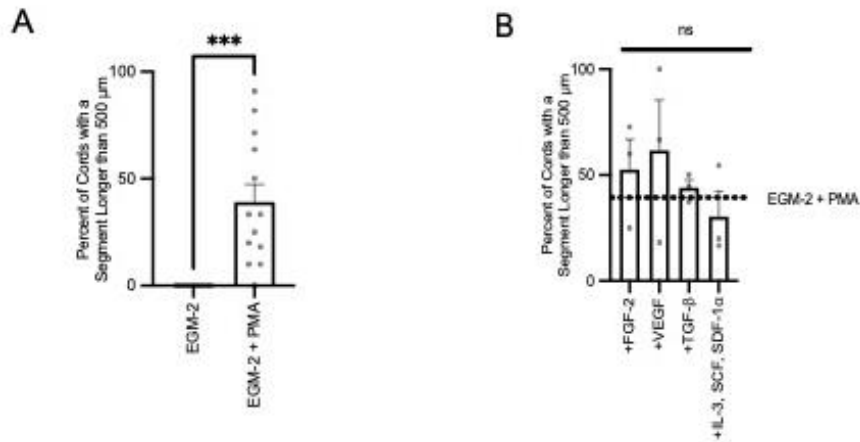


Figure 4.6 Adding pro-vasculogenic components to the media did not prevent scattering of HUVECs in patterned cords

A) The percent of cords per tissue that had at least one segment longer than 500 μm in length at 72 hours of culture in EGM-2 either containing or omitting 50 ng/mL PMA. Bars represent the mean \pm SEM. Each data point represents one independent tissue. T-test, $p < 0.001$. B) The percent of cords per tissue that had at least one segment longer than 500 μm in length at 72 hours of culture in EGM-2 + PMA with different media additives: 50 ng/mL VEGF, 50 ng/mL FGF-2, 50 ng/mL TGF- β , or a stem cell cytokine cocktail composed of 200 ng/mL each of SDF-1 α , SCF, and IL-3. Bars represent the mean \pm SEM. Each data point represents one independent tissue. One-way ANOVA with multiple comparisons to the control (EGM-2 + PMA), not significant.

We next sought to understand what fraction of FBS contributed to the scattering phenotype. Fractionation of the FBS using molecular weight cutoff filters demonstrated that the active component of FBS was greater than 200 kilodaltons (kDa) in molecular weight (Figure 4.7). Furthermore, the component was present in heat-inactivated FBS, charcoal-stripped FBS, and exosome-depleted FBS, suggesting

that the component was not part of the complement system, a lipophilic molecule, or an exosome, respectively. Proteinase K treatment of the FBS blocked its effects, suggesting that the active component of FBS contains a protein. We then tested a range of candidate proteins that were known to be present in plasma or serum^{213,214} (Figure 4.8) but none of the candidate proteins were sufficient to induce cell scattering from patterned cords.

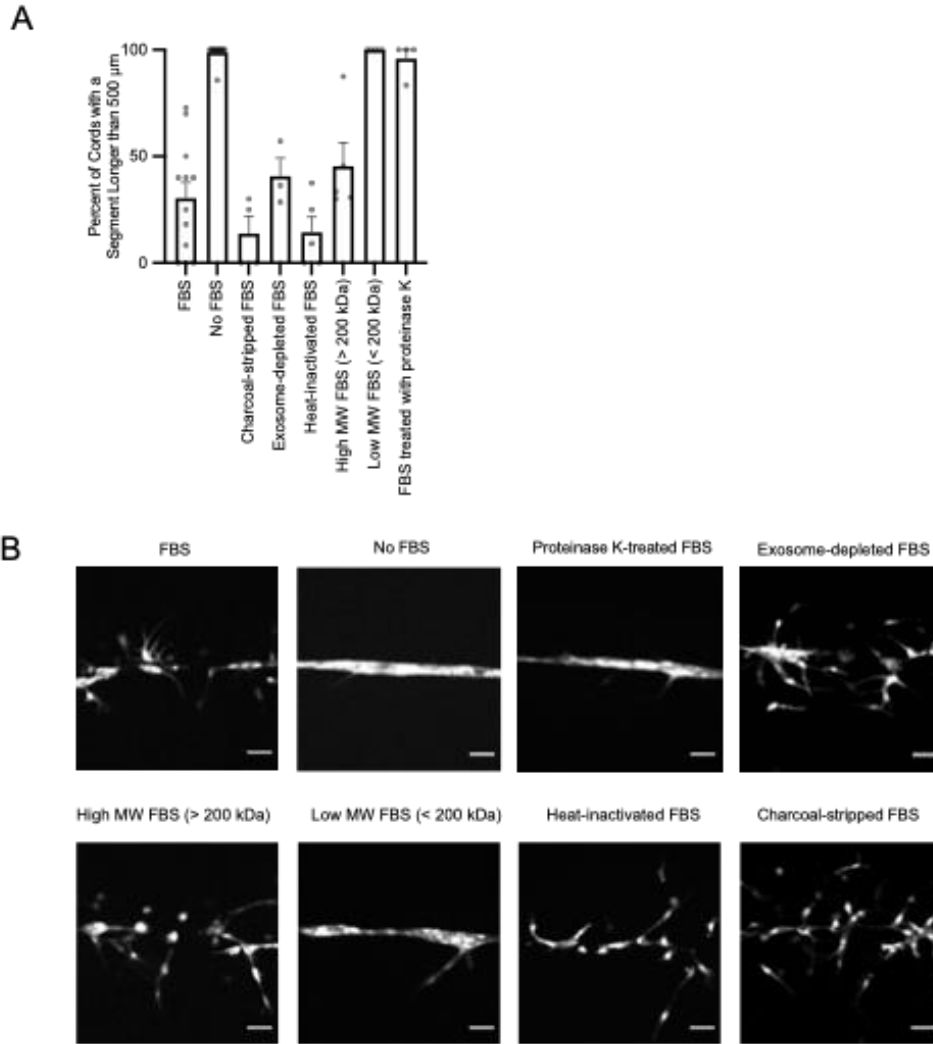


Figure 4.7 The component of FBS that is driving the HUVEC phenotype is a protein greater than 200 kDa.

HUVEC cords were cultured in EGM-2 + PMA with the addition of one of several FBS variants, including charcoal-stripped FBS, exosome-depleted FBS, heat-inactivated FBS, FBS treated for 1 hour with 100 $\mu\text{g}/\text{mL}$ proteinase K at 55°C before being neutralized with 100 $\mu\text{g}/\text{mL}$ PMSF, FBS that has been filtered to exclude components greater than 200 kDa, and FBS that has been filtered to be enriched for components greater than 200 kDa. A) Analysis of the percent of cords per tissue that had at least one segment longer than 500 μm in length at 72 hours of culture as a function of media condition. Data represented as mean \pm SEM with individual data points. All conditions were measured in at least three separate experiments. B) Representative images of cords cultured for 72h in different media formulations. Scale bar = 50 μm .

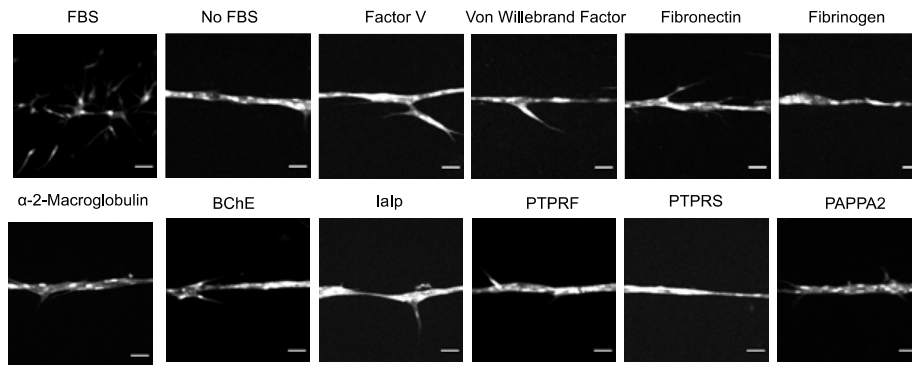


Figure 4.8 Examples of candidate proteins larger than 200 kDa that failed to recapitulate the phenotype of FBS.

Representative images of HUVEC cords cultured in serum-free media with the addition of recombinant proteins that fit the overall profile of being larger than 200 kDa and known to be present in serum.

To better understand how components of FBS were contributing to cell behaviors that resulted in cord destabilization, we examined individual cellular behaviors by using DPAC to pattern pairs of endothelial cells – a minimal “tissue” – that were initially separated by 25 μm (center-to-center distance) and cultured them in media with or without FBS (Figure 4.9). Time-lapse microscopy revealed striking differences in morphology and cell behavior due to the media composition. Endothelial cell pairs cultured with FBS had a star-shaped morphology, with protrusions extending in all directions. In contrast, endothelial cell pairs cultured in serum-free media tended to elongate and had fewer protrusions (Figure 4.9). FBS also resulted in more transient cell-cell adhesions, as measured by the fraction of time where the cells were in contact as well as the average number of instances where the cells separated over the course of the time-lapse (Figure 4.9). Thus, the high molecular weight fraction of FBS inhibits stabilization of cell-cell junctions and promotes cell

morphologies and patterns of motility that increase the probability of cells moving away from nearest neighbors.

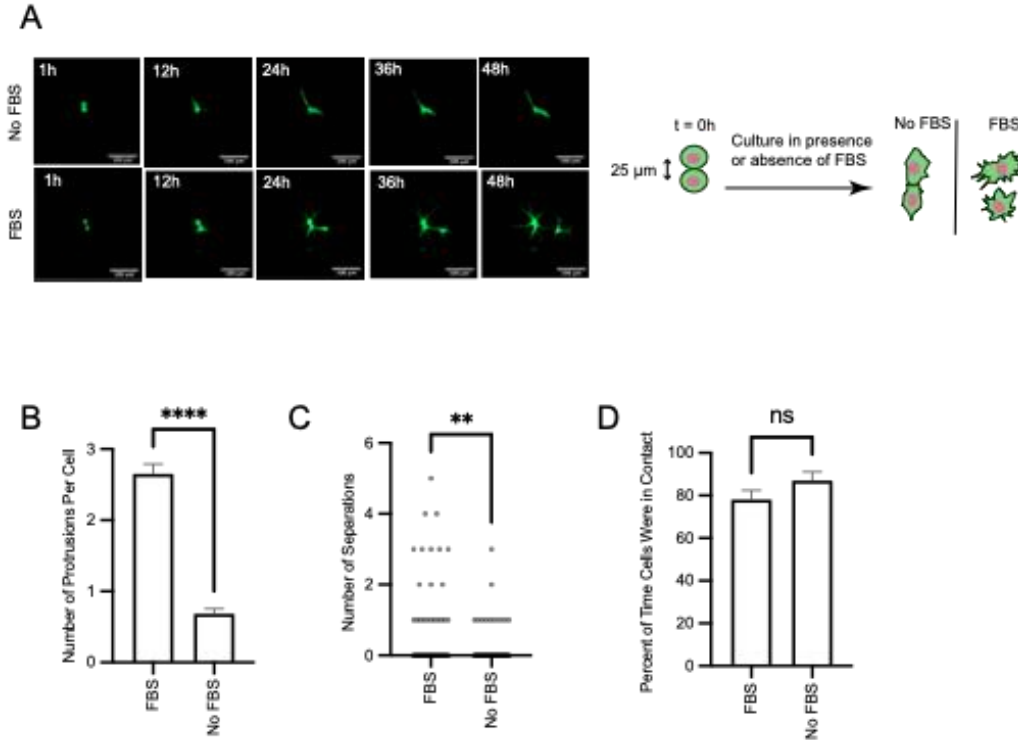


Figure 4.9 Observation of cell pairs reveals that FBS increases proliferation and extension of subcellular protrusions but inhibits the formation of stable cell-cell adhesions.

A) Pairs of HUVECs were patterned 25 μm apart (center to center distance) and cultured for 60 hours in either FBS-free EGM-2 + PMA or FBS-containing EGM-2 + PMA. Cell pairs were imaged once per hour between hours 13-60. B) Quantification of the number of protrusions per cell. Bars represent the mean \pm SEM. Each data point represents one cell. T-test, $p < 0.0001$. C) Quantification of the average number of instances over the time-lapse where the two cells in a pair lost contact with each other. Bars represent the mean \pm SEM. Each data point represents one cell pair. T-test, $p < 0.01$. D) Quantification of the average percent of frames that the cells in a pair were in contact with each other. Bars represent the mean \pm SEM. Each data point represents one cell pair. T-test, not significant.

Having identified conditions promoting cell behaviors consistent with stable cord formation, we investigated how these structures progress through the final stages of capillary morphogenesis (Figure 4.10). Endothelial cords cultured without FBS were stable for at least ten days with almost no change in cord morphology. Staining

for ZO-1 and claudin-5 revealed tight junctions between the endothelial cells of these microvessels. The presence of an endothelial-derived basement membrane around the endothelial cords was confirmed by staining for human collagen IV.

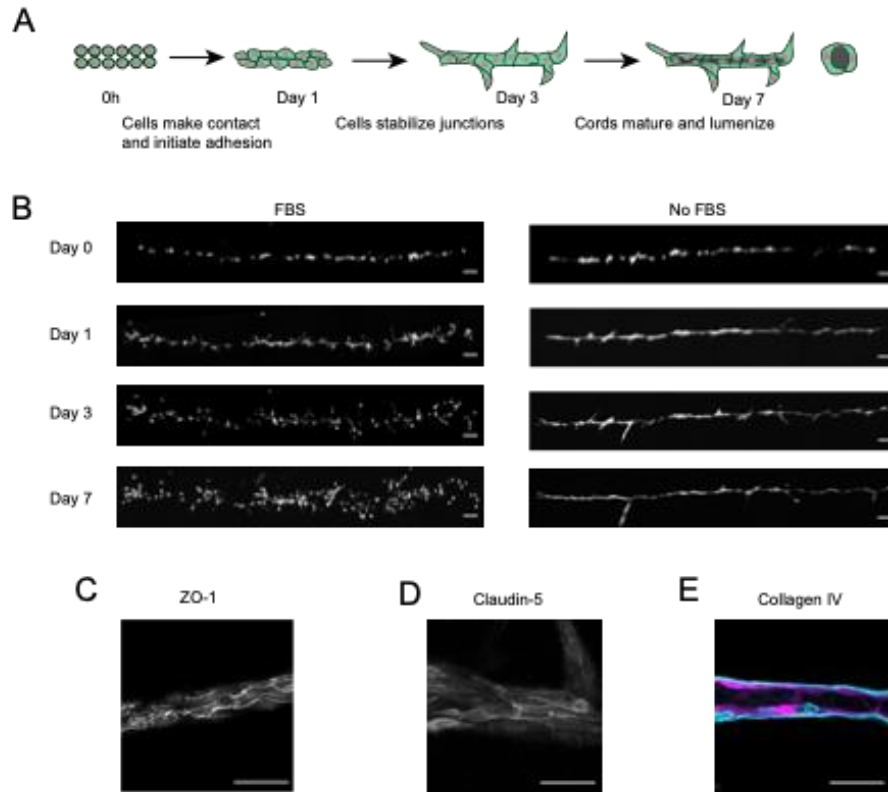


Figure 4.10 Extended culture of HUVEC cords in serum-free media led to the formation of stable, lumenized, and mature microvascular networks of controlled dimensions.

A) Diagram of the HUVEC cords progressing through the stages of vasculogenesis towards maturation and lumenization. B) HUVEC cords were cultured in EGM-2 + PMA either containing or omitting FBS for 7 days. The same cords were imaged each time, demonstrating the extent of cord morphology change over time. Scale bar: 100 μm . C) ZO-1 localized to the cell-cell junctions. Scale bar: 50 μm . D) The endothelial tight junction protein claudin-5 was present at cell-cell junctions. Scale bar: 50 μm . E) HUVEC cords (magenta) were able to synthesize a basement membrane around themselves (collagen IV, cyan). Scale bar: 50 μm .

While cords appeared stable in this assay and showed evidence of lumenization, we did not see evidence of lumenization over the distance necessary for perfusion.

Lumenization of blood vessels occurs through a number of mechanisms that likely

depend on the specific pathway of self-organization^{47,215,216}. We hypothesized that by increasing the cell-cell surface area, we could facilitate the formation of a lumen between endothelial cells²¹⁷. We repeated the cell patterning process to create three-layered HUVEC cords that were 30-75 μm in diameter (Figure 4.11). These larger cords responded similarly to FBS. Over seven days, cell debris accumulated in the center of these larger cords, consistent with the notion that they were undergoing lumenization by cavitation (Figure 4.12). To investigate this possibility, we cut the gel and vessel at one end, then pierced the other end with a hollow micropipette. Injecting PBS into the cords flushed out the cell debris, revealing a fully lumenized, perfusable microvessel (Figure 4.12). These microvessels were then perfused with 2 μm fluorescent microbeads, which traveled the length of the vessel. Confocal microscopy further confirmed the presence of a lumen. Mature microvessels were further able to incorporate other mural cell types. For example, when human brain vascular pericytes (HBVPs) were included as a layer during the DPAC process, they formed close associations with the endothelial cells and were found to be embedded within the vascular basement membrane (Figure 4.12). Thus, by using the microenvironment to control the vascular morphogenesis of patterned endothelial cells, we were able to create mature and perfusable microvessels. Since DPAC allows for the patterning of cells in arbitrary designs, we created a hierarchical microvascular network that approximated Murray's law with vessel diameters decreasing as the vessels branched¹⁴⁵ (Figure 4.12). Thus, by engineering the microenvironment to

control the process of vascular self-organization from patterned endothelial cells, we were able to create mature and perfusable microvessels.

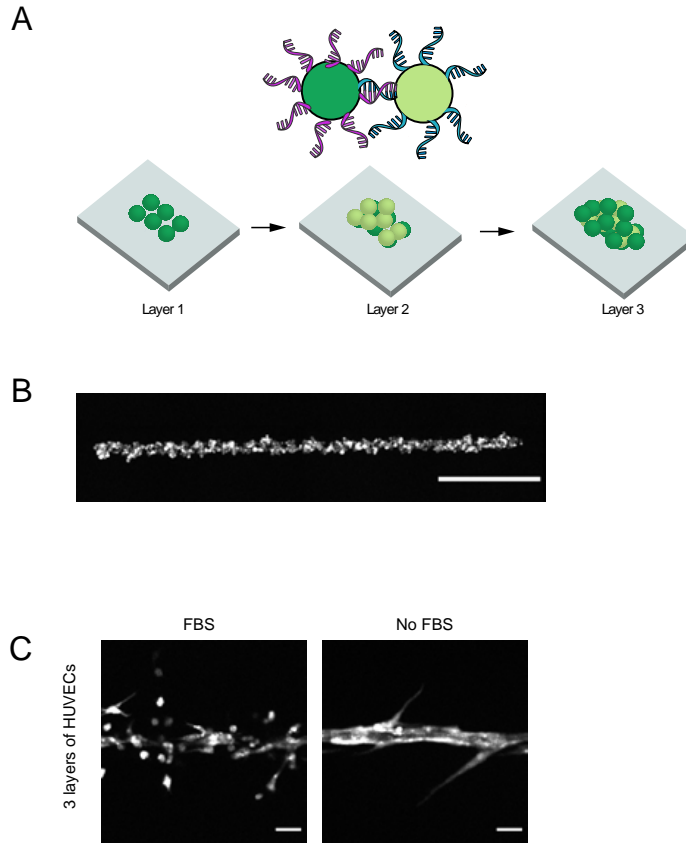


Figure 4.11 Multi-layered HUVEC cords also respond to FBS with increased sprouting.

A) Multi-layered cords can be created by first patterning one population of HUVECs as described in Figure 4.2, then adding a second population of HUVECs labeled with an oligo complementary to the first population of cells, then adding the first population of HUVECs again. Hybridization of the oligos dictates cell-cell adhesion, building up the tissue layer by layer. B) A three-layered HUVEC cord immediately after patterning. Scale bar = 500 μm. C) The response of three-layered HUVEC cords to FBS is similar to one-layered HUVEC cords. Scale bar = 50 μm.

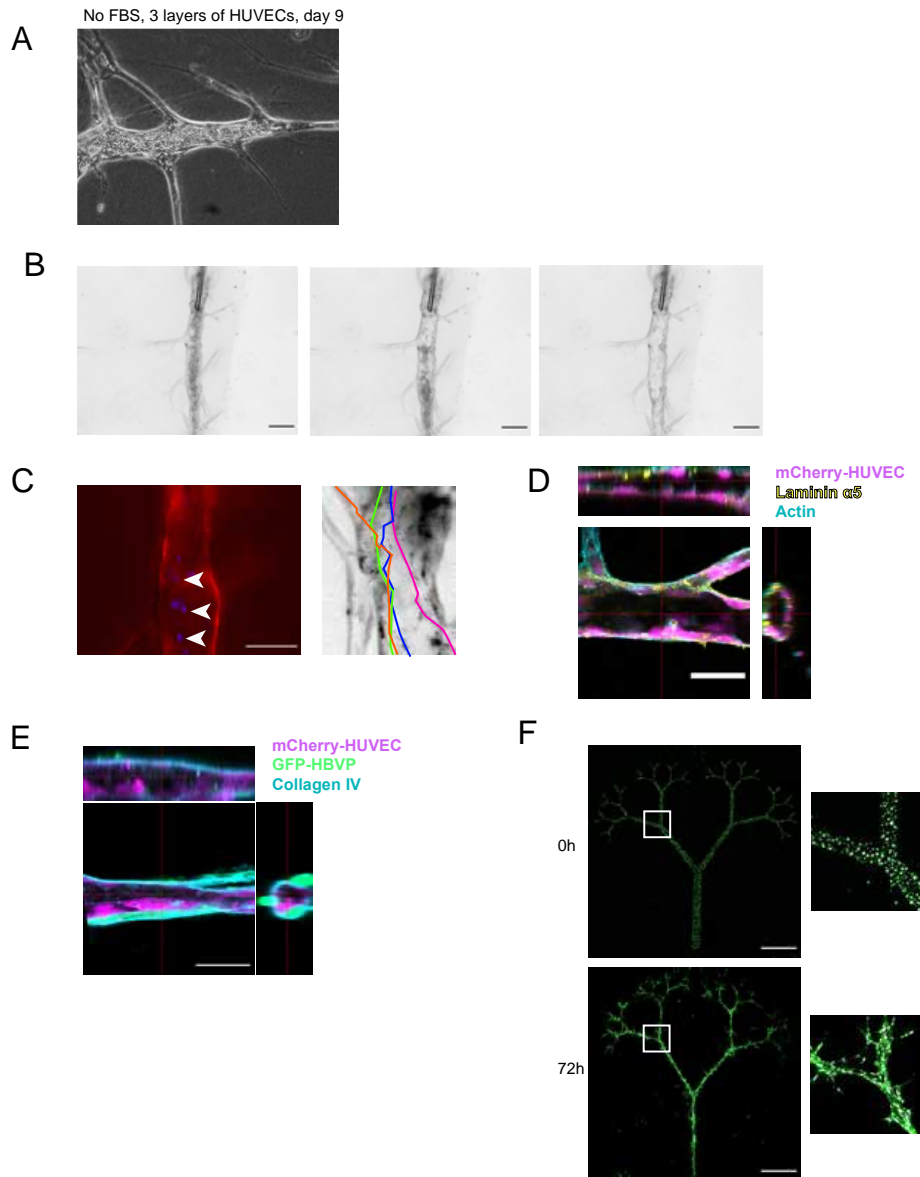


Figure 4.11 Engineering of lumenized, perfusable microvasculature that can be created with full control over vessel architecture.

A) Cell debris observed in the center of a three-layered HUVEC cord after 9 days of culture in serum-free EGM-2. B) Microinjection of PBS into a three-layered microvessel resulted in the removal of cell debris, revealing an intact lumen down the length of the microvessel. C) A three-layered mCherry-HUVEC microvessel (magenta) was perfused with 2 μm diameter blue fluorescent beads (arrowheads). Example bead traces for a different microvessel are shown to the right. D) Confocal microscopy of mCherry-HUVEC cords (magenta) revealed a continuous lumen as indicated by an empty channel surrounded by actin (cyan) and laminin $\alpha 5$ (yellow). E) A three-layered mCherry-HUVEC cord (magenta) was co-cultured with GFP-HBVPs (green), leading to the deposition of a collagen IV (cyan)-rich basement membrane. F) A stylized microvascular network tree with diameters ranging from 184 μm to 12 μm was created by

patterning HUVECs (cytoplasm, EGFP (green) and nuclei, H2B-mScarlet (magenta)) and culturing them in MG-COL1 for 72 hours.

4.5 Discussion

The goal of this study was to identify microenvironmental cues that could encourage the self-organization of patterned endothelial cells into functional microvessels in the context of engineered tissues. Understanding the “design rules” of vasculogenesis *in vitro* can help tissue engineers to efficiently vascularize engineered tissues. Using DPAC, we patterned endothelial cells with high spatial resolution and reproducibility, resulting in cords of endothelial cells with a similar diameter to capillaries (initially 35 μm before condensing into a 1-2 cell-wide line of 8-20 μm). These patterned cords provided us with a reliable assay to test the effects of a variety of microenvironmental cues on the self-organization of endothelial cells initially patterned close together. We found that collagen I was required in the surrounding ECM for the endothelial cells to form elongated structures. However, the endothelial cells scattered over the course of 72 hours. We found that by removing the FBS from the culture media, we could promote cell-cell adhesion and limit the extension of protrusions. Endothelial cords cultured in serum-free media maintained a continuous structure, lumenized, and showed indicators of maturity.

One of the initial steps required for vascular morphogenesis is for the endothelial cells to extend towards each other and make cell-cell adhesions. We found that matrix composition is critical for this process. We were initially interested in culturing the endothelial cords in a basement membrane extract, both to promote the formation of stable microvasculature and to enhance compatibility with possible organoid co-cultures^{35,41,194}. However, the patterned HUVEC cords were unable to maintain their structure in Matrigel, with the line of cells breaking up into several smaller clusters. Fluorescently labeling the matrix revealed that only HUVEC cords cultured in MG-COL1 were able to remodel the ECM, concentrating it in a sheath around themselves in a process known to involve cell contractility^{12,206}. We hypothesize that the endothelial cells require fibrillar matrices such as collagen I that they can exert tension upon in order to elongate and migrate towards each other. Using composite hydrogels like MG-COL1 may be the best solution for organoid co-cultures that require vascularization.

Our initial attempts at endothelial self-organization within the patterned cord assay led to the dissolution of the cord into individual endothelial cells and small clusters over 72 hours. Microenvironmental conditions that were successful within a bottom-up, randomly seeded vasculogenesis assay (Chapter 5) failed to promote self-organization when the endothelial cells were patterned to be initially close to each other. We had not fully appreciated the need to tailor the microenvironment based on

the spatial arrangement of the cells and the cell behaviors required for the desired stages of vascular morphogenesis. This point was further illustrated by the fact that soluble factors known to promote angiogenesis and vasculogenesis (VEGF, FGF, a stem cell cytokine cocktail)¹⁰³ did not improve cord cohesiveness. Pro-angiogenic factors are useful when tip cell-like behaviors such as migration and extension of protrusions are desired^{19,207}, but in the context of microvessel stabilization and maturation, they provided no additional benefit. Instead, we were only able to successfully guide self-organization of endothelial cells into stable microvasculature when we removed the pro-angiogenic FBS. When we closely examined the underlying cell behaviors, we found that FBS was promoting the extension of protrusions and the weakening of cell-cell junctions, both behaviors associated with angiogenic tip cells but not with stable microvasculature^{218,219}. Broadly, one can think of vasculogenesis as a process where endothelial cells must first migrate, proliferate, and extend protrusions in order to make contact with other endothelial cells, and then mature by stabilizing nascent cell-cell adhesions, polarizing, and lumenizing. By using high resolution cell patterning to place the endothelial cells adjacent to each other, we are effectively starting at the midway point of this process. We found that FBS promotes the cell behaviors associated with the early stages of vasculogenesis (proliferation, extension of protrusions) but inhibits the behaviors associated with the later stages of vasculogenesis (stabilization, maturation). We therefore suggest that the

microenvironment applied to engineered microvasculature must be tailored to the current state of the cells and the desired morphogenic behaviors.

The flexibility and high-resolution of DPAC allowed us to create microvessels of any desired shape and size, including capillary-sized microvessels (diameter $\sim 10 \mu\text{m}$) and branched vascular networks. Using this technique, we were able to learn more about the microenvironmental cues that can stimulate the self-organization of densely patterned endothelial cells into microvessels. We believe that there are exciting opportunities to combine this approach with other advanced methods for engineering microvasculature. For example, the microenvironmental cues identified in this paper could be applied to encourage the rapid self-organization of endothelial cells patterned via extrusion bioprinting¹⁴. DPAC could also be used in conjunction with biofabrication methods such as laser ablation¹²⁴ or the bioprinting of sacrificial materials^{115,119} that create endothelial-lined channels hundreds of microns in diameter. By combining fabrication methods, one could create an engineered tissue that is initially perfused with larger endothelial-lined channels but includes densely patterned endothelial cells branching from these channels. Over a few days, the patterned endothelial cells could self-organize into microvessels that anastomose with the channels. This approach would combine the advantages of DPAC (capillary-sized resolution, complete control over structure) with the scalability and perfusability of top-down biofabrication methods.

A limitation of this study is that the vessels were not continuously perfused during culture and were only perfusable after being pierced with a micropipette. Continuous perfusion might have facilitated lumen formation⁷⁰ and prevented the buildup of cell debris within the lumen. Additionally, the luminal shear stress may have aided maturation and quiescence^{220,221}. DPAC imposes many engineering constraints onto a potential microfluidic perfusion system, including the need to create multiple layers of hydrogel and PDMS and then sandwich them together while remaining watertight. Future work will need to be done to engineer a microfluidic device that can successfully perfuse DPAC-patterned microvessels throughout culture.

4.6 Conclusions

Creating hierarchical microvascular networks throughout an engineered tissue is a major goal in the tissue engineering field. We believe that this can be accomplished efficiently through a combination of putting the vascular cells into the initial network structure and by driving the endothelial cells to go through vascular morphogenesis. Using DPAC to pattern cells with high precision, we developed an assay to test how different microenvironmental cues can influence endothelial self-organization into microvessels. We found that collagen I is essential for the

endothelial cells to maintain the initial patterned structure. We also discovered that FBS present in the culture media was de-stabilizing the initial endothelial cord, resulting in scattering instead of tubulogenesis. By removing the FBS from the culture media, we were able to create stable, mature, and lumenized microvessels with precisely controlled geometry.

5 Effect of Endothelial Cell Density on Endothelial Self-Organization

Katelyn A. Cabral, Maxwell C. Coyle, and Zev J. Gartner

Author Contributions: K.A.C, M.C.C., and Z.J.G conceived the project. K.A.C. and M.C.C. performed experiments. K.A.C. and M.C.C. analyzed the data. Z.J.G. supervised experiments. K.A.C. wrote this chapter.

5.1 Abstract

Cell-cell interactions can drive individual and collective cell behaviors, leading to tissue morphogenesis. We observed that patterned HUVEC cords tended to scatter under microenvironmental conditions that resulted in successful vasculogenesis when the endothelial cells were seeded uniformly at a density of 2×10^6 cells/mL. This suggested to us that the spatial context, particularly the global cell density, was another aspect of the microenvironment that could regulate vasculogenesis *in vitro*. Increasing the total endothelial cell density by adding an un-patterned, adjacent layer of dense endothelial cells underneath the patterned endothelial lines resulted in increased cohesion of the endothelial cord. This density-driven phenomenon was limited to vascular cell types (both endothelial and mural). We hypothesized that the endothelial cells were communicating at a distance with each other, resulting in widespread

changes to endothelial cell behavior on the individual and collective scale. However, we were unable to determine the mechanism for this phenomenon. There was not sufficient evidence to support any potential roles of secreted molecules. Future experiments should analyze the effect of endothelial cell density on the endothelial transcriptome. These experiments could potentially identify both the potential “signal” that the endothelial cells use to communicate with each other as well as the subsequent responses.

5.2 Introduction

One parameter that we considered when engineering the microvasculature is cell density, which influences many aspects of the microenvironment. For cells that are initially evenly distributed throughout a tissue, the cell density informs the average distance between any two cells. Increased cell density also increases the total metabolism of the tissue, leading to increased consumption of nutrients and increased production of waste. Additionally, cells are capable of sensing changes in cell density and changing their behavior as a result. The best studied example of this is bacterial quorum sensing, in which collective cell behaviors are achieved as a result of the secretion and detection of extracellular communication molecules²²². Similarly, in vertebrate development, Gurdon et al. described a “community effect” in which the ability of cells to differentiate into muscle is dependent on neighboring cells also

differentiating the same way at the same time²²³. The interaction of cells with their neighbors results in large-scale coordination of cell behavior. The cells could be communicating through direct cell-cell contact, gap junction signaling, or the secretion of diffusible factors²²⁴. Saka et al. created a mathematical model of the community effect and found that having many cells present in the area is required for the phenomenon. Thus, cell density is a property of the microenvironment that could result in a change to cellular behavior and vascular morphogenesis.

The micropatterned endothelial cords described in previous chapters have a high local cell density, in that each cell is initially within a few microns of its nearest neighbors. However, the global cell density, considering the total number of cells per unit volume of extracellular matrix, is low, at an estimated 38,000 cells/mL. In contrast, the cell density of the human body is orders of magnitude is much higher, at approximately 400 million cells/mL (using estimates of 3×10^{13} total cells and assuming a total volume of 70 L for a “standard” 70 kg person)^{225,226}. Most of these cells are erythrocytes. Endothelial cells comprise 2-5% of the total cell count in the human body and would therefore have an approximate cell density of about 8 million cells/mL. Thus, the micropatterned endothelial cords were far less dense than normal human physiology.

To test whether cell density directly influences the self-organization of patterned endothelial cells into microvessels, we increased the global endothelial cell density by including a denser, non-patterned population of endothelial cells into an adjacent layer of the tissue. We observed that this change in global cell density altered both the collective and individual behaviors of the endothelial cells, resulting in a more cohesive cord structure after 72 hours of culture than at the typical lower endothelial cell density typically used in our cord assay. This effect was limited to vascular-related cell types. We tested several hypotheses that could potentially describe the mechanism underlying this density-dependent phenomenon, including the production of secreted molecules that could coordinate endothelial cell self-organization, the metabolism of pro-angiogenic molecules in the media, and changes to ECM mechanical properties as a function of cell density.

5.3 Methods

Detailed methods regarding ECM hydrogel formulation, microscopy, image quantification, and statistical analysis can be found in Chapters 3 and 4.

Cell culture:

As described earlier, human umbilical vein endothelial cells (HUVECs, Lonza) were used between passages 4 and 6 and fed with EGM-2 (Lonza). GFP-HUVECs

were created by transducing HUVECs with a pSicoR-EF1a-EGFP lentivirus and then sorting out GFP⁺ cells using a fluorescence-associated cell sorter (BD Aria II).

Human brain vascular pericytes (HBVPs) were purchased from Sciencell, used between passages 7 and 11, and fed with Pericyte Media (Sciencell). MCF10As were cultured in DMEM/F12 phenol-red free media containing 5% horse serum, 20 ng/mL EGF, 1 µg/mL hydrocortisone, 1 ng/mL cholera toxin, 10 µg/mL insulin, and 1% penicillin-streptomycin.

Vasculogenesis assay:

Wells of an 8-well chamber coverglass slide (Nunc® Lab-Tek™ Chambered Coverglasses, Thermo Fisher Scientific) were pre-coated with a solution of 50% Matrigel in PBS. This coating facilitated the adhesion of the cell-laden hydrogel to the slide. A cell suspension of HUVECs was counted using a Countess Automated Cell Counter (Applied Biosystems). An appropriate number of HUVECs were then pelleted in a 1.5 mL centrifuge tube. Meanwhile, a collagen I solution by neutralizing rat tail collagen I (Corning) with 0.3 M NaOH and mixing with 10X phosphate buffered saline and water. This collagen I solution was then added to growth factor reduced Matrigel (Corning) for a total gel composition of 6 mg/mL Matrigel and 2 mg/mL collagen I. The final ECM solution was then added to the HUVEC pellet and mixed thoroughly via pipetting to create a uniform cell suspension within the hydrogel. Thirty microliters of cell-laden hydrogel solution were added to each well of

the 8-well chamber coverglass slide. The hydrogels were polymerized by incubating for 45 minutes at 37°C. The hydrogels were then fed with 500 µL each of EGM-2 supplemented with 50 ng/mL phorbol 12-myristate 13-acetate (PMA, Sigma-Aldrich).

Cell patterning:

Endothelial cells were patterned using the original protocol of DPAC^{16,173}. The DNA patterns were created by spotting amine-modified oligos onto an aldehyde-functionalized slide (Nexterion AL, Nexterion) using a high-precision liquid deposition machine (Nano eNabler, Nanoforce Biosciences). The DNA patterns were composed of 10-15 µm diameter spots arranged into lines 2 spots wide by 80 spots long. The HUVECs were labeled with 1 µM of lipid-modified oligo and then passed through PDMS flow cells placed over the DNA-patterned surface, as described in Figure 3.2. Upon hybridization of the oligos, the HUVECs adhered to the surface. Non-adherent cells were washed away. The patterned lines of endothelial HUVECs were embedded within a hydrogel containing 6 mg/mL Matrigel, 2 mg/mL collagen I, and 2% Turbo DNase (Life Technologies) and incubated for 45 minutes at 37°C to polymerize. The hydrogel slab was then peeled off the aldehyde-functionalized slide and placed on top of a 30 µL drop of liquid hydrogel (6 mg/mL Matrigel and 2 mg/mL collagen I, hereafter referred to as MG-COL1) before being incubated at 37°C for an additional 45 minutes. For experiments where composite tissues were

created, the patterned HUVEC lines were placed on top of a cell-laden hydrogel droplet with a cell density of 2 million cells/mL (Figure 5.1).

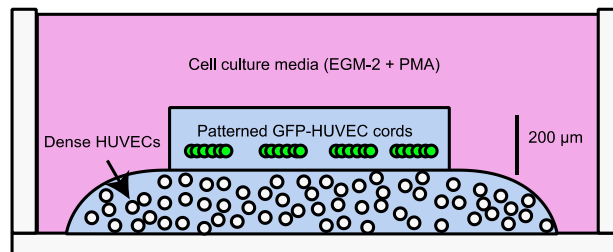


Figure 5.1 The experimental setup for composite DPAC tissues.

Patterned GFP-HUVEC cords were created using DPAC, embedded in MG-COL1, and then placed on top of a droplet of MG-COL1 seeded with 2 million HUVECs/mL.

Proteome profiler:

Conditioned media was collected after 24 hours of culture with HUVEC-laden MG-COL1 hydrogels (60,000 HUVECs in 30 μ L hydrogel, fed with 500 μ L EGM-2 + PMA). This conditioned media was analyzed using a Proteome Profiler Angiogenesis Array and a Proteome Profiler Cytokine Array (R&D Systems). These arrays contain an array of capture antibodies for proteins that have been well established to be involved with angiogenesis or cytokine signaling. Samples were incubated with the array membranes following manufacturer instructions. Membranes were then incubated with IRDye 800 CW Streptavidin and imaged on an infrared imaging system (LI-COR Biosciences). The signal corresponded to the amount of sample protein captured on each antibody spot. The relative fluorescence intensity of each image was measured using FIJI¹⁹⁹.

5.4 Results

During our optimization of the vasculogenesis of patterned HUVEC cords, as described in Chapter 4, we frequently observed that we could not draw direct parallels between patterned HUVEC cords and HUVECs that were uniformly dispersed within a hydrogel. For example, growth factors such as VEGF and FGF-2 that were well described to be pro-vasculogenic in the literature^{100,103} had no effect on the vasculogenesis of the patterned HUVEC cords (Figure 4.6). We found that HUVECs cultured with the same media (EGM-2 + PMA) and extracellular matrix (MG-COL1) behaved differently depending on the assay that was used. HUVECs that were initially uniformly seeded within a droplet of MG-COL1 at a cell density of 2 million cells/mL (hereafter referred to as “vasculogenesis assay”) were able to successfully elongate, migrate, link up with other endothelial cells, and form microvascular networks over the course of 72h (Figure 5.2). In contrast, the patterned HUVECs scattered away from each other. Furthermore, the presence or absence of fetal bovine serum (FBS), which was found to be a key effector of vascular morphogenesis in the patterned HUVEC cords (Chapter 4), had no effect on the structure of HUVEC networks formed during the vasculogenesis assay (Figure 5.3). Because the media, extracellular matrix, and cell source were held constant between these two assays, this would suggest that the spatial context in which the endothelial cells are cultured plays a

major influence in vascular morphogenesis and the response of the endothelial cells to microenvironmental cues.

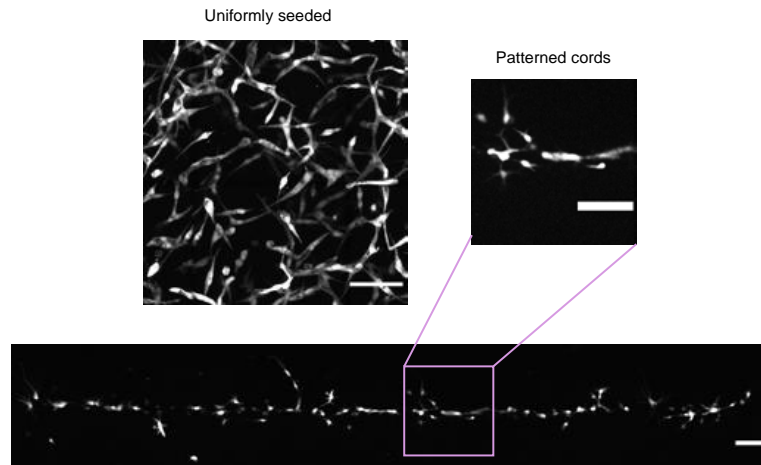


Figure 5.2 The spatial context influences the vasculogenesis of HUVECs.

HUVECs formed complex, elongated multicellular networks over 72 hours when uniformly seeded within an MG-COL1 hydrogel. Image depicts a maximum intensity projection of a tissue section 250 μm in height. HUVECs that were initially patterned into a thin line within an MG-COL1 hydrogel scattered into a discontinuous structure over 72 hours. Scale bar: 100 μm .

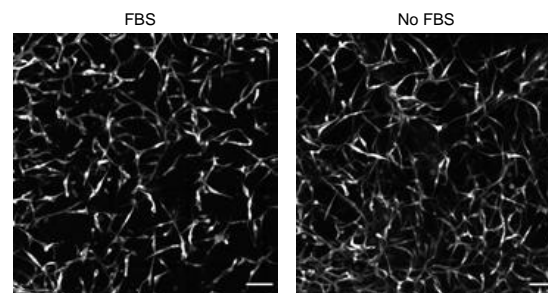


Figure 5.3 Fetal bovine serum (FBS) has no gross morphological effect on the vasculogenesis of GFP-HUVECs uniformly seeded within an MG-COL1 hydrogel.

Images are maximum intensity projections of a tissue section 250 μm in height. Scale bar: 100 μm .

In the patterned cords, the endothelial cells are patterned within a few microns of their nearest neighbors. However, the patterned cords are patterned far apart (1 millimeter in X and Y) and there are only ~1,900 cells total within the 50 μ L tissue. The local cell density is high, but the tissue-wide cell density is low. In the vasculogenesis assay, the cells start off further apart, with an average spacing of 50 microns for a hydrogel seeded at a cell density of 2 million cells/mL (Figure 5.4). Even though the cells in the vasculogenesis assay must travel further to reach each other, the overall cell density is much closer to the physiological endothelial cell density of ~8 million cells/mL of tissue.

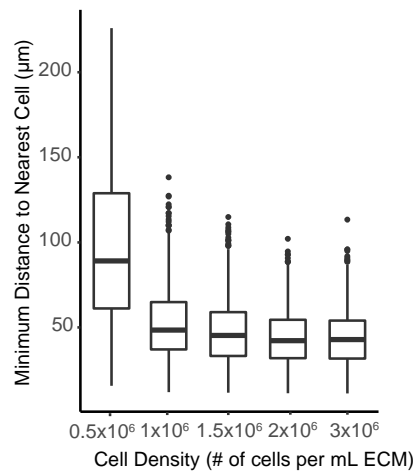


Figure 5.4 Initial cell-cell spacing in the vasculogenesis assay.

Endothelial cells were seeded uniformly within an MG-COL1 hydrogel and then imaged with a confocal microscope. The images were segmented with Imaris and the minimum distance from each cell to its nearest neighbor was calculated.

To explore the role of cell density in vasculogenesis, we created composite DPAC tissues in which the patterned GFP-HUVEC cords were placed on top of a hydrogel droplet containing 2 million non-fluorescent HUVECs/mL (Figure 5.1).

This increased the total cell density of the tissue to 1.2 million cells/mL. This inclusion of this denser, adjacent population of HUVECs resulted in significant changes to cord morphology at 72 hours, with less scattering, more cohesive cord structure, and fewer sprouts (Figure 5.5). The differences in cord morphology could not be explained by a difference in proliferation (Figure 5.6). This effect was not limited to HUVECs. Culture with a dense population of human brain vascular pericytes (HBVPs) resulted in much longer cord segments when cultured in an adjacent tissue layer at a density of 2 million cells/mL. The effect of dense HBVPs may or may not be related to the effect of dense HUVECs, as pericytes are well established as a stabilizer of endothelial cells^{81,91}. MCF10As did not cause the phenotype, suggesting that this effect is vascular-specific and not a function of general cell density (Figure 5.7). These data indicate that increasing the tissue-wide vascular cell density can alter the collective behavior of endothelial cells, promoting self-organization of patterned HUVECs into cohesive multicellular cords.

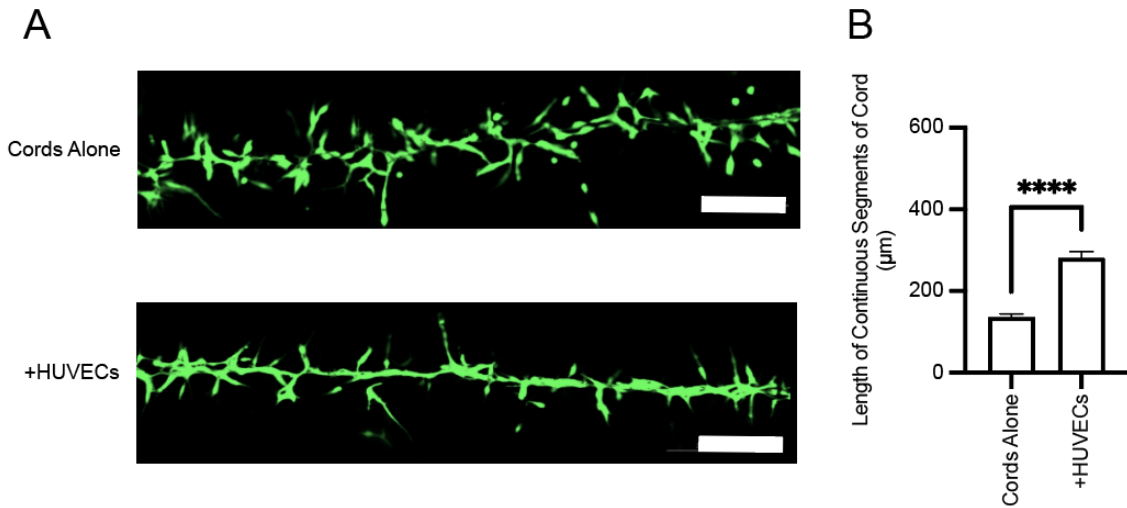


Figure 5.5 The addition of a dense population of HUVECs underneath the patterned HUVEC cords results in a more cohesive cord morphology.

A) Representative images of GFP-HUVEC cords cultured for 72 hours either alone or with the addition of a dense (2×10^6 cells/mL) population of HUVECs directly underneath. Scale bar: 200 μm . B) Quantification of the lengths of cord segments. Data represented as mean \pm SEM. Unpaired t-test, $p < 0.0001$.

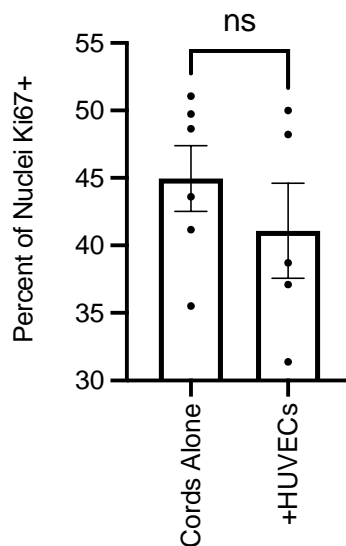


Figure 5.6 Assessment of proliferation in patterned GFP-HUVEC cords after culture with neighboring, dense endothelial cells.

GFP-HUVEC cords were either cultured alone or with a dense population of endothelial cells in an adjacent tissue layer. The cords were fixed after 72 hours and stained for the proliferation marker Ki67 and DAPI. T-test, no significant difference.

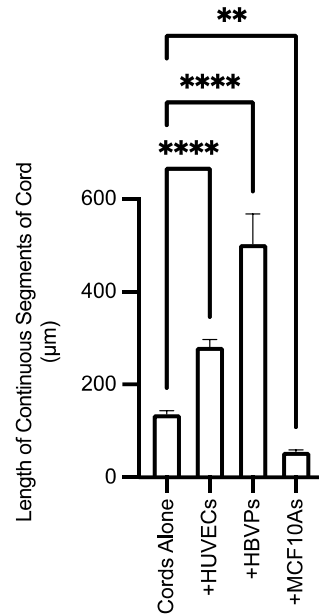


Figure 5.7 Comparison of different cell types in adjacent population to cords.

HUVECs, HBVPs, and MCF10As were cultured in a layer of MG-COL1 directly underneath patterned GFP-HUVEC cords at a cell density of 2×10^6 cells/mL. Only HUVECs and HBVPs were able to cause the GFP-HUVECs in the cord to self-organize into longer cord segments. One-way ANOVA followed by multiple comparisons to Cords Alone. ** = $p < 0.01$. **** = $p < 0.0001$.

Increasing the cell density resulted in tissue-wide changes to cell behavior, resulting in collective vasculogenesis of the cells into cords. This suggested to us that the HUVECs are collectively communicating with each other, and at a certain threshold of this communication signal, each cell adjusts its behavior. On a tissue-wide scale, this results in a shift from scattered, individual cells to long, multicellular endothelial cords. It was unclear by what mechanism the cells were communicating. Potential mechanisms could include direct cell-cell contact, mechanical or chemical changes to the extracellular matrix, secreted soluble proteins, or other short-range diffusible signals.

We hypothesized that a secreted protein was responsible for the observed reduction in angiogenic sprouting and change in endothelial cord morphology as a function of cell density. We analyzed media conditioned by dense HUVECs cultured in MG-COL1 using a Proteome Profiler assay to determine which angiogenesis-associated proteins were secreted by the endothelial cells. We found that the dense HUVECs secreted growth factors including members of the IGF1R family as well as several proteins involved in matrix remodeling (MMP-9, TIMP-1, uPA) (Figure 5.8). We also found that VEGF was depleted by 85% compared to non-conditioned media, corresponding to a final concentration of 0.3 ng/mL. VEGF is a well-established driver of angiogenesis^{18,227} and it is possible that excess amounts of VEGF could drive the scattering and sprouting phenotypes observed. We hypothesized that each endothelial cell uptakes a certain amount of VEGF, and that by increasing the total cell number of endothelial cells per milliliter of media, we were depleting the excess VEGF, allowing the endothelial cells in the cords to undergo vasculogenesis into long, multicellular cords. However, reducing the VEGF concentration of EGM-2 + PMA to 0.3 ng/mL did not improve the cohesiveness of the cords (Figure 5.9). To assess whether soluble factors secreted into the media were driving this phenotype, we cultured patterned HUVEC cords with media conditioned by dense HUVECs, diluted 1:1 with fresh media. The conditioned media was unable to recapitulate the more cohesive cord morphology seen in the composite DPAC tissues (Figure 5.10). This

result could be explained in a few ways: the endothelial cells are not communicating with each other through secreted soluble factors, the soluble factors are getting bound by the ECM and are not present in conditioned media, or that the soluble factors have a short half-life and do not remain functional in the conditioned media.

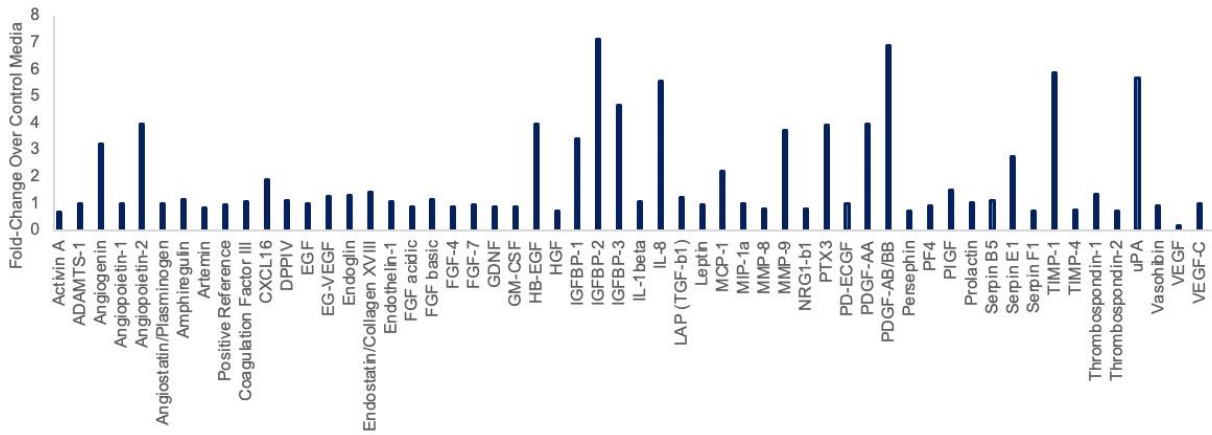


Figure 5.8 Analysis of secreted proteins found in conditioned media from dense HUVECs.

Conditioned media was collected from wells containing 2×10^6 HUVECs/mL in MG-COL1 and analyzed using a Proteome Profiler assay. Bars represent the fold-change in signal intensity over control media (EGM-2 + PMA that was cultured with cell-free MG-COL1).

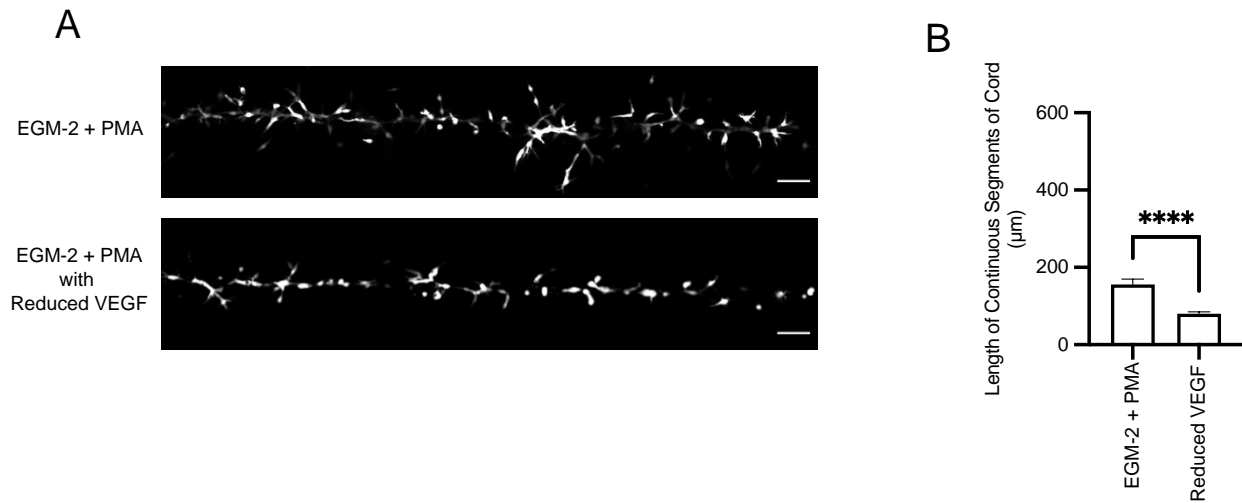


Figure 5.9 Reduction of VEGF in the media did not recapitulate the effect of dense, neighboring HUVECs.

A) Representative images of GFP-HUVEC cords after 72 hours of culture with either standard EGM-2 + PMA or a version with EGM-2 + PMA containing 0.3 ng/mL VEGF. B) Quantification of the cohesiveness of the GFP-HUVEC cords. The lengths of each continuous segment of each cord were measured. The bars represent the mean \pm SEM for each condition. Unpaired t-test, $p < 0.0001$.

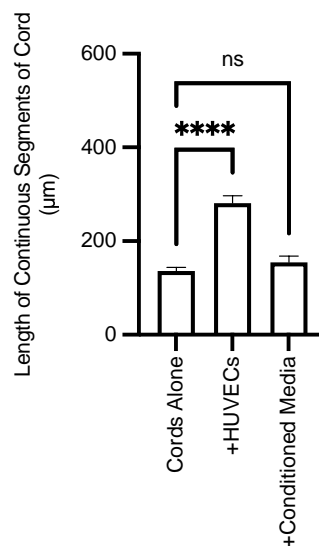


Figure 5.10 Conditioned media could not recapitulate effect of dense, adjacent HUVEC population on the self-organization of patterned GFP-HUVEC cords.

Conditioned media was collected from 60,000 HUVECs grown in MG-COL1 and fed daily with 500 μ L EGM-2 + PMA, diluted 1:1 with fresh media, and used to feed patterned GFP-HUVEC cords. The lengths of each continuous segment of each cord were measured. The bars represent the mean \pm SEM for each condition. One way ANOVA with multiple comparisons to Cords Alone. **** = $p < 0.0001$.

An alternate hypothesis is that the dense population of HUVECs influences the patterned GFP-HUVEC cords by inducing changes in ECM mechanical properties. Staining the ECM revealed that HUVECs remodel the surrounding ECM while undergoing vasculogenesis, wrapping it around themselves and aligning it towards the tips of new branches (Figure 5.11). This matches what other researchers have shown; endothelial cells can compact and align collagen I between themselves as they undergo vasculogenesis. In doing so, the endothelial cells create lines of tension that facilitate cell migration and elongation toward each other^{60,62,63}. Dense HUVECs cultured directly underneath GFP-HUVEC cords remodel their ECM, leading to an overall compaction or concentration of the ECM (Figure 5.11). Although one could predict that the highest tensional forces would be between two adjacent cells in a GFP-HUVEC cord, it is possible that the overall ECM remodeling caused by the dense HUVEC population is acting on the patterned GFP-HUVECs and causing the observed changes in vasculogenic behaviors.

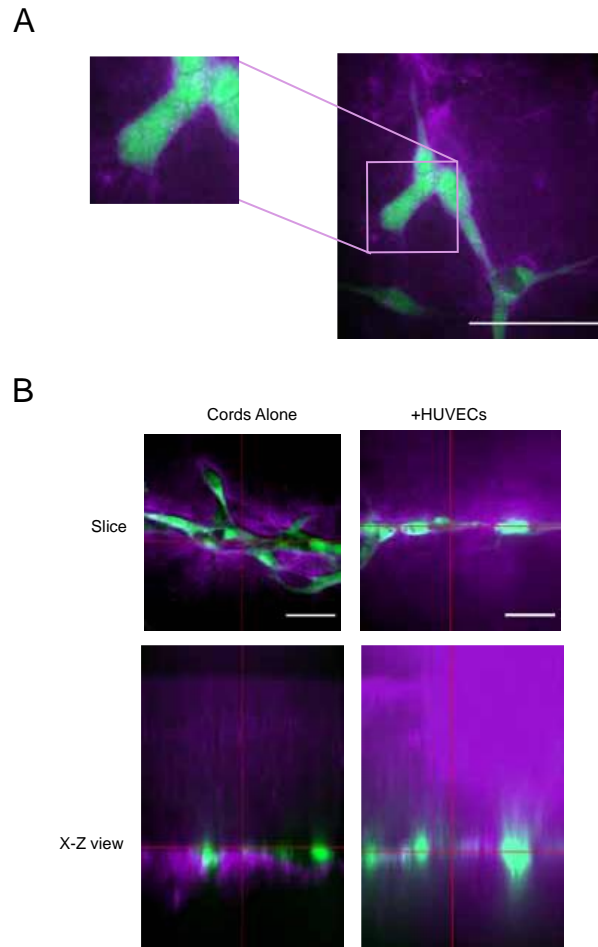


Figure 5.11 Densely seeded HUVECs remodel and concentrate the ECM.

An Alexa Fluor 647-conjugated NHS-ester was used to dye the ECM (magenta) and visualize how it was remodeled by HUVECs (green). A) Dense HUVECs (2×10^6 cells/mL) in MG-COL1 remodel their ECM by pulling it towards themselves and wrapping it around them as a sheath. Image taken after 48 hours of culture. Scale bar: 50 μm . B) Confocal imaging (300 μm total height, z-stack with slices 1.37 μm thickness) of GFP-HUVEC cords cultured with or without a dense population of HUVECs underneath revealed that the ECM becomes more concentrated because of the increased cell density. In cords cultured alone, the ECM is not concentrated except for a small sheath around the cord.

5.5 Discussion

In this chapter, we provide evidence for a community effect in vascular morphogenesis, with high cell density driving endothelial self-organization into long,

cohesive microvascular cords. We created composite tissues where the top portion of the tissue contained DPAC cords and the bottom part of the tissue where the endothelial cells were uniformly seeded at a density of 2 million cells/mL. This setup raised the total cell density of the tissue. The patterned endothelial cords cultured with the dense endothelial cells were better able to self-organize into continuous, cohesive cords than patterned endothelial cords cultured alone. This suggests that there is a cell-non-autonomous phenomenon at play. The endothelial cells are somehow able to detect the total cell density of the tissue and their vasculogenic behaviors change as a function of cell density. At low cell densities, the patterned cells scatter, and at the increased cell density, the patterned cells are much more likely to stay together as one cohesive cord.

The mechanism underlying this phenomenon is unknown. The cells seem to be communicating with each other and coordinating their behavior accordingly. However, there were no soluble cues recoverable in conditioned media that were sufficient to induce the phenotype. This negative result could be explained by a short half-life of the signaling molecule or the binding of certain growth factors to the ECM (preventing it from entering conditioned media). An alternate explanation for the observed phenotype could be that the cells are actively depleting the media (or ECM) of certain pro-angiogenic components as a function of total cell number, and that the dense population of endothelial cells underneath the patterned cords is acting as a

sink for unwanted pro-angiogenic components. We briefly tested this idea by testing whether the depletion of VEGF from the media would be able to recapitulate the phenotype caused by the addition of the dense HUVECs. Though there is no direct evidence to support this, we could also speculate that the active component of FBS that causes scattering in patterned cords (Chapter 4) could also be internalized or metabolized as a function of total cell number. If that were true, the dense HUVEC population could be influencing the self-organization of the patterned endothelial cords by removing some of the excess FBS from the culture.

To test the hypothesis that widespread remodeling of the ECM by the dense HUVECs is causing the observed phenotype in the patterned cords, future research should use rheology and/or atomic force microscopy to measure the stiffness of cell-free MG-COL1 hydrogels and MG-COL1 hydrogels containing 2×10^6 HUVECs/mL after 48 hours of culture. If the dense HUVECs are making the MG-COL1 hydrogels significantly stiffer, one could artificially crosslink cell-free MG-COL1 gels to match that stiffness and then assess the self-organization of GFP-HUVECs patterned into a cord. If increased hydrogel stiffness is successful at recapitulating the phenotype, that would suggest that the observed density-dependent phenomena is solely based on mechanics.

Future work on this project should include a transcriptomic analysis of patterned HUVECs cultured with and without the adjacent population of dense HUVECs. The pattern of gene expression that is upregulated/downregulated by the addition of the dense HUVECs might provide some insight into both the signal by which the endothelial cells are communicating as well as the response by the patterned HUVECs. A complementary transcriptomics experiment could compare endothelial cells cultured at a range of cell densities (1×10^5 cells/mL - 5×10^6 cells/mL) and see how gene expression varies within each endothelial cell as a function of cell density. It would also be useful to separate out the effects of cell number and cell density. This could be achieved by increasing and/or decreasing the volume of the gel containing dense HUVECs without changing the cell density. This would change the number of cells in total (and cells per mL of media) without changing the distance between cells. This may be helpful to discern between mechanisms related specifically to cell density (like quorum sensing) and mechanisms that are a result of the number of cells (like cells consuming or metabolizing certain media components).

6 Discussion

Vascularization is essential for the success of engineered tissues and organs. As the field of tissue engineering matures and progress is made towards the goal of replacing damaged organs, the challenge of how to vascularize engineered tissues is of high priority. One strategy for accomplishing tissue vascularization is to bioprint the endothelial and mural cells into a network structure and to encourage self-organization of the cells into microvessels through manipulation of the microenvironment. The primary objective of my dissertation research was to understand the rules that govern the self-organization of patterned endothelial cells into functional capillary-like microvessels.

6.1 Accomplishments

To accomplish this research, we developed an improved DPAC protocol for the creation of spatially defined cell patterns and microtissues with extremely high precision. Compared to previous iterations of this protocol^{16,173}, this protocol can be done simply, inexpensively, and without the use of expensive reagents or specialized equipment. Although the primary goal of developing this protocol was to make the technique widely accessible to other researchers, it also helped me to accomplish my research more efficiently, cheaply, and at higher throughput. In particular, switching

from the slow printing of DNA by the Nano eNabler (3 hours per slide) to the much faster photopatterning of DNA¹⁷⁸ (less than 2 hours per batch of 5 slides) allowed me to do many more experiments and with higher reproducibility.

The creation of patterned capillary-sized lines of endothelial cells using DPAC provided me with a useful and highly reproducible assay for testing how the microenvironment influences the self-organization of endothelial cells into capillaries. By starting with the same initial boundary conditions in every experiment, I could change one aspect of the microenvironment and observe how it affected the overall microvessel morphology. The ultimate aim of this dissertation was to identify the microenvironmental cues necessary for pre-patterned endothelial cells to fully reconstitute mature microvasculature, defined as a perfusable endothelial tube with a continuous lumen at least 5 μm wide, an intact basement membrane with laminin and collagen IV, and permeability similar to in vivo vasculature of approximately 1×10^{-8} m/s. I was able to accomplish most, but not all of this goal by providing a microenvironment that promoted self-organization and vascular stabilization. I was able to engineer perfusable endothelial tubes with a continuous, millimeters-long lumen. This vasculature was stable, with few changes in vascular morphology after 7 days and viability maintained for at least two weeks (data not shown). These engineered microvessels were surrounded by a basement

membrane that included collagen IV. The microvessels had claudin-5 and ZO-1 present at their cell-cell junctions, indicating the presence of tight junctions.

6.2 Problems Left to Solve

I was unable to assess whether the engineered microvessels had permeability like that of capillaries *in vivo*. The presence of tight junctions and smooth VE-cadherin junctions suggests that they may have had adequate permeability²²⁸, but this has yet to be determined. To assess permeability, I could inject 70 kDa FITC-dextran into the lumen and measure fluorescence outside the lumen over time to measure it¹⁴⁰.

However, since the lumen is open on both ends during the injection, it's possible that there would be extra background fluorescence from FITC-dextran coming from the inlet or outlet of the microvessel. If the vascular permeability was too high and the microvessels were leaky, I could address this problem by adding pericytes on top of the endothelial cords²²⁹ or reducing the concentration of VEGF in the culture media¹⁰¹.

Another limitation of the work presented in this dissertation was that these endothelial cords were cultured under static conditions and could not be perfused continuously during culture. In the early stages of microvessel development, the presence of interstitial fluid flow would have promoted vasculogenesis and the formation of lumens⁷³. After the microvessels had lumenized, fluid shear stress could

be applied, promoting endothelial alignment, maturation, and quiescence²²¹. Having a fully perfused engineered capillary network could promote the survival of surrounding tissues and facilitate studies of intravasation/extravasation of immune cells and the response of endothelial cells to pro-thrombotic or pro-inflammatory signals. DPAC imposes several engineering constraints on any perfusion device, including the requirement to remove the tissue intact from a glass slide and add a hydrogel precursor solution adjacent to the patterned cells. The need for separate tissue layers for the tissue fabrication step makes it more difficult to form a leak-proof seal²³⁰. This problem could be overcome in a few ways. One option could be to use a biocompatible, quick-acting adhesive such as a cyanoacrylate glue to glue the two halves of the device together. Another solution could be to create a rigid plastic jig that is held together by screws, clamps, or magnets^{231,232}. This could exert uniform pressure across the microfluidic device, improving the seal between the PDMS layers so that media could not leak out. An alternate approach would be to modify a micromanipulator so that it contained several microneedles, each connected to a syringe pump. Each developing microvessel could be punctured with an inlet needle and an outlet needle, resulting in a constant stream of fluid through the lumen of the vessel. A disadvantage of this approach is that it would only be possible after 3-5 days of culture when the endothelial cords had lumenized.

6.3 Significance within field of microvascular tissue engineering

My vascularization philosophy is to provide the initial network structure for endothelial and mural cells and then encourage vasculogenic cell behaviors using the microenvironment. This will promote the efficient formation of microvascular networks within engineered tissues. This is similar to the strategy employed by Brassard and colleagues, where they bioprinted endothelial cells at a high density into an ECM and allowed them to form vascular tubes over six days¹⁴. I believe that this hybrid approach to engineering microvasculature, that harnesses both the power of biofabrication technology and the intrinsic self-organization, will prove to be the most efficient method of fabricating microvascular networks in the 10-100 μm size range.

A strength of this work is that we were able to engineer lumenized microvessels with higher spatial resolution and control than anyone else in the field. This allowed us to create structures that were truly capillary sized as well as hierarchical microvascular networks that mimic those found in vivo. I think DPAC is an ideal method for applications that would involve modeling the interactions between the vasculature and other cell types. For example, one could replicate the specific structure of the glomerulus and its spatial relationships to the other cell types of the kidney¹²⁴ by using DPAC to pattern all of the relevant cell types. However, the specific method used to place the cells, DPAC, is not well suited for all applications

because it lacks scalability in three dimensions. For larger, more three-dimensional tissues, I would instead propose that cell-dense extrusion bioprinting be used as the fabrication method¹⁴. The same design rules that I discovered during my dissertation research (collagen I is required, limit the amount of serum in the media to prevent scattering, etc.) can easily be applied to cell-dense extrusion bioprinting methods. I hope that this would facilitate and expedite the formation of perfusable microvasculature. Furthermore, this method could easily be combined with top-down and/or bottom-up microvascular tissue engineering strategies. It would be possible to create a multi-material bioprinted tissue that includes endothelial cells uniformly dispersed within the stroma (bottom-up), dense lines of endothelial cells about 50 μm in diameter (hybrid), and endothelial-lined sacrificial channels in the 500 – 1000 μm range (top-down). Initially, media would only be carried through the large endothelial-lined channels. After a few days, the dense lines of endothelial cells would self-organize into perfused microvessels. Meanwhile, the uniformly dispersed endothelial cells in the bulk of the tissue would be undergoing vasculogenesis to form capillary networks. The final product would be a hierarchical vascular network that could perfuse the tissue efficiently and re-organize itself to meet the needs of the tissue.

6.4 Unresolved Questions

One theme that came up during this research project was the importance of spatial context in the response of endothelial cells to microenvironmental cues. For example, as described in Chapter 4, endothelial cells in DPAC-patterned cords respond very strongly to FBS. However, when the endothelial cells are arranged as a monodispersion of cells at a density of 2×10^6 cells/mL, there are no gross differences in microvascular network formation as a function of FBS (Figure 5.2). Endothelial cells in DPAC cords and endothelial cells uniformly seeded in the hydrogels are exposed to the same microenvironment – the same media, the same ECM. The only difference between the two experiments is the relative density and spacing of cells to each other. It is unclear by what mechanism the endothelial cells are sensing the cell density or other spatial contexts. To gain some insight into this mechanism, a transcriptomic analysis of cells cultured at different global cell densities should be done. This might provide clues as to both the signal that is affecting individual and collective endothelial cell behavior as well as the response that it induces in endothelial cells to cause those behaviors.

Another open question is the identity of the component in FBS that is driving such a marked change in both individual and collective endothelial cell behavior. It must be protein in nature, as treatment of the FBS with proteinase K, a non-specific

protease, abrogated the effects of FBS. Further, we know that it has a high molecular weight, greater than 200 kilodaltons. There are not that many proteins of such size known to be present at high concentrations in serum, especially those known to influence angiogenesis, yet all tested candidate proteins were unable to recapitulate the phenotype caused by FBS. Thus, the active component is either a protein that has not been previously connected with endothelial cell behavior or is part of a complex of smaller proteins. Either way, this molecule(s) and the way it affects endothelial cells would represent a previously un-studied aspect of endothelial cell biology. There are a few ways that one could go about trying to identify this mystery molecule(s). One approach is to use proteomics – fractionating the FBS using a high-performance liquid chromatography instrument, identifying which fractions can drive the scattering phenotype, and then performing mass spectrometry on the successful fractions to identify the proteins present. Alternately, a transcriptomic approach could be taken, where we could collect RNA from HUVEC cords cultured with or without FBS and identify the genes that are upregulated or downregulated in response to FBS. The clusters of genes that are differentially expressed across conditions may suggest that the active component of FBS is a member of certain signaling pathways. Follow-up experiments with proteins in these pathways may confirm the identity of the active component.

6.5 Future Directions

The self-organization of organ-specific endothelial cells would be an interesting topic for further research. Endothelial cells are heterogeneous, differing substantially based not only on vessel type (artery vs capillary vs vein), but also on the specific organ in which they reside^{94–96,233,234}. Endothelial cells adapt their gene expression, morphology, secretome, and behavior to meet the needs of their local niche.

Endothelial cells in the brain are tightly adhered to each other and have a thick basement membrane to form the blood-brain barrier, while sinusoidal endothelial cells in the liver have large fenestrations, or gaps, in between the cells to maximize fluid exchange. There is much that is unknown about the process by which these organ-specific microvascular networks arise during development. Moreover, as the biomedical field has become more interested in creating 3D microphysiological systems to model various diseases and test drugs on them^{3,4,235}, it would be beneficial to be able to create organ-specific microvascular networks *in vitro* that mimic the specific structure and functionality of the organs being studied. DPAC could be used as a platform to study the self-organization of these organ-specific microvascular networks. Primary organ-specific endothelial cells or immature iPSC-derived endothelial cells could be patterned into microvessels that are intertwined with the other cell types in the niche, including parenchymal and stromal cells. Using this platform, we could learn a great deal about the interactions between the different cell

types in an organ's vascular niche and how different components of the microenvironment, including ECM, paracrine factors, and direct cell-cell contact, influence the self-organization and maturation of endothelial cells into organ-specific microvasculature. Because DPAC is a flexible technique, the relative positioning of various cell types to the vasculature, the initial structure of the endothelial cells, and the composition of the ECM could be studied individually and in combination to assess the influence of those factors on the development of organ-specific microvasculature.

6.6 Conclusion

In summary, I developed an assay to systematically test how different aspects of the microenvironment influence the self-organization of pre-patterned endothelial cells into capillary-like microvessels. I found that in order to guide vasculogenesis of these patterned endothelial cells, I needed to tailor the microenvironment to promote the desired cell behaviors. I hope that this work sheds some insight onto the rules governing the self-organization of endothelial cells *in vitro* and guides future tissue engineers to create more complex and sophisticated vascularized tissues.

References

1. Aboulkheyr Es, H., Montazeri, L., Aref, A. R., Vosough, M. & Baharvand, H. Personalized Cancer Medicine: An Organoid Approach. *Trends Biotechnol.* **xx**, 1–14 (2018).
2. Huch, M., Knoblich, J. A., Lutolf, M. P. & Martinez-Arias, A. The hope and the hype of organoid research. *Development* **144**, 938–941 (2017).
3. Marx, U. Biology-inspired microphysiological system approaches to solve the prediction dilemma of substance testing. *ALTEX* 1–64 (2016).
4. Kamm, R. D. *et al.* Perspective: The promise of multi-cellular engineered living systems. *APL Bioeng.* **2**, 040901 (2018).
5. Stephens, N., Sexton, A. E. & Driessen, C. Making Sense of Making Meat: Key Moments in the First 20 Years of Tissue Engineering Muscle to Make Food. *Front. Sustain. Food Syst.* **3**, (2019).
6. Hirsch, T. *et al.* Regeneration of the entire human epidermis using transgenic stem cells. *Nature* **551**, 327–332 (2017).
7. Giwa, S. *et al.* The promise of organ and tissue preservation to transform medicine. *Nat. Biotechnol.* **35**, 530–542 (2017).
8. Khademhosseini, A. & Langer, R. A decade of progress in tissue engineering. *Nat. Protoc.* **11**, 1775–1781 (2016).
9. Krogh, A. The number and distribution of capillaries in muscles with calculations of the oxygen pressure head necessary for supplying the tissue. *J. Physiol.* **52**, 409–415 (1919).
10. Folkman, J. & Hochberg, M. Self-regulation of growth in three dimensions. *J. Exp. Med.* **138**, (1973).
11. Griffith, L. G. & Swartz, M. a. Capturing complex 3D tissue physiology in vitro.

- Nat. Rev. Mol. Cell Biol.* **7**, 211–224 (2006).
12. Utzinger, U., Baggett, B., Weiss, J. A., Hoying, J. B. & Edgar, L. T. Large-scale time series microscopy of neovessel growth during angiogenesis. *Angiogenesis* 219–232 (2015).
 13. Auger, F. a, Gibot, L. & Lacroix, D. The pivotal role of vascularization in tissue engineering. *Annu. Rev. Biomed. Eng.* **15**, 177–200 (2013).
 14. Brassard, J. A., Nikolaev, M., Hübscher, T., Hofer, M. & Lutolf, M. P. Recapitulating macro-scale tissue self-organization through organoid bioprinting. *Nat. Mater.* (2020).
 15. Han, S. *et al.* Constructive remodeling of a synthetic endothelial extracellular matrix. *Sci. Rep.* **5**, 18290 (2015).
 16. Todhunter, M. E. *et al.* Programmed synthesis of three-dimensional tissues. *Nat. Methods* **12**, 975–981 (2015).
 17. Chung, A. S. & Ferrara, N. Developmental and Pathological Angiogenesis. *Annu. Rev. Cell Dev. Biol.* **27**, 563–584 (2011).
 18. Potente, M., Gerhardt, H. & Carmeliet, P. Basic and therapeutic aspects of angiogenesis. *Cell* **146**, 873–87 (2011).
 19. Betz, C., Lenard, A., Belting, H. & Affolter, M. Cell behaviors and dynamics during angiogenesis. *Development* **143**, 2249–2260 (2016).
 20. Folkman, J. Tumor Angiogenesis: Therapeutic Implications. *Nejm* **285**, (1971).
 21. Jain, R. K. Antiangiogenesis Strategies Revisited: From Starving Tumors to Alleviating Hypoxia. *Cancer Cell* **26**, 605–622 (2014).
 22. Chung, A. S., Lee, J. & Ferrara, N. Targeting the tumour vasculature: insights from physiological angiogenesis. *Nat. Rev. Cancer* **10**, 505–514 (2010).
 23. Tonnesen, M. G., Feng, X. & Clark, R. A. F. Angiogenesis in wound healing. *J.*

- Investig. Dermatology Symp. Proc.* **5**, 40–46 (2000).
24. Kumar, P. *et al.* Role of angiogenesis and angiogenic factors in acute and chronic wound healing. *Plast. Aesthetic Res.* **2**, 243 (2015).
 25. Góth, M. I., Hubina, E., Raptis, S., Nagy, G. M. & Tóth, B. E. Physiological and pathological angiogenesis in the endocrine system. *Microsc. Res. Tech.* **60**, 98–106 (2003).
 26. Arevalo, J. F. *et al.* Intravitreal bevacizumab (avastin) for proliferative diabetic retinopathy: 6-Months follow-up. *Eye* **23**, 117–123 (2009).
 27. Morgan, J. T., Shirazi, J., Comber, E. M., Eschenburg, C. & Gleghorn, J. P. Fabrication of centimeter-scale and geometrically arbitrary vascular networks using in vitro self-assembly. *Biomaterials* **189**, 37–47 (2018).
 28. Perry, L., Flugelman, M. Y. & Levenberg, S. Elderly Patient-Derived Endothelial Cells for Vascularization of Engineered Muscle. *Mol. Ther.* **25**, (2017).
 29. Crosby, C. O. *et al.* Quantifying the vasculogenic potential of iPSC-derived endothelial progenitors in collagen hydrogels. *Tissue Eng. Part A* 1–44 (2019).
 30. Moya, M. L., Hsu, Y.-H., Lee, A. P., Hughes, C. C. W. & George, S. C. In Vitro Perfused Human Capillary Networks. *Tissue Eng. Part C Methods* **19**, 730–737 (2013).
 31. Sobrino, A. *et al.* 3D microtumors in vitro supported by perfused vascular networks. *Sci. Rep.* **6**, 31589 (2016).
 32. Mazio, C., Casale, C., Imperato, G., Urciuolo, F. & Netti, P. A. Recapitulating spatiotemporal tumor heterogeneity in vitro through engineered breast cancer microtissues. *Acta Biomater.* (2018).
 33. Lee, H., Park, W., Ryu, H. & Jeon, N. L. A microfluidic platform for

- quantitative analysis of cancer angiogenesis and intravasation. *Biomicrofluidics* **8**, 054102 (2014).
34. Bersini, S. *et al.* A microfluidic 3D invitro model for specificity of breast cancer metastasis to bone. *Biomaterials* **35**, 2454–2461 (2014).
 35. Pham, M. T. *et al.* Generation of human vascularized brain organoids. *Neuroreport* **1** (2018).
 36. Nie, Y. Z. *et al.* Recapitulation of hepatitis B virus–host interactions in liver organoids from human induced pluripotent stem cells. *EBioMedicine* **35**, 114–123 (2018).
 37. Homan, K. A. *et al.* Flow-enhanced vascularization and maturation of kidney organoids in vitro. *Nat. Methods* **16**, 255–262 (2019).
 38. Takebe, T. *et al.* Vascularized and functional human liver from an iPSC-derived organ bud transplant. *Nature* **499**, 481–4 (2013).
 39. Osaki, T., Sivathanu, V. & Kamm, R. D. Vascularized microfluidic organ-chips for drug screening, disease models and tissue engineering. *Curr. Opin. Biotechnol.* **52**, 116–123 (2018).
 40. Paek, J. *et al.* Microphysiological Engineering of Self-Assembled and Perfusable Microvascular Beds for the Production of Vascularized Three-Dimensional Human Microtissues. *ACS Nano* (2019).
 41. Zhang, S., Wan, Z. & Kamm, R. D. Vascularized organoids on a chip: strategies for engineering organoids with functional vasculature. *Lab Chip* 473–488 (2021).
 42. Fleischer, S., Tavakol, D. N. & Vunjak-Novakovic, G. From Arteries to Capillaries: Approaches to Engineering Human Vasculature. *Adv. Funct. Mater.* **1910811**, 1–23 (2020).
 43. Bogorad, M. I. *et al.* Review: in vitro microvessel models. *Lab Chip* **15**, 4242–

- 4255 (2015).
44. Risau, W. & Flamme, L. Vasculogenesis. *Cell Dev. Biol* **1**, 73–91 (1995).
 45. Schmidt, A., Brixius, K. & Bloch, W. Endothelial precursor cell migration during vasculogenesis. *Circ. Res.* **101**, 125–136 (2007).
 46. Downs, K. M. Florence Sabin and the mechanism of blood vessel lumenization during vasculogenesis. *Microcirculation* **10**, 5–25 (2003).
 47. Lammert, E. & Axnick, J. Vascular lumen formation. *Cold Spring Harb. Perspect. Med.* **2**, a006619 (2012).
 48. Wacker, A. & Gerhardt, H. Endothelial development taking shape. *Curr. Opin. Cell Biol.* **23**, 676–85 (2011).
 49. Hogan, B. M. & Schulte-Merker, S. How to Plumb a Pisces: Understanding Vascular Development and Disease Using Zebrafish Embryos. *Dev. Cell* **42**, 567–583 (2017).
 50. Fish, J. E. & Wythe, J. D. The molecular regulation of arteriovenous specification and maintenance. *Dev. Dyn.* **244**, 391–409 (2015).
 51. Eelen, G., Treppe, L., Li, X. & Carmeliet, P. Basic and Therapeutic Aspects of Angiogenesis Updated. *Circ. Res.* **127**, 310–329 (2020).
 52. Tsuji-Tamura, K. & Ogawa, M. Morphology regulation in vascular endothelial cells. *Inflamm. Regen.* **38**, 25 (2018).
 53. Davis, G. E., Bayless, K. J. & Mavila, A. Molecular basis of endothelial cell morphogenesis in three-dimensional extracellular matrices. *Anat. Rec.* **268**, 252–275 (2002).
 54. Park, Y. K. *et al.* In Vitro Microvessel Growth and Remodeling within a Three-dimensional Microfluidic Environment. *Cell. Mol. Bioeng.* **7**, 15–25 (2014).
 55. Nowak-Sliwinska, P. *et al.* Consensus guidelines for the use and interpretation of

- angiogenesis assays. Angiogenesis* (Springer Netherlands, 2018).
56. Whisler, J. a, Chen, M. B. & Kamm, R. D. Control of Perfusable Microvascular Network Morphology Using a Multiculture Microfluidic System. *Tissue Eng. Part C. Methods* **20**, 1–38 (2013).
 57. Bersini, S. *et al.* Cell-microenvironment interactions and architectures in microvascular systems. *Biotechnol. Adv.* (2016).
 58. Francis, M. E., Uriel, S. & Brey, E. M. Endothelial cell-matrix interactions in neovascularization. *Tissue Eng. Part B. Rev.* **14**, 19–32 (2008).
 59. Gordon, E., Schimmel, L. & Frye, M. The Importance of Mechanical Forces for in vitro Endothelial Cell Biology. *Front. Physiol.* **11**, 1–20 (2020).
 60. Rosenfeld, D. *et al.* Morphogenesis of 3D vascular networks is regulated by tensile forces. *Proc. Natl. Acad. Sci.* **113**, 201522273 (2016).
 61. Sieminski, A. L., Hebbel, R. P. & Gooch, K. J. The relative magnitudes of endothelial force generation and matrix stiffness modulate capillary morphogenesis in vitro. *Exp. Cell Res.* **297**, 574–584 (2004).
 62. Korff, T. & Augustin, H. G. Tensional forces in fibrillar extracellular matrices control directional capillary sprouting. *J. Cell Sci.* **112** (Pt 1, 3249–3258 (1999).
 63. McLeod, C. *et al.* Microscopic matrix remodeling precedes endothelial morphological changes during capillary morphogenesis. *J. Biomech. Eng.* **135**, 71002 (2013).
 64. Kniazeva, E. & Putnam, A. J. Endothelial cell traction and ECM density influence both capillary morphogenesis and maintenance in 3-D. *Am. J. Physiol. Physiol.* **297**, C179–C187 (2009).
 65. Yamamura, N., Sudo, R., Ikeda, M. & Tanishita, K. Effects of the Mechanical Properties of Collagen Gel on the In Vitro Formation of Microvessel Networks

- by Endothelial Cells. *Tissue Eng.* **13**, 1443–1453 (2007).
66. Mason, B. N., Starchenko, A., Williams, R. M., Bonassar, L. J. & Reinhart-King, C. A. Tuning three-dimensional collagen matrix stiffness independently of collagen concentration modulates endothelial cell behavior. *Acta Biomater.* **9**, 4635–4644 (2013).
 67. Rao, R. R., Peterson, A. W., Ceccarelli, J., Putnam, A. J. & Stegemann, J. P. Matrix composition regulates three-dimensional network formation by endothelial cells and mesenchymal stem cells in collagen/fibrin materials. *Angiogenesis* **15**, 253–64 (2012).
 68. Ghajar, C. M. *et al.* The effect of matrix density on the regulation of 3-D capillary morphogenesis. *Biophys. J.* **94**, 1930–1941 (2008).
 69. Brown, A. *et al.* Engineering PEG-based hydrogels to foster efficient endothelial network formation in free-swelling and confined microenvironments. *Biomaterials* **243**, 119921 (2020).
 70. Abe, Y. *et al.* Balance of interstitial flow magnitude and vascular endothelial growth factor concentration modulates three-dimensional microvascular network formation. *APL Bioeng.* **3**, 036102 (2019).
 71. Ng, C. P., Helm, C.-L. E. & Swartz, M. a. Interstitial flow differentially stimulates blood and lymphatic endothelial cell morphogenesis in vitro. *Microvasc. Res.* **68**, 258–264 (2004).
 72. Hernández Vera, R. *et al.* Interstitial fluid flow intensity modulates endothelial sprouting in restricted Src-activated cell clusters during capillary morphogenesis. *Tissue Eng. Part A* **15**, 175–85 (2009).
 73. Kim, S., Chung, M., Ahn, J., Lee, S. & Jeon, N. L. Interstitial flow regulates the angiogenic response and phenotype of endothelial cells in a 3D culture model. *Lab Chip* **16**, 4189–4199 (2016).

74. Hsu, Y.-H. *et al.* Full range physiological mass transport control in 3D tissue cultures. *Lab Chip* **13**, (2012).
75. Vickerman, V. & Kamm, R. D. Mechanism of a flow-gated angiogenesis switch: early signaling events at cell-matrix and cell-cell junctions. *Integr. Biol. (Camb)*. **4**, 863–74 (2012).
76. Song, J. W., Daubriac, J., Tse, J. M., Bazou, D. & Munn, L. L. RhoA mediates flow-induced endothelial sprouting in a 3-D tissue analogue of angiogenesis. *Lab Chip* **12**, 5000 (2012).
77. Bonvin, C., Overney, J., Shieh, A. C., Dixon, J. B. & Swartz, M. a. A multichamber fluidic device for 3D cultures under interstitial flow with live imaging: Development, characterization, and applications. *Biotechnol. Bioeng.* **105**, 982–991 (2010).
78. Helm, C.-L. E., Fleury, M. E., Zisch, A. H., Boschetti, F. & Swartz, M. a. Synergy between interstitial flow and VEGF directs capillary morphogenesis in vitro through a gradient amplification mechanism. *Proc. Natl. Acad. Sci. U. S. A.* **102**, 15779–15784 (2005).
79. Shirure, V. S., Lezia, A., Tao, A., Alonzo, L. F. & George, S. C. Low levels of physiological interstitial flow eliminate morphogen gradients and guide angiogenesis. *Angiogenesis* **20**, 493–504 (2017).
80. Vilanova, G., Burés, M., Colominas, I. & Gomez, H. Computational modelling suggests complex interactions between interstitial flow and tumour angiogenesis. *J. R. Soc. Interface* **15**, (2018).
81. Armulik, A., Genove, G. & Betsholtz, C. Pericytes: Developmental, Physiological, and Pathological Perspectives, Problems, and Promises. *Dev. Cell* **21**, 193–215 (2011).
82. Bergers, G. & Song, S. The role of pericytes in blood-vessel formation and

- maintenance. *Neuro. Oncol.* **7**, 452–464 (2005).
83. Waters, J. P. *et al.* In vitro self-assembly of human pericyte-supported endothelial microvessels in three-dimensional coculture: a simple model for interrogating endothelial-pericyte interactions. *J. Vasc. Res.* **50**, 324–31 (2013).
 84. Kim, S., Lee, H., Chung, M. & Jeon, N. L. Engineering of functional, perfusable 3D microvascular networks on a chip. *Lab Chip* **13**, 1489–500 (2013).
 85. Purtscher, M., Rothbauer, M., Holnthoner, W., Redl, H. & Ertl, P. Establishment of Vascular Networks in Biochips Using Co-cultures of Adipose Derived Stem Cells and Endothelial Cells in a 3D Fibrin Matrix. in *IFMBE Proceedings* (eds. Lacković, I. & Vasic, D.) **45**, 313–317 (Springer International Publishing, 2015).
 86. Grainger, S. J., Carrion, B., Ceccarelli, J. & Putnam, A. J. Stromal cell identity influences the in vivo functionality of engineered capillary networks formed by co-delivery of endothelial cells and stromal cells. *Tissue Eng. Part A* **19**, 1209–22 (2013).
 87. Rohringer, S. *et al.* Mechanisms of vasculogenesis in 3D fibrin matrices mediated by the interaction of adipose-derived stem cells and endothelial cells. *Angiogenesis* **17**, 921–933 (2014).
 88. Margolis, E. A. *et al.* Stromal Cell Identity Modulates Vascular Morphogenesis in a Microvasculature-on-a-Chip Platform. *Lab Chip* (2021).
 89. Kosyakova, N. *et al.* Differential functional roles of fibroblasts and pericytes in the formation of tissue-engineered microvascular networks in vitro. *npj Regen. Med.* **5**, (2020).
 90. Song, H. H. G. *et al.* Transient Support from Fibroblasts is Sufficient to Drive Functional Vascularization in Engineered Tissues. *Adv. Funct. Mater.* **30**, 1–13 (2020).

91. Gaengel, K., Genové, G., Armulik, A. & Betsholtz, C. Endothelial-mural cell signaling in vascular development and angiogenesis. *Arterioscler. Thromb. Vasc. Biol.* **29**, 630–638 (2009).
92. Campisi, M. *et al.* 3D self-organized microvascular model of the human blood-brain barrier with endothelial cells, pericytes and astrocytes. *Biomaterials* **180**, 117–129 (2018).
93. Pati, S. *et al.* Human Mesenchymal Stem Cells Inhibit Vascular Permeability by Modulating Vascular Endothelial Cadherin/ β -Catenin Signaling. *Stem Cells Dev.* **20**, 89–101 (2011).
94. Jakab, M. & Augustin, H. G. Understanding angiodiversity: insights from single cell biology. *Development* **147**, dev146621 (2020).
95. Minami, T., Muramatsu, M. & Kume, T. Organ/tissue-specific vascular endothelial cell heterogeneity in health and disease. *Biol. Pharm. Bull.* **42**, 1609–1619 (2019).
96. Augustin, H. G. & Koh, G. Y. Organotypic vasculature: From descriptive heterogeneity to functional pathophysiology. *Science (80-.)*. **357**, (2017).
97. Diaz-Santana, A., Shan, M. & Stroock, A. D. Endothelial cell dynamics during anastomosis in vitro. *Integr. Biol.* **7**, 454–466 (2015).
98. Chen, X. *et al.* Prevascularization of a fibrin-based tissue construct accelerates the formation of functional anastomosis with host vasculature. *Tissue Eng. Part A* **15**, 1363–1371 (2009).
99. Phng, L.-K., Stanchi, F. & Gerhardt, H. Filopodia are dispensable for endothelial tip cell guidance. *Development* **140**, 4031–40 (2013).
100. Patel-Hett, S. & D'Amore, P. A. Signal transduction in vasculogenesis and developmental angiogenesis. *Int. J. Dev. Biol.* **55**, 353–363 (2011).

101. Koch, S., Tugues, S., Li, X., Gualandi, L. & Claesson-Welsh, L. Signal transduction by vascular endothelial growth factor receptors. *Biochem. J.* **437**, 169–183 (2011).
102. Yu, P. *et al.* FGF-dependent metabolic control of vascular development. *Nature* (2017).
103. Stratman, A. N., Davis, M. J. & Davis, G. E. VEGF and FGF prime vascular tube morphogenesis and sprouting directed by hematopoietic stem cell cytokines. *Blood* **117**, 3709–3719 (2011).
104. Smith, A. O., Bowers, S. L. K., Stratman, A. N. & Davis, G. E. Hematopoietic stem cell cytokines and fibroblast growth factor-2 stimulate human endothelial cell-pericyte tube co-assembly in 3D fibrin matrices under serum-free defined conditions. *PLoS One* **8**, 1–19 (2013).
105. Montesano, R. & Orci, L. Tumor-promoting phorbol esters induce angiogenesis in vitro. *Cell* **43**, 469–477 (1985).
106. Bayless, K. J. & Davis, G. E. Sphingosine-1-phosphate markedly induces matrix metalloproteinase and integrin-dependent human endothelial cell invasion and lumen formation in three-dimensional collagen and fibrin matrices. *Biochem. Biophys. Res. Commun.* **312**, 903–913 (2003).
107. Wang, W. Y., Lin, D., Jarman, E. H., Polacheck, W. J. & Baker, B. M. Functional angiogenesis requires microenvironmental cues balancing endothelial cell migration and proliferation. *Lab Chip* **20**, 1153–1166 (2020).
108. Chrobak, K. M., Potter, D. R. & Tien, J. Formation of perfused, functional microvascular tubes in vitro. *Microvasc. Res.* **71**, 185–196 (2006).
109. Polacheck, W. J., Kutys, M. L., Tefft, J. B. & Chen, C. S. Microfabricated blood vessels for modeling the vascular transport barrier. *Nat. Protoc.* **14**, 1425–1454 (2019).

110. Kim, J. A. *et al.* Collagen-based brain microvasculature model in vitro using three-dimensional printed template. *Biomicrofluidics* **9**, (2015).
111. van Dijk, C. G. M. *et al.* A new microfluidic model that allows monitoring of complex vascular structures and cell interactions in a 3D biological matrix. *Lab Chip* (2020).
112. Zheng, Y. *et al.* In vitro microvessels for the study of angiogenesis and thrombosis. *Proc. Natl. Acad. Sci. U. S. A.* **109**, 9342–7 (2012).
113. Menon, N. V., Tay, H. M., Wee, S. N., Li, K. H. H. & Hou, H. W. Micro-engineered perfusable 3D vasculature for cardiovascular diseases. *Lab Chip* (2017).
114. Wu, W., Deconinck, A. & Lewis, J. a. Omnidirectional printing of 3D microvascular networks. *Adv. Mater.* **23**, 178–183 (2011).
115. Miller, J. S. *et al.* Rapid casting of patterned vascular networks for perfusable engineered three-dimensional tissues. *Nat. Mater.* **11**, 768–774 (2012).
116. Golden, A. P. & Tien, J. Fabrication of microfluidic hydrogels using molded gelatin as a sacrificial element. *Lab Chip* **7**, 720–725 (2007).
117. Skylar-Scott, M. A. *et al.* Biomanufacturing of organ-specific tissues with high cellular density and embedded vascular channels. *Sci. Adv.* **5**, eaaw2459 (2019).
118. Maharjan, S. *et al.* Symbiotic Photosynthetic Oxygenation within 3D-Bioprinted Vascularized Tissues. *Matter* **4**, 217–240 (2021).
119. Kinstlinger, I. S. *et al.* Generation of model tissues with dendritic vascular networks via sacrificial laser-sintered carbohydrate templates. *Nat. Biomed. Eng.* (2020).
120. Grigoryan, B. *et al.* Multivascular networks and functional intravascular topologies within biocompatible hydrogels. *Science* **364**, 458–464 (2019).

121. Heintz, K. A. *et al.* Fabrication of 3D Biomimetic Microfluidic Networks in Hydrogels. *Adv. Healthc. Mater.* **5**, 2153–2160 (2016).
122. Heintz, K. A., Mayerich, D. & Slater, J. H. Image-guided, Laser-based Fabrication of Vascular-derived Microfluidic Networks. *J. Vis. Exp.* (2017).
123. Arakawa, C. K., Badeau, B. A., Zheng, Y. & DeForest, C. A. Multicellular Vascularized Engineered Tissues through User-Programmable Biomaterial Photodegradation. *Adv. Mater.* **1703156**, 1–9 (2017).
124. Rayner, S. G. *et al.* Multiphoton-Guided Creation of Complex Organ-Specific Microvasculature. *Adv. Healthc. Mater.* **2100031**, 2100031 (2021).
125. Lee, A. *et al.* 3D bioprinting of collagen to rebuild components of the human heart. *Science (80-.).* **365**, 482–487 (2019).
126. Miri, A. K. *et al.* Effective bioprinting resolution in tissue model fabrication. *Lab Chip* **19**, 2019–2037 (2019).
127. Linville, R. M., Boland, N. F., Covarrubias, G., Price, G. M. & Tien, J. Physical and Chemical Signals That Promote Vascularization of Capillary-Scale Channels. *Cell. Mol. Bioeng.* **9**, 73–84 (2016).
128. Ambrosi, D., Bussolino, F. & Preziosi, L. A Review of Vasculogenesis Models. *J. Theor. Med.* **6**, 1–19 (2005).
129. Vailhé, B., Vittet, D. & Feige, J. J. In vitro models of vasculogenesis and angiogenesis. *Lab. Invest.* **81**, 439–452 (2001).
130. Szöke, K., Reinisch, A., Østrup, E., Reinholt, F. P. & Brinchmann, J. E. Autologous cell sources in therapeutic vasculogenesis: In vitro and in vivo comparison of endothelial colony-forming cells from peripheral blood and endothelial cells isolated from adipose tissue. *Cytotherapy* (2015).
131. Hsu, Y.-H., Moya, M. L., Hughes, C. C. W., George, S. C. & Lee, A. P. A

- microfluidic platform for generating large-scale nearly identical human microphysiological vascularized tissue arrays. *Lab Chip* **13**, 2990–8 (2013).
132. Palladino, A. *et al.* Induced Pluripotent Stem Cells as Vasculature Forming Entities. *J. Clin. Med.* **8**, 1782 (2019).
 133. Morin, K. T. & Tranquillo, R. T. In vitro models of angiogenesis and vasculogenesis in fibrin gel. *Exp. Cell Res.* **319**, 2409–2417 (2013).
 134. Koh, W., Stratman, A. N., Sacharidou, A. & Davis, G. E. In vitro three dimensional collagen matrix models of endothelial lumen formation during vasculogenesis and angiogenesis. *Methods Enzymol.* **443**, 83–101 (2008).
 135. Belair, D. G., Schwartz, M. P., Knudsen, T. & Murphy, W. L. Human iPSC-derived endothelial cell sprouting assay in synthetic hydrogel arrays. *Acta Biomater.* **39**, 12–24 (2016).
 136. Helm, C.-L. E., Zisch, A. H. & Swartz, M. A. Engineered blood and lymphatic capillaries in 3-D VEGF-fibrin-collagen matrices with interstitial flow. *Biotechnol. Bioeng.* **96**, 167–176 (2007).
 137. Bersini, S. *et al.* Cell-microenvironment interactions and architectures in microvascular systems. *Biotechnol. Adv.* **34**, 1113–1130 (2016).
 138. Jeon, J. S. *et al.* Generation of 3D functional microvascular networks with human mesenchymal stem cells in microfluidic systems. *Integr. Biol. (Camb)*. **6**, 555–63 (2014).
 139. Alonzo, L. F., Moya, M. L., Shirure, V. S. & George, S. C. Microfluidic device to control interstitial flow-mediated homotypic and heterotypic cellular communication. *Lab Chip* (2015).
 140. Wang, X., Phan, D. T. T., George, S. C., Hughes, C. C. W. & Lee, A. P. Engineering anastomosis between living capillary networks and endothelial cell-

- lined microfluidic channels. *Lab Chip* **16**, 282–290 (2015).
141. Chen, M. B. *et al.* Inflamed neutrophils sequestered at entrapped tumor cells via chemotactic confinement promote tumor cell extravasation. *Proc. Natl. Acad. Sci.* **115**, (2018).
 142. Jeon, J. S. *et al.* Human 3D vascularized organotypic microfluidic assays to study breast cancer cell extravasation. *Proc. Natl. Acad. Sci.* **112**, 201501426 (2015).
 143. Bi, Y. *et al.* Tumor-on-a-chip platform to interrogate the role of macrophages in tumor progression. *Integr. Biol. (Camb)*. **12**, 221–232 (2020).
 144. White, S. M. *et al.* Longitudinal In Vivo Imaging to Assess Blood Flow and Oxygenation in Implantable Engineered Tissues. *Tissue Eng. Part C Methods* **18**, 697–709 (2012).
 145. Murray, C. D. The physiological principle of minimum work applied to the angle of branching of arteries. *J. Gen. Physiol.* **9**, 835–841 (1926).
 146. Laurent, J. *et al.* Convergence of microengineering and cellular self-organization towards functional tissue manufacturing. *Nat. Biomed. Eng.* **1**, 939–956 (2017).
 147. Brassard, J. A. & Lutolf, M. P. Engineering Stem Cell Self-organization to Build Better Organoids. *Cell Stem Cell* **24**, 860–876 (2019).
 148. Hoch, E., Tovar, G. E. M. & Borchers, K. Bioprinting of artificial blood vessels: current approaches towards a demanding goal. *Eur. J. Cardiothorac. Surg.* **46**, 1–12 (2014).
 149. Malheiro, A., Wieringa, P., Mota, C., Baker, M. & Moroni, L. Patterning Vasculature: The Role of Biofabrication to Achieve an Integrated Multicellular Ecosystem. *ACS Biomater. Sci. Eng.* **2**, 1694–1709 (2016).
 150. Yang, G. *et al.* Fabrication of centimeter-sized 3D constructs with patterned endothelial cells through assembly of cell-laden microbeads as a potential bone

- graft. *Acta Biomater.* (2020).
151. Baranski, J. D. *et al.* Geometric control of vascular networks to enhance engineered tissue integration and function. *Proc. Natl. Acad. Sci. U. S. A.* **110**, 7586–91 (2013).
 152. Stevens, K. R. *et al.* In situ expansion of engineered human liver tissue in a mouse model of chronic liver disease. *Sci. Transl. Med.* **9**, (2017).
 153. Kreeger, P. K., Strong, L. E. & Masters, K. S. Engineering Approaches to Study Cellular Decision-Making. *Annu. Rev. Biomed. Eng.* 49–72 (2018).
 154. Goubko, C. a. & Cao, X. Patterning multiple cell types in co-cultures: A review. *Mater. Sci. Eng. C* **29**, 1855–1868 (2009).
 155. Sun, W. *et al.* The bioprinting roadmap. *Biofabrication* **12**, 022002 (2020).
 156. Liu, W. F. & Chen, C. S. Cellular and multicellular form and function. *Adv. Drug Deliv. Rev.* **59**, 1319–1328 (2007).
 157. Duffy, R. M., Sun, Y. & Feinberg, A. W. Understanding the Role of ECM Protein Composition and Geometric Micropatterning for Engineering Human Skeletal Muscle. *Ann. Biomed. Eng.* (2016).
 158. Chen, S. *et al.* Interrogating cellular fate decisions with high-throughput arrays of multiplexed cellular communities. *Nat. Commun.* **7**, 10309 (2016).
 159. Shaya, O. *et al.* Cell-Cell Contact Area Affects Notch Signaling and Notch-Dependent Patterning. *Dev. Cell* **40**, 505-511.e6 (2017).
 160. Rao, N. *et al.* A co-culture device with a tunable stiffness to understand combinatorial cell–cell and cell–matrix interactions. *Integr. Biol.* **5**, 1344 (2013).
 161. Sriraghavan, V., Desai, R. A., Kwon, Y., Mrksich, M. & Chen, C. S. Micropatterned dynamically adhesive substrates for cell migration. *Langmuir* **26**, 17733–17738 (2010).

162. Wong, L., Pegan, J. D., Gabela-Zuniga, B., Khine, M. & McCloskey, K. E. Leaf-inspired microcontact printing vascular patterns. *Biofabrication* **9**, 021001 (2017).
163. Chen, T. H. *et al.* Directing tissue morphogenesis via self-assembly of vascular mesenchymal cells. *Biomaterials* (2012).
164. Lin, C. & Khetani, S. R. Micropatterned co-cultures of human hepatocytes and stromal cells for the assessment of drug clearance and drug-drug interactions. *Curr. Protoc. Toxicol.* **2017**, 1–23 (2017).
165. Hui, E. E. & Bhatia, S. N. Micromechanical control of cell-cell interactions. *Proc. Natl. Acad. Sci. U. S. A.* **104**, 5722–5726 (2007).
166. D’Arcangelo, E. & McGuigan, A. P. Micropatterning strategies to engineer controlled cell and tissue architecture in vitro. *Biotechniques* **58**, 13–23 (2015).
167. Martinez-Rivas, A., González-Quijano, G. K., Proa-Coronado, S., Séverac, C. & Dague, E. Methods of micropatterning and manipulation of cells for biomedical applications. *Micromachines* **8**, (2017).
168. Lee, S. *et al.* Simple Lithography-Free Single Cell Micropatterning using Laser-Cut Stencils. *J. Vis. Exp.* 1–9 (2020).
169. Strale, P. O. *et al.* Multiprotein Printing by Light-Induced Molecular Adsorption. *Adv. Mater.* **28**, 2024–2029 (2016).
170. Melero, C. *et al.* Light-induced molecular adsorption of proteins using the primo system for micro-patterning to study cell responses to extracellular matrix proteins. *J. Vis. Exp.* **2019**, 1–19 (2019).
171. Reid, J. A., Mollica, P. M., Bruno, R. D. & Sachs, P. C. Consistent and reproducible cultures of large-scale 3D mammary epithelial structures using an accessible bioprinting platform. *Breast Cancer Res.* 1–13 (2018).
172. Wang, Z., Lee, S. J., Cheng, H.-J., Yoo, J. J. & Atala, A. 3D Bioprinted

- Functional and Contractile Cardiac Tissue Constructs. *Acta Biomater.* (2018).
173. Todhunter, M. E., Weber, R. J., Farlow, J., Jee, N. Y. & Gartner, Z. J. Fabrication of 3D Microtissue Arrays by DNA Programmed Assembly of Cells. *Curr. Protoc. Chem. Biol.* **8**, 147–178 (2016).
 174. Csizmar, C. M., Petersburg, J. R. & Wagner, C. R. Programming Cell-Cell Interactions through Non-genetic Membrane Engineering. *Cell Chem. Biol.* **25**, 931–940 (2018).
 175. Weber, R. J., Liang, S. I., Selden, N. S., Desai, T. A. & Gartner, Z. J. Efficient targeting of fatty-acid modified oligonucleotides to live cell membranes through stepwise assembly. *Biomacromolecules* **15**, 4621–4626 (2014).
 176. Hughes, A. J. *et al.* Engineered Tissue Folding by Mechanical Compaction of the Mesenchyme. *Dev. Cell* **44**, 165-178.e6 (2018).
 177. Weber, R. J. *et al.* Rapid Organoid Reconstitution by Chemical Micromolding. *ACS Biomater. Sci. Eng.* (2016).
 178. Scheideler, O. J. *et al.* Recapitulating complex biological signaling environments using a multiplexed, DNA-patterning approach. *Sci. Adv.* **6**, (2020).
 179. Viola, J. M. *et al.* Guiding Cell Network Assembly using Shape-Morphing Hydrogels. *Adv. Mater.* **2002195**, e2002195 (2020).
 180. Mohammad, A., Davis, M., Aprelev, A. & Ferrone, F. A. Note: Professional grade microfluidics fabricated simply. *Rev. Sci. Instrum.* **87**, 1–4 (2016).
 181. Lee, O. J., Chuah, H. S., Umar, R., Chen, S. K. & Yusra, A. F. I. Construction of cost effective homebuilt spin coater for coating amylose-amylopectin thin films. *J. Fundam. Appl. Sci.* **9**, 279 (2018).
 182. Webb, K., Hlady, V. & Tresco, P. A. Relative importance of surface wettability and charged functional groups on NIH 3T3 fibroblast attachment, spreading,

- and cytoskeletal organization. *J. Biomed. Mater. Res.* **41**, 422–430 (1998).
183. Microchem. SU-8 2000 Permanent Epoxy Negative Photoresist. Processing Guidelines for: SU-8 2025, SU-8 2035, SU-8 2050, SU-8 2075. 1–5 (2019). Available at: <https://kayakuam.com/wp-content/uploads/2019/09/SU-82000DataSheet2025thru2075Ver4.pdf>.
 184. McGinnis, C. S. *et al.* MULTI-seq: sample multiplexing for single-cell RNA sequencing using lipid-tagged indices. *Nat. Methods* **16**, 619–626 (2019).
 185. Maxfield, F. R. & van Meer, G. Cholesterol, the central lipid of mammalian cells. *Curr. Opin. Cell Biol.* **22**, 422–429 (2010).
 186. Luo, J., Yang, H. & Song, B. L. Mechanisms and regulation of cholesterol homeostasis. *Nat. Rev. Mol. Cell Biol.* **21**, 225–245 (2020).
 187. Liu, L., Tan, L., Yao, J. & Yang, L. Long non-coding RNA MALAT1 regulates cholesterol accumulation in ox-LDL-induced macrophages via the microRNA-17-5p/ABCA1 axis. *Mol. Med. Rep.* **21**, 1761–1770 (2020).
 188. Palte, M. J. & Raines, R. T. Interaction of nucleic acids with the glycocalyx. *J. Am. Chem. Soc.* **134**, 6218–6223 (2012).
 189. Mali, P. *et al.* Barcoding cells using cell-surface programmable DNA-binding domains. *Nat. Methods* **10**, 403–406 (2013).
 190. Hsiao, S. C. *et al.* Direct cell surface modification with DNA for the capture of primary cells and the investigation of myotube formation on defined patterns. *Langmuir* **25**, 6985–6991 (2009).
 191. Gartner, Z. J. & Bertozzi, C. R. Programmed assembly of 3-dimensional microtissues with defined cellular connectivity. *PNAS* 1–5 (2009).
 192. Collinet, C. & Lecuit, T. Programmed and self-organized flow of information during morphogenesis. *Nat. Rev. Mol. Cell Biol.* (2021).

193. Song, H. H. G., Rumma, R. T., Ozaki, C. K., Edelman, E. R. & Chen, C. S. Vascular Tissue Engineering: Progress, Challenges, and Clinical Promise. *Cell Stem Cell* **22**, 340–354 (2018).
194. Rajasekar, S. *et al.* IFlowPlate—A Customized 384-Well Plate for the Culture of Perfusable Vascularized Colon Organoids. *Adv. Mater.* **32**, 1–12 (2020).
195. Griffith, C. K. *et al.* Diffusion limits of an in vitro thick prevascularized tissue. *Tissue Eng.* **11**, 257–266 (2005).
196. White, S., Pittman, C. & Hingorani, R. Implanted Cell-Dense Prevascularized Tissues Develop Functional Vasculature that Supports Reoxygenation Following Thrombosis. *Tissue ...* **00**, 1–13 (2014).
197. Wu, P. K. & Ringeisen, B. R. Development of human umbilical vein endothelial cell (HUVEC) and human umbilical vein smooth muscle cell (HUVSMC) branch/stem structures on hydrogel layers via biological laser printing (BioLP). *Biofabrication* **2**, (2010).
198. Wisdom, K. M. *et al.* Matrix mechanical plasticity regulates cancer cell migration through confining microenvironments. *Nat. Commun.* **9**, (2018).
199. Schindelin, J. *et al.* Fiji: An open-source platform for biological-image analysis. *Nat. Methods* **9**, 676–682 (2012).
200. Cabral, K. A. *et al.* Simple, Affordable, and Modular Patterning of Cells using DNA. *J. Vis. Exp.* (2021).
201. Lancaster, M. A. *et al.* Cerebral organoids model human brain development and microcephaly. *Nature* **501**, 373–379 (2013).
202. Sato, T. *et al.* Single Lgr5 stem cells build crypt-villus structures in vitro without a mesenchymal niche. *Nature* **459**, 262–5 (2009).
203. Jamieson, P. R. *et al.* Derivation of a robust mouse mammary organoid system

- for studying tissue dynamics. *Development* dev.145045 (2016).
doi:10.1242/dev.145045
204. Yeung, T. *et al.* Effects of substrate stiffness on cell morphology, cytoskeletal structure, and adhesion. *Cell Motil. Cytoskeleton* **60**, 24–34 (2005).
 205. Ban, E. *et al.* Mechanisms of Plastic Deformation in Collagen Networks Induced by Cellular Forces. *Biophys. J.* **114**, 450–461 (2018).
 206. Buchmann, B. *et al.* Mechanical plasticity of collagen directs branch elongation in human mammary gland organoids. *Nat. Commun.* **12**, 2759 (2021).
 207. Gerhardt, H. *et al.* VEGF guides angiogenic sprouting utilizing endothelial tip cell filopodia. *J. Cell Biol.* **161**, 1163–1177 (2003).
 208. Fischer, R. S., Lam, P.-Y., Huttenlocher, A. & Waterman, C. M. Filopodia and focal adhesions: An integrated system driving branching morphogenesis in neuronal pathfinding and angiogenesis. *Dev. Biol.* **451**, 86–95 (2019).
 209. Nishizuka, Y. The role of protein kinase C in cell surface signal transduction and tumour promotion. *Nature* **308**, 693–698 (1984).
 210. Nguyen, D.-H. T. *et al.* Biomimetic model to reconstitute angiogenic sprouting morphogenesis in vitro. *Proc. Natl. Acad. Sci. U. S. A.* **110**, 6712–7 (2013).
 211. Gavard, J. & Gutkind, J. S. VEGF controls endothelial-cell permeability by promoting the β -arrestin-dependent endocytosis of VE-cadherin. *Nat. Cell Biol.* **8**, 1223–1234 (2006).
 212. Bentley, K. *et al.* The role of differential VE-cadherin dynamics in cell rearrangement during angiogenesis. *Nat. Cell Biol.* **16**, 309–21 (2014).
 213. Anderson, N. L. & Anderson, N. G. The Human Plasma Proteome. *Mol. Cell. Proteomics* **1**, 845–867 (2002).
 214. Zheng, X. *et al.* Proteomic analysis for the assessment of different lots of fetal

- bovine serum as a raw material for cell culture. Part IV. Application of proteomics to the manufacture of biological drugs. *Biotechnol. Prog.* **22**, 1294–1300 (2006).
215. Zeeb, M., Strilic, B. & Lammert, E. Resolving cell-cell junctions: Lumen formation in blood vessels. *Curr. Opin. Cell Biol.* **22**, 626–632 (2010).
 216. Xu, K. & Cleaver, O. Tubulogenesis during blood vessel formation. *Semin. Cell Dev. Biol.* **22**, 993–1004 (2011).
 217. Strilić, B. *et al.* Electrostatic cell-surface repulsion initiates lumen formation in developing blood vessels. *Curr. Biol.* **20**, 2003–2009 (2010).
 218. Szymborska, A. & Gerhardt, H. Hold me, but not too tight—endothelial cell–cell junctions in angiogenesis. *Cold Spring Harb. Perspect. Biol.* **10**, (2018).
 219. Tung, J. J., Tattersall, I. W. & Kitajewski, J. Tips, stalks, tubes: Notch-mediated cell fate determination and mechanisms of tubulogenesis during angiogenesis. *Cold Spring Harb. Perspect. Med.* **2**, 1–14 (2013).
 220. Baeyens, N. *et al.* Vascular remodeling is governed by a VEGFR3-dependent fluid shear stress set point. *Elife* **4**, 1–16 (2015).
 221. Baeyens, N. & Schwartz, M. A. Biomechanics of vascular mechanosensation and remodeling. *Mol. Biol. Cell* **27**, 7–11 (2016).
 222. Mukherjee, S. & Bassler, B. L. Bacterial quorum sensing in complex and dynamically changing environments. *Nat. Rev. Microbiol.* **17**, 371–382 (2019).
 223. Gurdon, J. B. A community effect in animal development. *Nature* **336**, 772–774 (1988).
 224. Gurdon, J. B., Lemaire, P. & Kato, K. Community effects and related phenomena in development. *Cell* **75**, 831–834 (1993).
 225. Sender, R., Fuchs, S. & Milo, R. Revised Estimates for the Number of Human

- and Bacteria Cells in the Body. *PLoS Biol.* **14**, 1–14 (2016).
226. Bianconi, E. *et al.* An estimation of the number of cells in the human body. *Ann. Hum. Biol.* **40**, 463–471 (2013).
227. Koch, S. & Claesson-Welsh, L. Signal transduction by vascular endothelial growth factor receptors. *Cold Spring Harb. Perspect. Med.* **2**, 1–21 (2012).
228. Gavard, J. Endothelial permeability and VE-cadherin: A wacky comradeship. *Cell Adhes. Migr.* **8**, 158–164 (2014).
229. Bichsel, C. a., Hall, S. R. R., Schmid, R. a., Guenat, O. T. & Geiser, T. Primary Human Lung Pericytes Support and Stabilize In Vitro Perfusable Microvessels. *Tissue Eng. Part A* **21**, 2166–2176 (2015).
230. Temiz, Y., Lovchik, R. D., Kaigala, G. V. & Delamarche, E. Lab-on-a-chip devices: How to close and plug the lab? *Microelectron. Eng.* **132**, 156–175 (2015).
231. Foncy, J. *et al.* Reversible magnetic clamp of a microfluidic interface for the seric detection of food allergies on allergen microarrays. *Microelectron. Eng.* **158**, 16–21 (2016).
232. Abhyankar, V. V., Wu, M., Koh, C.-Y. & Hatch, A. V. A Reversibly Sealed, Easy Access, Modular (SEAM) Microfluidic Architecture to Establish In Vitro Tissue Interfaces. *PLoS One* **11**, e0156341 (2016).
233. Przysinda, A., Feng, W. & Li, G. Diversity of Organism-Wide and Organ-Specific Endothelial Cells. *Curr. Cardiol. Rep.* **22**, (2020).
234. Rafii, S., Butler, J. M. & Ding, B.-S. Angiocrine functions of organ-specific endothelial cells. *Nature* **529**, 316–325 (2016).
235. Esch, M. B. *et al.* How multi-organ microdevices can help foster drug development. *Adv. Drug Deliv. Rev.* **69–70**, 158–169 (2014).

Publishing Agreement

It is the policy of the University to encourage open access and broad distribution of all theses, dissertations, and manuscripts. The Graduate Division will facilitate the distribution of UCSF theses, dissertations, and manuscripts to the UCSF Library for open access and distribution. UCSF will make such theses, dissertations, and manuscripts accessible to the public and will take reasonable steps to preserve these works in perpetuity.

I hereby grant the non-exclusive, perpetual right to The Regents of the University of California to reproduce, publicly display, distribute, preserve, and publish copies of my thesis, dissertation, or manuscript in any form or media, now existing or later derived, including access online for teaching, research, and public service purposes.

Katelyn Ashley Cabral
Author Signature

6/4/2021
Date